UNIVERSITY OF KWAZULU-NATAL

COLLEGE OF AGRICULTURE, ENGINEERING AND SCIENCE

SIMULATION AND EXPERIMENTAL EVALUATION OF A HYBRID FLAT-PLATE VACUUM INSULATED PHOTOVOLTAIC AND THERMAL POWER MODULE

Oyieke Andrew Young Apuko

213570041

Dissertation submitted in fulfilment of the requirements of the award of the degree of
Master of Science in Mechanical Engineering

Supervisor:

Dr. Freddie L. Inambao

December 2014

"As the candidate's Academic Supervisor, I agree to the Submission of this Thesis"

.......DR. FREDDIE L. INAMBAO...........   ....

       Name of Supervisor   Signature

DECLARATION 1 - PLAGIARISM

I, **Oyieke Andrew Apuko Young**, declare that:

1. The research reported in this thesis, except where otherwise indicated, is my original research.

2. This thesis has not been submitted for any degree or examination at any other university.

3. This thesis does not contain other persons' data, pictures, graphs or other information, unless specifically acknowledged as being sourced from other persons.

4. This thesis does not contain other persons' writing, unless specifically acknowledged as being sourced as being sourced from other researchers. Where other written sources have been quoted, then:

   (a) Their words have been re-written but the general information attributed to them has been referenced.

   (b) Where their exact words have been used, then their writing has been placed in italics and inside quotation marks and referenced.

5. This thesis does not contain text, graphics of tables copied and pasted from the internet, unless specifically acknowledged, and the source being detailed in the thesis and in the references sections.

Signed:

....

DECLARATION 2 - PUBLICATIONS

The following papers have been published:

1. **Oyieke Andrew Y. A**. and Inambao F.L., "Experimental performance analysis of flat plate vacuum insulated hybrid photovoltaic and thermal power module for domestic applications in South Africa". Submitted to *Energy Sources, Part A: Recovery, Utilization and Environmental effects*

2. **Oyieke Andrew Y. A**. and Inambao F.L., "Simulation and performance evaluation of a vacuum insulated hybrid solar photovoltaic/thermal power module for domestic applications in South Africa". *In: Proceedings of the 13th International Conference on Sustainable Energy Technologies (SET2014)* CD Rom, Geneva, Switzerland, 25th − 28th August, 2014.

3. **Oyieke Andrew Y.A.** and Inambao F.L., "Water based hybrid photovoltaic and thermal (PV/T) flat-plate solar collectors: Status and opportunities". *In: Proceedings of the 13th BIE Biennial Conference* CD Rom, Gaborone, Botswana, 15th − 18th October, 2013, pp. 85-98.

In all the above listed papers, I Oyieke Andrew Young Apuko was the main and corresponding author, whilst Dr. Freddie L. Inambao was the co-author and my research supervisor.

Signed:

....

ACKNOWLEDGEMENTS

ABSTRACT

Current Photovoltaic (PV) technologies are characterised by low conversion efficiencies due to the inability to fully absorb solar radiation within the spectral range. This results in the generation of residual heat and raised cell temperatures. The high temperatures are undesirable for efficient operation of the PV and must be controlled hence the development of hybrid Photovoltaic and Thermal (PV/T) systems. Whereas electrical energy generation is prioritized in PV/T systems, the thermal component has often been overlooked and only used as an action to enhance electrical efficiency. They operate at low thermal efficiencies compared to conventional solar thermal systems since they are meant to reduce the PV cell temperatures. In this dissertation, a flat-plate Vacuum Insulated Photovoltaic and Thermal (VIPV/T) system has been thermodynamically simulated and experimentally evaluated in order to assess the thermal and electrical performance as well as conversion efficiencies.

A simulation model of a hybrid PV/T system made of specified components was developed to accurately predict the performance. To assess the influence of the vacuum insulation on the system's electrical and thermal performance, a numerical energy balance equation for the VIPV/T system was formulated and implemented in TRNSYS environment using temperatures, current, voltage and power flows over medium-term duration (daily cycle) under local climatic conditions. Parametric and sensitivity studies conducted on the VIPV/T collector to determine the optimum inclination angle realised a value of 35°. The effect of changes in the PV/T system configuration e.g. with and without PV glass encapsulation has also been studied. The application of vacuum insulation allowed for the removal of PV cell glass encapsulation. This option was found to increase the optical performance by 8 %.

The experimentation was carried out under steady-state conditions in accordance to ISO 9806-1:1994 standard, at the University of Kwazulu-Natal, Durban, Kwazulu-Natal province, -29^o97'N, 30^o95'E, South Africa. The experimental results of the system operating temperatures and energy gains were compared with the simulation results obtained in TRNSYS based on the actual daily weather data and were found to be within the allowable margin of variation of 5 %. The VIPV/T has shown an improved overall efficiency of 9.5 % and thermal efficiency of 16.8 %, while electrical efficiency marginally reduced by 0.02 % compared to the conventional PV/T. This is due to increased heat retention capabilities resulting in raised PV module temperatures. The temperatures require high degree of controls and were regulated by controlling the water flow rates.

The simulated annual performance results for VIPV/T gave thermal, electrical and overall efficiencies of 18 %, 11 % and 29 % respectively. The solar fraction, overall exergy and primary energy saving efficiencies were 39 %, 29 % and 27 % respectively.

Key Words: *Vacuum Insulation, Hybrid, photovoltaic, thermal Power Module*.

TABLE OF CONTENTS

LIST OF FIGURES

LIST OF TABLES

LIST OF SYMBOLS

Roman symbols

Symbol	Description	Units
A	Area of the collector	m^2
k_b	Bond width	kJ/kg
I	Current	A
D	Diameter	m
W	Distance between the central axes of the tubes	m
e	Electric charge (1.602×10^{-19})	C
$\dot{m}$	Fluid mass flow rate	kg/s
Q	Heat (thermal) energy	kJ/kg
P	Power	W
G	Solar Irradiance	W/m^2
c_p	Specific Heat capacity of the fluid	kJ/kgk
T	Temperature	^{o}C
k	Thermal conductivity	kJ/kg
V	Voltage	V
v	Wind speeds	m/s

Dimensionless symbols

Symbol	Description	Units
ex	Exergy	$[-]$
F	Fin efficiency	$[-]$
F'	Fin efficiency factor	$[-]$

F_R	Heat removal factor	[−]
h	Heat transfer coefficient	[−]
N	Number of glass covers	[−]
Nu	Nusselt number	[−]
U_L	Overall thermal loss coefficient	[−]
Pr	Prandlt number	[−]
Re	Reynold's number	[−]
f	Solar fraction	[−]
C	Thermal conductance	[−]
U_t	Thermal loss coefficient through the top	[−]
U_e	Thermal loss coefficient through the edges	[−]
U_b	Thermal loss coefficient through the back	[−]

Greek symbols

α	Absorptance	[−]
γ	Bond thickness	m
β	Collector inclination angle	^oC
ρ	Density	kJ/m^3
η	Efficiency	[−]
ε	Emittance	[−]
ξ	Exergy efficiency	[−]
δ	Plate thickness	m
σ	Stephan Boltzmann's constant	kJ/kg
μ	Temperature coefficient of the PV at reference conditions	[−]

| τ | Transmittance | $[-]$ |

Subscripts

a	Ambient
Aux	Auxiliary
$back$	Back b Bond
C	Carnot
c	Collector
a	Diode
el	Electrical
e	External
f	Final
g	Glass
in	Inlet
i	Internal
L,th	Load, thermal
L,el	Load, electrical
Max	Maximum
mp	Mean plate outOutlet
oc	Open circuit
o	Overall
p	Plate
ph	Photo
$pgen$	Power generation

ref	Reference
sc	Short circuit
th	Thermal
t	Top
u	Useful
wm	Water, mean

ACRONYMS AND ABBREVIATIONS

AC	Alternating Current
AMY	Actual Meteorological Year
N_3H	Ammonia
$A-Si$	Amorphous Silicon
$BiPV$	Building integrated Photovoltaic
$BIPV\ T$	Building Integrated Photovoltaic and Thermal
BOS	Balance-of-System
CdS	Cadmium Sulphide
$CdTe$	Cadmium Telluride
CFC	Chlorofluorocarbon
CIS	Copper Indium Diselenide
$CLFR$	Compact Linear Fresnel Reflector
CO_2	Carbon Dioxide
$CPBT$	Cost-Payback Time
CPC	Compound Parabolic Collector
CPV	Concentrating Photovoltaic
$CPV\ T$	Concentrating Photovoltaic and Thermal
Cu_2S	Cuprous Sulphide
DC	Direct Current
DCS	Direct Circulation Systems

EES	Engineering Equations Solver
ETC	Evacuated Tube Collector
FLC	Fresnel Lens Collector
FPC	Flat-Plate Collector
GaAs	Gallium Arsenide
GHG	Greenhouse Gas
HFC	Heliostat Field Collector
ICS	Indirect Circulation Systems
IPV TS	Integrated Photovoltaic Thermal System
LCA	Life Cycle Assessment
LCC	Life Cycle Cost
LFR	Linear Fresnel Reflector
CH4	Methane
Pc − Si	Polycrystalline Silicon
PDR	Parabolic Dish Reflector
PTC	Parabolic Trough Collector
PV	Photovoltaic
PV/T	Photovoltaic/Thermal
RES	Renewable Energy Source
Si	Silicon
TMY	Typical Meteorological Year
TPV	Thermophotovoltaic

TRNSY S   Transient Simulation System

V IPV/T   Vacuum Insulated Photovoltaic and Thermal

CHAPTER 1

INTRODUCTION

Energy has played an integral role in the development of humanity, both at domestic and industrial levels of application, since ancient times. Energy conversion and consumption patterns greatly contribute to global economic growth and environmental sustainability. The development of solar conversion technologies range from new designs to efficiency improvement of existing ones. However, consumption patterns depend on affordability rather than availability of energy resources to the consumers; therefore, it makes economic sense to focus more attention on energy conversion technologies rather than consumption methodologies [1].

1.1   Background

Energy resources are broadly categorized as renewable or alternative and non-renewable or conventional energy. Consideration for safety and economic aspects, as well as, environmental effects should not be overlooked in the choice of energy sources used in our daily activities. For both domestic and industrial applications, energy is used in the form of electrical and thermal. Electrical energy is used to power machines, home appliances and lighting as well as cooking when converted into heat energy among other applications. Heat energy, otherwise known as thermal energy, plays a critical role in human activities and can be used as low-temperatures or low grade as well as high-temperatures or high grade [1].

The global shift of attention to and investment in renewable and environmentally friendly energy resources such as hydroelectric, wind, tidal or ocean currents, biomass, geothermal and solar among others, can be traced to the oil crisis in the 1970s, the world wide environmental challenges of global warming, ozone layer degradation and the need for efficient use of available energy resources [2]. Whereas renewable energy sources are known to be free from contaminants, inexhaustible and plentiful, some forms may be intermittent and costly to harness since they are dependent on the climatic conditions [3].

1

1.2   South African Energy Scenario

The Republic of South Africa leads the African continent in terms of energy generation and use. According to the National Energy Regulator (NER), 93 % of the current South African energy is generated from burning fossil fuels (coal), which translates to an annual consumption of coal of approximately 94.1 million tonnes. Consequently, a substantial amount of Green House Gases (GHG) are emitted to the environment, most notably, an estimated 169.3 million tonnes, 2154 tonnes, 1.5 million tonnes, 684000 tonnes and 59640 tonnes of CO_2, NO_2, SO_2, NO_x and particulates respectively [4].

The theoretical potential of renewable energy reaching the South African landmass is estimated to be about 280 Terawatts which is 6500 times greater than the current 43 Gigawatt generation capacity of power stations. The potential of solar energy alone is estimated to be 850 000$PJ/year$ which is way above the consumption of 587$PJ/year$ and 621$PJ/year$ generated by coal-fired plants [5]. As can be seen in the solar radiation distribution map for South Africa shown in figure 1 [5], more intensity is experienced towards the inland North, while along the coastline less solar intensity is experienced.
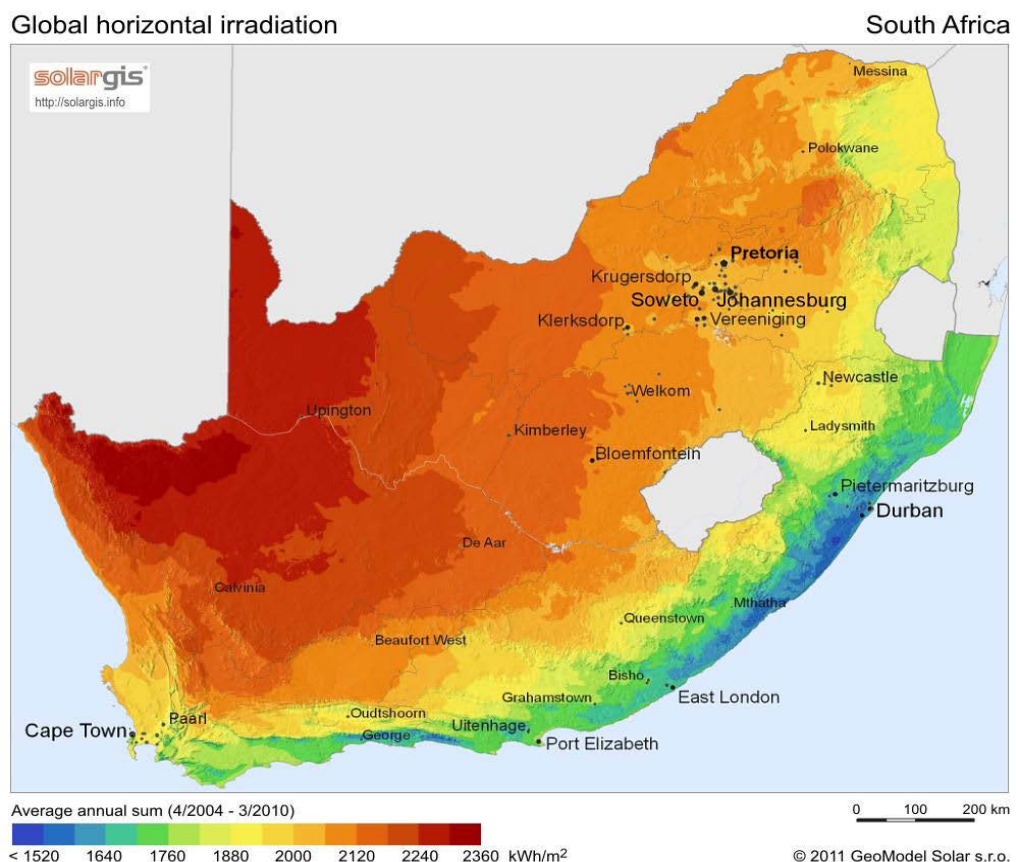
Figure 1: The South African GIS solar map

Owing to the diffuse and intermittent nature of solar energy, the technical, economic and market potentials for solar energy harnessing systems are still far below the theoretical potential.

Renewable Energy Sources (RES) such as solar, hydroelectricity, wind, biomass and geothermal which together currently account for only 7 % of energy generated in South Africa. As this proportion increases there will be a significant reduction in reliance on conventional fuel burning plants which in turn, will mitigate environmental degradation. Sustainable RES must be able to support livelihood in areas of application such as cooking, lighting, space heating/cooling, water heating and powering appliances.

Approximately 70 % and 30 % of energy generated in South Africa is used for industrial and building and residential applications respectively. To date, it still remains a challenge to produce adequate, affordable, reliable and sustainable energy supplies, even though electricity supply has improved from one-third to two-thirds since 1994. The current generation and application of energy poses increasing danger to the environment and the livelihood of the population. The main challenge is how to move to much cleaner and efficient power generation and use while at the same time continuing to extend affordable access to state of the art energy technologies, particularly to serve poor rural house-holds. Environmental soundness must be cost effective and affordable otherwise the technology is not sustainable.

In the global thermal energy and power scenario, solar thermal heating potential total capacity in operation stands at $147GW$ while total energy produced is $87TWh$ as can be seen in figure 2. This shows that only 62 % of the installed capacity is utilized due to undetermined factors. One of the probable reasons could be low conversion efficiencies. This justifies any action, study, research or implementation of energy efficiency improvement in these systems.

Solar energy has gained popularity in the recent past because of its sustainability and environmental friendliness but has not been fully exploited to bridge the current energy gaps due to costly harnessing systems. However, there are good prospects that costs may come down in the near future by developing novel and efficient technologies of conversion of solar energy [6]. Considering the enormous amount of untapped solar energy resources, the South African government recently initiated a roll out of subsidized solar water heating systems project for the new state housing programs. However, it will make more economic

3

sense if the thermal and electrical systems are pooled together to form hybrid Photovoltaic/Thermal (PV/T)systems that can be supplied under the same program. It is foreseen that the results of this study may well impact on household energy gains so positively contribute to livelihoods within the republic of South Africa.
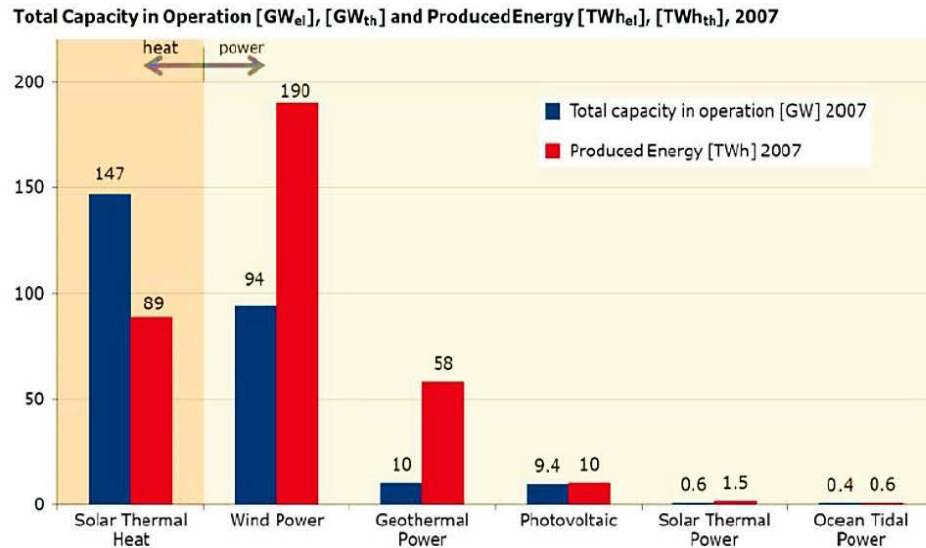
Figure 2: The global solar thermal energy use

The present study focuses on improving the efficiency of the transformation of solar radiation to electrical and thermal energy. A vacuum flat-plate Photovoltaic/Thermal (PV/T) collector was tested experimentally to determine the thermal and electrical conversion efficiency. An assessment of performance by modelling and simulation was carried out and the results obtained compared with the experimental values for validation.

1.3   Research motivation

The major problem of the current Photovoltaic (PV) technologies which inhibits their application is their low conversion efficiency of solar radiation to electrical energy. This is due to the fact that PV cells are unable to fully absorb solar radiation within the spectral range, resulting in heat dissipation to the surrounding atmosphere and raised temperatures. The high temperatures are undesirable for operation of PV modules and need to be controlled in order to achieve relatively higher efficiencies, which provide an opportunity for addition of a thermal unit within the same system to form a hybrid PV/T system.

However, electrical energy generation is given priority in hybrid PV/T systems thereby relegating thermal energy outputs to merely being electrical energy generation efficiency improvement mechanisms. This means that these systems have relatively lower thermal

efficiencies compared to individual solar thermal collectors. Therefore, this study seeks to investigate vacuum insulation as an intervention to improve thermal efficiency in a PV/T system without compromising electrical efficiency and to make it competitive with the individual thermal units possible.

1.4 Aim and objectives of study

The main aim of the study is to carry out modelling, simulation and experimental performance analysis of a Vacuum Insulated hybrid Photovoltaic and Thermal (VIPV/T) power module.

The objectives can specifically be stated as follows:

i To develop a simulation model in TRNSYS program made of specified components into which detailed manufacturer's data can be entered so as to accurately evaluate the functional properties of the Vacuum Insulated Hybrid Photovoltaic and Thermal (VIPV/T) system.

ii To conduct an out-door experiment on the hybrid VIPV/T and conventional air-insulated PV/T subjected to the same weather conditions and input parameters.

iii To assess the influence of vacuum insulation on the electrical and thermal performance of the PV/T system using temperatures and power flow over medium-term duration (daily cycle) based on the model developed.

iv To compare the results of the simulation and experimental studies in order to check the functionality, validity and accuracy of the TRNSYS model developed.

1.5 Research questions

The key research questions addressed in this study are as follows.

i What functional components combinations constitute a complete working hybrid PV/T system in TRNSYS program?

ii What are the component combinations, configurations and measurements that enable performance characterization of VIPV/T systems in comparison to PV/T systems?

iii What effect does the inclusion of a vacuum insulation layer have on the electrical and thermal performance of the PV/T system?

iv To what extent do the simulation and experimental results compare?

5

1.6   Contribution of the research

The main contributions of this study are as follows:

1. Develop and validate the TRNSYS model with experimental results under real/actual conditions. This provides a tool for sizing and performance analysis of PV/T for specified applications.

2. Significant improvement in the thermal performance of PV/T systems in addition to improved physical feasibility of applying vacuum envelope insulation where higher thermal output is desired.

3. Further promote the application of solar energy where conventional fossil fuels would have been used.

1.7   Scope of the research

The research study was formulated to achieve the stated objectives with respect to modelling, simulation and experimental performance analysis of hybrid VIPV/T in comparison to conventional PV/T. The VIPV/T and PV/T collector under consideration were limited to Flat-Plate types.

Even though there are numerous modelling and simulation tools for solar systems, this study was conducted using Transient Systems simulation (TRNSYS) software by way of component identification, connections and mathematical assignments. The numerical results generated were further processed, analysed and presented using Engineering Equations Solver (EES) software.

The weather input data was limited to Durban, Kwazulu-Natal, South Africa. For simulation, TRNSYS inbuilt Typical Meteorological Year (TMY) data file was used while for experimental study, the actual measured meteorological data was used. Hence, the results presented are specific to the city of Durban, South Africa, but can be expanded to include any other location. The validation of the simulation results was carried out by comparing both scenarios.

1.8   The general research outline

The research was conducted under a structured and systematic program from start to end. A comprehensive literature survey was carried out in order for the researcher to become familiar with the field of study. The preparatory procedures then followed, involving

learning of simulation software, experimental design and procurement of experimental apparatus. A simulation model was developed, tested and refined during the course of running the experiments. The results of both exercises were then compared for validity and relevant conclusions were drawn and recommendations made. The details of the research outline are presented in figure
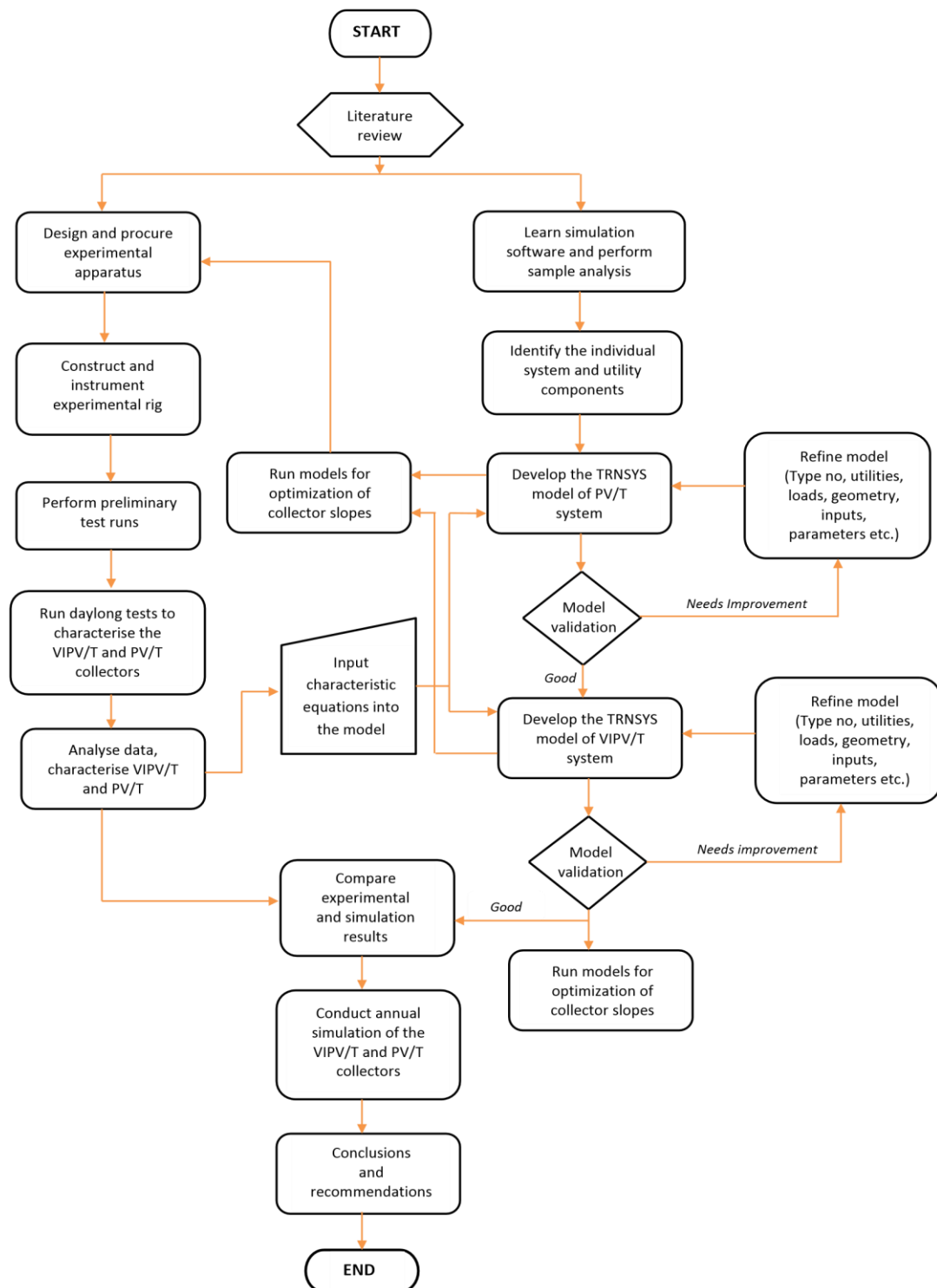
Figure 3: General research outline

1.9   Organization of the thesis

The dissertation is structured as follows:

1. Chapter 1 gives an introduction to the subject of the research study. The project is defined then the subject is objectively and systematically structured under the following sections: the background, research motivation, aims and objectives, scope and research questions. The organization of the dissertation and the research outline are also given.

2. Chapter 2 presents a critical review of literature in the field of PV/T including but not limited to past works by other researchers, physics of heat transport solar collectors, the concept of vacuum insulation, solar energy conversion systems; photovoltaic, solar water heating and hybrid photovoltaic systems and their performance assessment.

3. Chapter 3 presents modelling and simulation in which the modelling software is described and the TRNSYS model is developed and described in terms of the individual components. The model is simulated, results are presented and discussed in terms of daily (short-term) and annual (long-term) thermal energy and electrical energy outputs in relation to thermal, electrical, overall, exergy and primary energy saving efficiencies. The effect of vacuum insulation is also analysed.

4. Chapter 4 presents the experimental study including aims and objectives. Materials and equipment are identified and described. The experimental set-up and procedures are stipulated. A detailed discussion of experimental results is also presented in terms of the weather parameters, useful energy generated, hot water temperatures, efficiencies and electrical power generated.

5. Chapter 5 gives a comprehensive and detailed comparison of simulation and experimental results in terms of thermal outputs, useful heat energy, and variation of hot water temperatures, electrical energy outputs and thermal, electrical, overall exergy and primary energy saving efficiencies.

6. Chapter 6 presents a summary of the main conclusions of the study and relevant recommendations are drawn based on the results obtained.

1.10 Chapter Summary

In this chapter, an in-depth and precise introduction to the energy conversion technology and systems has been highlighted. The current energy scenario in the republic of South Africa and global solar thermal energy status are also provided. In order to give an insight of the study; the motivation, objectives, contributions, questions, scope, outline and organization of the research have also been clearly defined.

The next chapter presents a comprehensive systematic critical analysis of state-of-the-art of solar conversion energy and related technologies in order to appreciate the scholarly contributions of other researchers as well as identify the knowledge gaps. An extensive literature survey and critical review of existing technologies in terms of methodologies and obtained results will be used to justify the need for this study.

CHAPTER 2

LITERATURE REVIEW

This chapter gives an overview of the solar energy application categories as well as a review of the past research works carried out on the subject of solar PV/T technology. Solar energy conversion technologies, applications and performance evaluation theories are highlighted.

Hybrid PV/T solar systems technology is rapidly developing, but the adoption is still limited to prototypes for demonstration except for a few small scale projects initiated in Germany and Turkey. Despite the cost effective improvements on solar energy conversion, the uptake rate is still lower than the independent PV and thermal systems; however, the air-based systems have gained popularity in the built environment where standard practice requires PV cooling [7].

The air-based systems are relatively inexpensive compared to water-based systems and are not recommended for use on buildings located in low latitude regions because ambient day temperatures in these regions are above 20^oC for most of the year therefore effective electricity generation is limited to short periods. The water-based types are recommended for use in low latitude regions since the mains water supply temperatures are below 20^oC throughout the year. The dual water-air based types are new technologies with promising results in all regions. They have a mechanism of utilising either water or air, whichever is more effective at the time [8]. Most of the literature covered relating to the studies in the area of PV/T in this section are on water based since this is the subject of this study.

2.1   Review of past work on PV/T water based systems

Past and ongoing research points to considerable gains in hybrid PV/T technology with regard to overall improvement of the system's efficiency. These studies are related but not limited to the performance evaluation of different types of PV/T configurations, geometrical optimization, and operational parameters associated with PV/T. Design, experimental, simulation and modelling studies have been conducted using different techniques, software and simulation tools resulting in a common trend of producing useful outcomes. Numerous theories have been proposed, design configurations suggested and

simulation results obtained. Some of the works highlighted in this chapter are classified as: design studies, experimental studies, theoretical and analytical studies, modelling and simulation studies and finally the combination of experimental and simulation studies.

2.1.1 Design studies

Proper design and sizing of solar systems is a multifaceted procedure involving both predictable(collector, inverter, battery etc.) and the unpredictable (weather data) components. Studies on the design aspects of PV/T modules involve design techniques, material combinations, PV cells and thermal plated attaching techniques and their respective analysis.

Sadness et al., [9] examined the behaviour of a merged PV/T collector built by attaching single-crystal Si cells on top of a black plastic solar heat absorber (unglazed PV/T system). They suggested that this PV/T concept should be exploited in low-grade heat domestic applications such as room heating and sanitary hot water applications while sustaining the electrical efficiency.

Chow [10] built up an exciting model of a clear solitary glazing flat-plate PV/T collector with a sheet and pipe theory. He revealed that fin effectiveness and quality of the attachment connecting the collector and sheet beneath the cells are the vital aspects which limit the realizable total efficiency. He realized improvement in electrical efficiency of about 2 % at stream level of 0.01 *kg/s* corresponding to a plate-bond heat transfer coefficient of about 10,000 W/m^2K. The metallic tubes or fins are usually bonded to the PV module by means of a metallic medium to facilitate heat transfer, to guarantee no gap provision in the metallic pipes to PV module link. An extra 60 % thermal efficiency was realized too.

In the works of Huang et al. [11], an "integrated photovoltaic and thermal solar system (IPVTS)" was examined in comparison to a normal individual solar water heater. They used a p-Si PV module for construction of a PV/T collector built in an IPVTS and introduced the theory of primary-energy saving efficiency in the assessment of PV/T systems. The primary-energy saving efficiency of IPVTS exceeded 60 %, while the temperature difference between the tank water the PV module was around 4^oC. This was greater than for conventional solar water heating or PV units. The typical efficiency on a daily basis reached 38 % constituting approximately 76 % of that of a normal solar water

11

heating unit utilizing glass covered collectors which recorded 50.50 %. They concluded that improvement in the functionality of a PV/T collector can be achieved by directly packing all the components in one whole system i.e. the heat-absorbing plate, PV cells and glazing to constitute a glazed collector. Further, the production costs of the PV/T collector and IPVTS could also be decreased and made cost-effective.

2.1.2 Experimental studies

Experimental studies, ranging from single to arrayed systems of modules, have been carried out to measure an assortment of operational parameters such as temperature, flow rates and thermal and electrical power conversion rates. Most notable outcome of these studies was to determine the actual performance of PV/T systems in different operational environments, ascertaining the relationships between theoretical investigations and practical applications and validating the simulation models.

Tripanagnostopoulos et al. [12] considered appropriate thermal contacts connecting the module with the collector in unglazed combined PV/T systems. They showed that the boundary extents of the PV module and the collector in a PV/T configuration should be equivalent for greater overall efficiency. They additionally conducted experimental studies on unglazed pc-Si dual PV/T units that used both water and air as cooling media based on the prevailing climatic conditions and thermal load [13]. The prototypes were founded on conventional PV modules of distinct dimensions having booster drawn-out reflectors incorporated on the plane ridge of a building and recorded greater electrical and thermal yield. Their observation was that PV cooling increased energy conversion efficiency of the modules and improved the overall system efficiency. Enhancement of the performance was accomplished by supplementary covering to upsurge thermal output, installation of booster turgid reflectors to upturn the energy system's output and offering agility in system design. This enhanced system attained a growth in total energy output by up to 30 %. However, they did not make a recommendation regarding the best cooling medium for the system.

Agrawal and Tiwari [14] analysed both monocrystalline and a-Si Building Integrated Photovoltaic Thermal (BIPVT) in comparison to an equivalent Building Integrated Photovoltaic (BIPV) schemes installed on the roof of a building to produce electricity. They established that the BIPVT produced superior electrical yield, and additional heat energy for space-heating. They also created a thermodynamic model that described energy,

12

exergy and Life Cycle Cost (LCC) with respect to the BIPVT system. Their outcomes indicated that even though the monocrystalline BIPVT system was better to an extent, and was appropriate for domestic users because of their energy and exergy efficiencies, the a-Si BIPVT system was the most cost-effective. The a-Si BIPVT system realized energy and exergy efficiencies in the regions of 33.54 % and 7.13 % respectively under the complex weather environment prevalent in New Delhi.

Elswijk et al. [15] installed large PV/T arrays on residential buildings and established that the use of PV/T could save around 38 % in roof area compared to PV and solar thermal modules arranged side-by-side. More recently, Zondag et al. [16] carried out testing of a PV/T solar boiler with water storage tanks. They evaluated performances and categorized the PV/T water-based collectors into four major types namely sheet-and-tube collectors, channel collectors, free- flow collectors and two absorber collectors. They found that the covered sheet-and-tube system was the most promising PV/T concept for tap water heating with mean annual solar efficiencies in the range of 34 % to 39 %.

Joshi et al. [1] determined the "fill factor" experimentally and evaluated its effect on the performance characteristics of a PV and PV/T system founded on energy and exergy efficiencies. They found that energy efficiency of the PV/T system ranged from 33 % to 45 %. The corresponding exergy efficiency for the PV/T system was 11.3 % to 16 % and for the PV system 7.8 % to 13.8 %. Chow et al. [17] performed an experimental study on a wall mounted combined centralized photovoltaic and hot water collector that attained thermal and electrical efficiencies of 38.9 % and 8.56 %. Erdil et al. [18] introduced the concept of venting to release excess pressure build up in a hybrid PV/T module. A daily 2.8 *kWh* thermal energy could be stored as pre-heated water for domestic utilization at the expense of 11.5 % electrical energy loss.

He et al., [19] constructed and tested a thermosiphonic PV/T water heating system with a polycrystalline PV module on an aluminium-alloy flat-box absorber that attained a maximum thermal efficiency of 40 %. Following this development, Robles et al. [20] constructed and studied an experimental model of a PV/T hybrid system with a bi-facial PV module with a set of reflecting planes to enhance the electric energy production. This system attained an overall efficiency of 60 %, for which the electrical efficiency turned out to be 16.4 %.

13

2.1.3 Theoretical and analytical studies

Studies on the theories and analysis of performance of PV/T water heating systems revolve around revealing energy balance and temperature changes through different layers of PV/T materials [21] [22]; optimization of the structural/geometrical parameters (e.g. dimensions and sizes, connections, shapes); establishing the favourable operating conditions such as fluid flow rates and pressures; energy and exergy analytical models to study the overall energy use; performance of integrated systems [23];and 1D, 2D and 3D models for energy transfer calculation across modules and energy efficiencies [24].

In earlier work on the theoretical analysis of PV/T systems, Florschuetz [21] extended the Hottel-Whiller equation to model PV/T collectors and developed a linear relationship to predict the effect of cell operating temperatures on the PV/T system efficiency. In relation to this study, Jones and Underwood [25] derived an unsteady-state model expression for PV module temperature in terms of irradiance and ambient temperature.

Meir et al. [26] conducted a study to determine the performance of solar systems using a calorimetric technique and concluded that the method requires minimal monitoring equipment because hardly any parameters require recording and scrutiny. The conformity of solar gain was roughly ±10 %which is comparatively on the high side but is adequate in reference to the numerical nature of the boundary conditions for solar problems. A lesser figure was preferred for these systems.

Charron et al., [27] presented a hypothetical study on double-facades incorporating photovoltaics (PV) and powered blinds in which they investigated the effects of a variety of design parameters with regards to exploitation of solar energy. They realized an increase in wholesome thermal-electric efficiency of up to 25 % but power production was lowered by 21 % when PV modules were placed midway in the cavity. The optimum dimensions of the fins attached to the PV back plate to sustain the above results were found to be 0.015m by 0.002m and positioning the blinds in the central division of the cavity improved efficiency by 5 %. They claimed that by means of this performance optimization method, thermal-electric efficiency in excess of 60 % can be achieved. However, they concluded that, it would be virtually impossible to provide universal design procedures for Building Integrated Photovoltaic and Thermal (BIPV/T) double-facades and recommended further research probably by use of refined models to create these guidelines.

14

Hendrie [22] developed a theoretical model for flat-plate PV/T solar collectors and used it to study the thermal and electrical performance of an air and a liquid based PV/T solar collector and found that when the PV modules were operational, the air and liquid based units obtained slightly lower thermal efficiencies which were 40.4 % and 32.9 % respectively.

The extent of the existing theoretical models have adequate depth and breadth to expose the PV/T technology, predict its performance, optimize the system's configuration and propose favourable operating conditions. However, more studies need to be conducted on dynamic performance under prolonged periods e.g. yearly.

2.1.4 Modelling and simulation studies

Extensive work on modelling and simulation of PV/T systems have been instigated and carried out by several researchers based on a simple energy balance of each component of the PV/T system, in order to identify and analyse various performance parameters.

Kalogirou et al. [8] in their study of use of PV/T solar systems in industry suggested a hybrid PV/T system entailing p-Si and a-Si cell PV units fixed to copper pane and tubing heat removal components. The industrial use of these systems were suitably considered and examined in TRNSYS platform. The study encompassed industrial process heat configuration running at two distinct capacity temperatures. They observed that the electrical output of the p-Si cell was superior to that of the a-Si cell but thermally, the a-Si cell achieved better solar fraction outcome. A non-hybrid PV panel yields approximately 25 % additional electrical power but wastes a lot of thermal energy that is critical to some industrial applications.

Kalogirou [28] used TRNSYS software to model and simulate a hybrid PV/T solar system limiting his studies to Nicosia, Cyprus and found out that for the system to operate optimally the water flow rate needs to be regulated at 25*l/h*. Further, he established that the mean annual efficiency of the PV system improved marginally by 4.8 %, from 2.8 % to 7.7 % and provided coverage of hot water needs of 49 %. In the overall scale, the annual efficiency of the system was found to be 31.7 %. Because of the relatively low value of flow rate obtained in these results, he recommended the system apply thermosiphon technique for water circulation.

15

Kalogirou et al. [29] made use of the TRNSYS program to simulate a hybrid PV/T solar system for home water heating and electricity generation employing the sheet and duct technique. Their system simulation involved the use of pc-Si and a-Si panel joined together with a heat absorber plate configured typically as a flat-plate collector with an absorber created out of copper metal. Translucent protection was applied to lessen the transmission losses from the absorber to the ceiling of still air film stuck between absorber and glazing. They obtained electrical and thermal efficiencies of 6.7 % and 33 % respectively.

Bergene and Lovvik [30] conducted an energy transfer study on PV/T water system composed of flat-plate solar collector and PV cells. They developed algorithms of hybrid PV/T systems to be used in simulation. Their claim was that the model could predict the heat removed from the system and the power generated. The model predicted system efficiencies of between 60-80 % but experienced difficulties in comparing the simulation and relevant experimental results since the system parameters of their model were not explicitly stated and as a result recommended the system for residential applications.

Da Silva et al. [31] used surface response methodology and the modular strategy approach available in Matlab/Simulink platform to simulate water based $6m^2$ hybrid PV/T collector solar system made of polycrystalline Silicon cells. Their study was limited to a four persons family residence. They claimed that this methodology proved to be essential in performing transient simulation of solar systems due to its good size, integration with other computational tools, and shorter development time. Their results recorded a solar fraction of 67 % annually and interestingly 24 % efficiency in the overall scale: typically, 9 % and 15 % electrical and thermal efficiencies respectively. They recommended further improvements such as inclusion of vacuum or low pressure noble gases to replace PV cells encapsulation with a view to improving module emittance and ensuring that the air is not oxidized or degraded.

One-dimensional analytical models to predict the thermal and electrical performances of both liquid and air-based flat-plate PV/T collectors were derived by Raghuraman [32]. The analyses took into account the temperature difference between the primary absorber (PV cells) and secondary absorber (thermal flat-plate). Tiwari and Sodha Tiwari developed a thermal model for an Integrated Photovoltaic and Thermal Solar collector (IPVTS) system and compared it with the model for a conventional solar water heater by

16

Huang et al. [11].The simulations predicted a daily primary-energy saving efficiency of around 58 %, which was within good agreement range with the experimental value obtained by Huang et al at 61.3 %.

To predict the operational temperatures of a PV module and its heat-removal fluid during periods of fluctuating irradiance and discontinuous fluid flow in a transient condition, Chow [17] developed an explicit dynamic model based on the control volume finite-difference approach for a single-glazed flat-plate water heating PV/T collector that attained a maximum overall efficiency of over 70 % for a perfect collector and might decrease to less than 60 % for a low-quality collector.

Anderson et al. [33] designed a novel fixed angle roof mounted Building Integrated Photovoltaic and Thermal (BIPVT) solar collector and simulated it in TRNSYS software to assess the performance. They conducted sensitivity analysis on fluid flow rates, bond conductance and glass covering and found that improving bond conductance while optimizing flow rate improved maximum thermal efficiency by about 5 %. However, a greater challenge lies on the architectural disparities of buildings roofs making it difficult to install and achieve optimality to operate except on flat roofs.

From the literature investigated it is evident that a wide range of simulation models have been developed and used to analyse performance of hybrid PV/T collectors. TRNSYS and Matlab/Simulink leads in the list of simulation software and provides a good platform for solar system studies. However, for more accurate analysis, there is a need to provide universal and standardised climatic data sets and formats for simulation to avoid variations in results.

2.1.5 Combination of experimental and simulation studies

In order to offer detailed insights on hybrid PV/T water heating, researchers have conducted extensive simulation studies and carried out experiments to validate their simulation models, analyse errors, evaluate electrical and thermal efficiencies in different climatic conditions [8] [11] [19] [24] [34], determine heat removal effectiveness of water as a cooling medium [17], establish optimum fluid flow rates and temperature distribution across various layers [35]. In addition to the above highlights, other relevant works from the literature study have been singled out and cited as follows.

17

Jie Ji et al. [36] conducted validation analysis of a combined PV/T free flow water boiling system. Their assessment outcomes indicated that the normal everyday main energy reserved reached up to 65 %. The PV cell lamination factor was 0.63 and forward facing glazed cover transmissivity recorded as 0.83 as soon as the hot water capacity per unit heat absorbing area surpassed 80 kg/m^2. These simulation outcomes implied that the greater the PV cell lamination factor and front glass cover transmissivity, the more superior the total system performance.

Sandiness and Rekstad [9] simulated temperature distribution, thermal and electrical performance of a PV/T unit made of a polymer solar heat collector attached to single-crystal silicon PV cells, using an analytical model derived from the Hottel-Whiller model and experimentally tested the unit. Their simulation results were in agreement with the experimental data which showed that the solar energy absorbed by the panel could be significantly reduced (10 % of incident energy) by pasting solar cells onto the absorbing surface. They recommended that the combined PV/T concept should be applied in relatively low temperatures to give the desired cooling effects.

To investigate quantitative performance predictions of a hybrid PV/T system, Dubey and Tiwari [37] developed an analytical model to describe the performance of multiple PV/T flat-plate collectors as a function of design and climatic parameters. They validated this model with experimental results and attained increased efficiency in the range of 33-64 % mainly due to the increase in glazing area. The useful thermal energy yield was about 4.17 - 8.66kWh and electrical energy yield increased from0.052 - 0.123kWh depending on the number of collectors.

Agarwal and Garg [38] designed the prototypes of thermosiphonic flat-plate PV/T water heaters with PV cells pasted directly onto the absorber plate. They performed experimental runs on the prototypes in thermosiphonic and pumped circulation flow modes and determined the heat loss coefficient for the tank and the overall heat transfer coefficients of the PV/T module. Their model equations were enhanced to incorporate solar cells and reflectors for which the results were found to be in perfect agreement with the experiments.

Zondag et al. [24], developed dynamic 3D model and steady state 3D, 2D and 1D models and used them to assess the electrical and thermal yield of PV/T.

The 1D steady state model was found to be more appropriate for combined PV/T collector performance analysis since it performed 30 times as fast as the 2D which was also 25 times as fast as the 3D models. They obtained thermal and electrical efficiencies of 33 % and 6.7 % respectively as compared to 54 % and 7.2 % for individual conventional thermal collector and PV modules respectively subjected to similar operating conditions. However, 2D, and 3D models were more flexible in their applicability and suggested further scrutiny.

To sum it up, combined modelling and experimental studies reported are numerous and in good agreement with most theoretical results, providing a promising precursor to development of real world applications. Combined modelling, simulation and experimental studies provide a good and more accurate technique of analysis. Modelling and simulation technique provide results for virtual experiments while real experimental performance provide a platform for benchmarking the simulation models resulting in more accurate solutions compared to individual separate cases. However, further study opportunities lie in aspects of measuring of the long term dynamic performance of the system in varying operational conditions.

2.1.6 Convection suppression in solar thermal collectors

Numerous studies and development of modifications and special designs of solar flat-plate collectors have been reported. Consequently, a common goal of efficiency improvement by heat loss reduction has been the major drive in these studies. One of the techniques in application has been to suppress convective heat loss via the two covers.

As reported in Duffie et al. [3], the use of slats and honey comb to prevent fluid motion in the collector, thereby reducing convective losses was introduced in 1978 by Meyers et al. and Arnold et al. The use of slats only reduces convection for aspect ratios less than 0.5, above which an increase is inevitable. However, in an inappropriate design, these strategies may give rise to increase rather than reduction in convective losses. The honeycomb initially showed limited impact on heat transfer in as far as horizontal aspect ratios past unity is concerned. The application of honeycomb technique however,

19

adversely reduced the solar radiation hitting the absorber plate impacting energy conversion negatively.

The use of transparent aerogels with fine silica particles and micro-pores has also been applied to reduce convective heat transfer due to its ability to transmit a large amount of solar radiation but have very feeble thermal stability and rapid degradability when exposed to prolonged harsh weather conditions [39].

In a bid to improve radiative features of solar collectors, enclosures have also been proposed and have shown great potential. However, the positive radiative gains are overridden by increased convective losses. Moreover, this configuration presents structural and geometrical challenges when it comes to PV/T applications [40].

Air gaps have found widespread application to date in flat-plate solar thermal collectors and have been widely adopted for PV/T applications. Air particles are set in motion when subjected to elevated temperatures hence propagate convective currents of heat towards the surface as an avenue for thermal loss. The composition of air presents a challenge to the PV cells as direct contact accelerates rapid cell degradation hence shortened life. This has led to additional encapsulation of cells which in turn negatively affects the optical properties of the collectors.

The use and application of a vacuum envelope between the PV cells and the top glazing presents a valid convective loss suppression avenue thereby restricting heat transfer to radiation and conduction. The residual heat emitted from the cells is insulated from bouncing back to the top cover by the vacuum medium. One of the strengths of a vacuum with regards to heat transmission is its high resistance to heat flow. Therefore, in this study the air gap in a conventional PV/T has been replaced with a vacuum envelope to form a vacuum insulated photovoltaic and thermal (VIPV/T) collector.

2.1.7 Opportunities for advancement of PV/T water heating

A considerable amount of research and studies have been conducted on PV/T water heating systems as is evident in this review. However there are more opportunities and widespread areas of growth for this technology as summarized in this section.

Research on optimization and sizing of PV/T systems is now well advanced, but research on enhancement of geometrical and dimensional parameters of the PV/T with a view to

20

improving their thermal and electrical performance is lacking. The concept of sheet and tube is by now well established as the most effective configuration adopted for PV/T heat exchange, but there is still an opportunity to establish additional methods for improving heat transfer. An optimal design configuration of a PV/T system would be able to provide electricity as well a shot water cost-effectively compared to isolated PV and solar thermal units.

There is a need to advance dynamic simulations under real conditions to reflect the fluctuating nature of climatic parameters up on which the performance of PV/T systems is premised. Factors such as fluctuation in ambient temperatures, solar radiation, and wind speeds are crucial to the system's performance and are not easy to predict with regard to their respective long term effects. This fact has a bearing on the economic and environmental analysis which is presently restricted to simulation in laboratories, and hence the need for long-term measurements. In order to increase PV/T systems' attractiveness it is vital to formulate a universal model that can be used for all varying climatic conditions.

Further improvements, such as inclusion of vacuum or low pressure noble gases to replace PV cell encapsulations, with a view to improving module emittance and ensuring that the air is not oxidized or degraded, can be accomplished. Moreover, no literature was found regarding the design, modelling, simulation and subsequent experimental validation studies of vacuum flat-plate PV/T collectors – the subject matter of this research study.

2.2 Solar energy conversion technologies

The application of solar energy is limited to photovoltaic (PV) and thermal systems for electric and heat energy supplies respectively. The current state-of-the-art solar thermal system technologies available are typically 2-4 times more efficient and 1⁄3 to 1⁄2 times cheaper than PV systems. Solar photovoltaic and thermal systems can however be amalgamated to form one integral unit known as a hybrid photovoltaic/thermal power module for both electricity and heat energy generation. These conversion systems are illustrated in figure 4. These technologies are further explained in the following section for in-depth understanding.
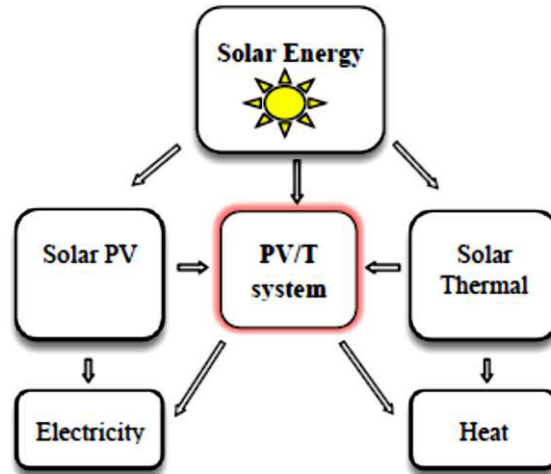
Figure 4: The solar energy conversion tree

2.2.1 Photovoltaic Systems

Photovoltaic (PV) units are solid-state appliances that directly convert the sun's radiant energy into electrical energy. PV cells are made of multiple slim sheets of semiconducting matter that generate electrical charges when struck by a beam of light due to the photovoltaic effect. This photovoltaic effect occurs when an electron is energized by the equivalent energy of the photon it engrosses. When this energy exceeds the band-gap in a semiconducting material, the electron possessing the excess energy will be detached from the atom and move freely into the conduction-band. The electron may be mobilized by an electric field created in the PV material utilizing a p-n junction to generate current which is conducted away to the connected loads [3].

On the other hand, should there be insufficient photon energy to permit electron release into the band-gap, the electron reattaches itself to the atom, thus contributing to generation of kinetic energy which cumulatively gives rise to elevated temperatures. Only a single electron can be released at a time irrespective of the amount of photon energy in relation to the band-gap energy which explains the low efficiency associated with PV cells [6].

A PV cell is made of the PV substance, a metallic framework, glazing and supports. These components optimize the cell function and enable maximum absorption of sunlight and power output. The PV substance can be monocrystalline or polycrystalline silicon or composite. The metal framework enhances the current conduction from bottom and top surfaces of the solar cell. The glazing, mostly a solitary layer, is placed on topside of the cell to ensure maximum absorption of sunlight. For some types of PV cells, the upper side

is enclosed with a see-through conductor functioning equally as a conductor and as glazing. A fully assembled PV cell has two terminals i.e. the positive and negative terminals for connecting loads.

Since relatively little electric power can be obtained from one cell, several cells are combined and encapsulated to make a module (panel). Several modules can be joined together into an array to provide the required electrical power yield and to allow for future expansion of the system in response to growing demand. PV units vary in size, ranging from *milliwatt* (*mW*) to *Megawatt* (*MW*), in addition, the units are modular, i.e., several units can be combined without difficulty to increase productivity [28].

2.2.1.1 Types of PV cell materials

The most common PV materials in use are monocrystalline silicon cells, multicrystalline silicon cells, amorphous silicon, and thermophotovoltaics as described by Kalogirou [29].

Monocrystalline silicon cells have a single unbroken crystal lattice configuration with no defect or contamination. They are highly efficient, normally in the region of 15 % but require an expensive and complicated manufacturing process. On the other hand, multicrystalline silicon cells are formed by various granules of monocrystalline silicon in a relatively simple and inexpensive manufacturing process involving casting the liquefied polycrystalline silicon to make blocks, which are then sliced into extremely slim wafers and brought together to form complete cells. However, their typical efficiencies are in the region of 12 % [7].

Amorphous silicon cells comprise silicon particles in a slim uniform sheet instead of a crystal configuration. They are more efficient at soaking up beams of light than cSi, enabling them to be thinner than c-Si and can be fixed onto a variety of stiff and elastic substrates, making them perfect for use on arched and foldable surfaces. Their typical efficiencies are in the region of 6 %, but are simple and inexpensive to manufacture. Thermophotovoltaics utilize the infra-red segment of radiant energy radiation, other than sunlight. An entire thermophotovoltaic (TPV) arrangement consists of fuel, burner, heat exchanger, long-wave photon recuperation means, PV cell, and residual heat recovery component. TPV units accept radiation, both in wide and narrow bands, emanating at a lower temperature range of 1300 *K*– 1800 *K* and a detachment of a few centimetres [7].

2.2.1.2 Applications of photovoltaics

PV systems can be used in stand-alone or grid connected modes depending on the size and location of use. The former is independent of the existing main grid network and the power generated is usually accumulated in batteries designed for use in remote locations with no access to the main grid, while the latter connects and feeds power to the main power distribution network [6].

PV modules are intended for external applications subjected to harsh open air environment, such as aquatic, tropical, frosty, and arid regions. The modular nature of the PV cells make them suitable for array configurations where several modules are linked either in series or parallel to provide appropriate current and voltage yields [29]. In recent times PV solar systems have found use in a wide range of areas, most notably, in infrastructural developments such as information exchange networks on ground and in space, secluded power generation, isolated inspection of systems in inhabitable spaces, illumination, water circulation pumps and battery charging.

The basic arrangement of a PV system is given in figure 5. In this configuration, the electric power generated from the module goes through the controller for conditioning, and then is transmitted directly to the load for immediate use or to the battery for storage for use at a later no-sunshine period.
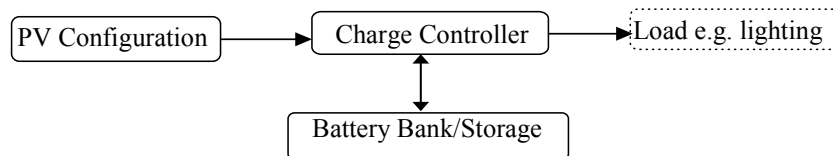
Figure 5: Principle of solar power scheme

2.2.2 Solar hot water systems

Solar hot water systems, also called solar thermal systems, are popular in domestic applications due to their simplicity and general viability. A variety of solar thermal systems are in existence but generally, they consist of solar energy harnessing, transmission and storage units. The solar collector absorbs radiant energy of the sun, converts it to thermal energy which is then transferred to a heat sensitive fluid owing from end to end of the collector. The thermal energy is either conserved as heat energy or utilized immediately.

24

Hot water systems can either be direct flow, where water temperature is increased directly as it flows into the harnessing unit or indirect where water gains heat from hot circulating fluid from the collector via a heat exchanger [29].

Depending on how the heat transfer fluid is transported, solar water heating systems can also be categorized as natural (passive) systems in which circulation occurs by convective currents due to the buoyancy effect or induced circulation (active) systems in which heating fluid is pumped to flow throughout the collector. The classifications of these systems are shown in table 1 [29].

Table 1: Solar water heating systems

Passive Systems	Active Systems
Thermosiphon (Direct and Indirect)	Direct Circulation (or open loop active) systems
Integrated Collector Storage	Indirect Circulation (closed loop active) systems, internal and external heat exchangers Air systems Heat pump systems Pool heating

In Direct Circulation Systems (DCS) as shown in figure 6, water is circulated from the reservoir to the collector unit with aid of a pump (active system) or by thermosiphonic reaction. These are demonstrated in figure 6 (a) and figure 6 (b) respectively. The heated water is directed back to the storage vessel ready for use when required. Due to the pumping action this system offers flexibility in tank installation position, either above, below, or side by side with the collector. To prevent energy loss due to reverse flow when the pump stops, there is need for installation of a spring-mounted valve flow control.

25

(a) Passive direct thermosiphon   **(b) Active (pumped) direct circulation**
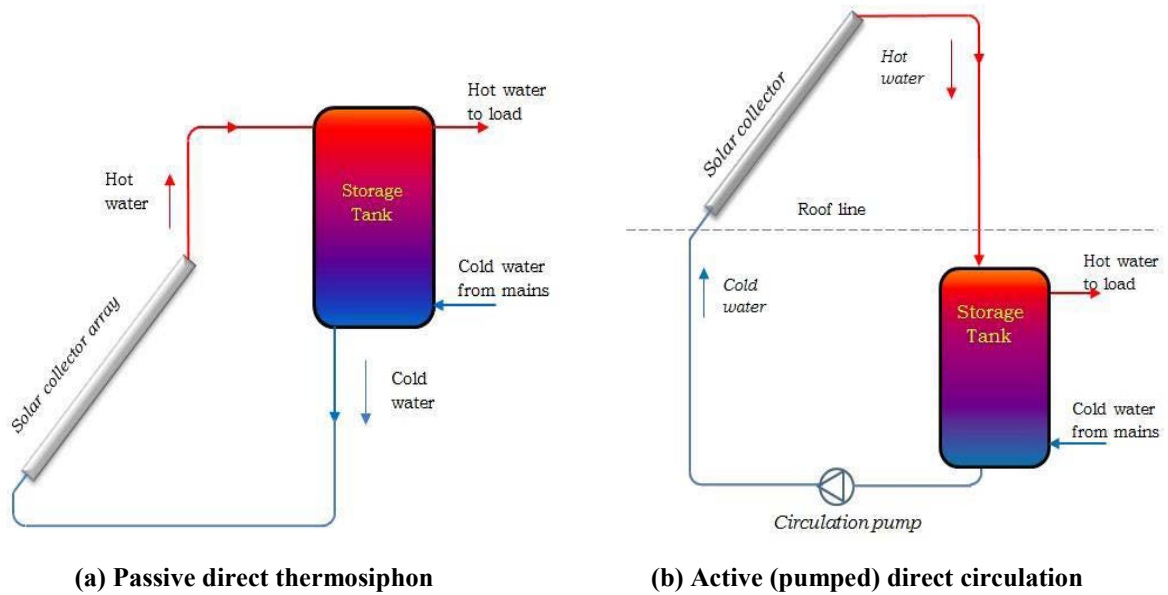
Figure 6: Typical direct solar water heating systems

DCS water systems can be supplied with water from cold-water storage tank or straight from service water pipelines; however, in situations where the mains water pressure surpasses the collector operating pressure, pressure relief valves and pressure-reducing valves should be included in the system. DCS systems are not suitable in regions with excessively hard or acidic water due to scaling of collector tubes resulting in clogging or severe corrosion. On the other hand, they are applicable in sub-zero or frosty conditions if a dump valve is installed beneath the collector to offer extra shielding against freezing under extremely cold temperatures should there be no power and the pump does not run [6].

In Indirect Circulation Systems (ICS) a heat sensitive fluid, most commonly a water ethylene glycol solution is distributed over the collector's closed-loop to the heat exchanger in which it heats the water. The position of the heat-exchanger can be within or on the surface of (mantle-tank), or outside the storage tank. Since the collection ring is closed, provision for bulging and a pressure-relief valve are essential. To protect the heat-transfer fluid against degrading or corroding, there should be sufficient control of excess heat. ICS systems can be active or passive as shown in figure 7 (a) and figure 7 (b) respectively. As a maintenance measure, the fluid must be inspected yearly and replaced after the prescribed period provided by the manufacturers making them costly to build and run. Typical ICS collector configurations with external heat exchangers are illustrated in   figure 7.

26
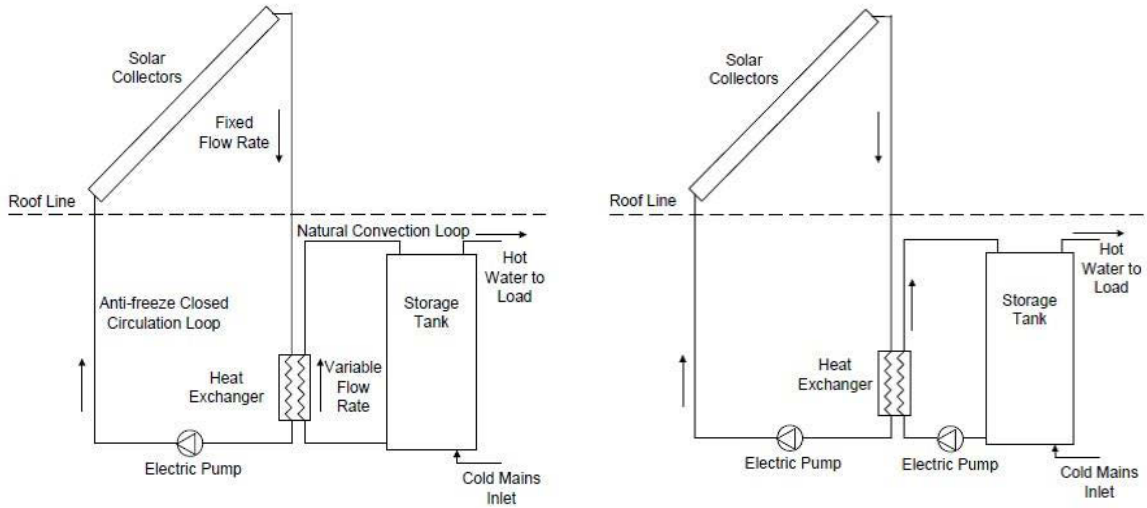
(a) Indirect natural convection system   **(b) indirect pumped system**

Figure 7: Typical indirect solar water heating systems

2.2.2.1 Solar thermal collectors

Solar thermal energy conversion depends on the collector which is a special kind of heat-exchanger with solar radiation absorbing capability and transfer of the thermal energy absorbed to the working fluid. The design of the collector depends on the temperature and general application requirements. The prime objective is to obtain the highest possible thermal output. It soaks up solar energy at elevated temperatures and transfers the heat to a fluid (typically air, water, or oil) circulating in the collector.

Solar collectors are essentially categorized into non-concentrating/stationary and concentrating. Non-concentrating collectors use one plane for capturing and absorbing sunlight, while sun-tracking concentrating collectors use curved-in shiny planes to capture and focus the sun-rays to a receiver, thus raising the temperatures. Concentrating-collectors are most appropriate for high-heat purposes. Solar collectors can as well be classified by the kind of heat-transfer fluid used and whether glazed or unglazed. A variety of collectors can be applied in solar water-heating systems, including flat-plate, evacuated-tube and compound-parabolic [29]. A comprehensive and detailed classification of various solar collectors of solar energy is illustrated in table 2 [41].

Table 2: Classification of various solar collectors

Solar Energy Technologies	Solar Thermal Collectors	Concentrating Parabolic Collectors	Parabolic Trough Collector
			Linear Fresnel Reflector (LRF)
			Parabolic Dish
			Central Receiver
		ETC Collectors	
		Solar Thermal Collectors	
	Solar Photovoltaic (PV) Technology	Silicon solar Cells	Single Crystalline Silicon
			Polycrystalline Silicon
			Amorphous Crystalline
		II-V group Solar cells	Gallium arsenide
			Indium Phosphide
		Thin Film Solar Cells	
	Solar PV/Thermal Technology	Liquid PV/T Collectors	
		Air PV/T Collectors	
		Solar Thermal Collectors	

♦ **Stationary collectors**

Stationary-collectors are permanently fixed in operating positions and do not have the capability of tracing the movement of the sun. The major collector types in this category are Flat-plate collectors (FPC), Stationary compound-parabolic collectors (CPC) and Evacuated-tube collectors (ETC).

Compound Parabolic Collectors (CPC) are capable of redirecting the entire direct radiation to the absorbing unit in broad ranges, depending on the design. As the name suggests, the concentrating unit is manufactured in a parabolic shape designed to capture maximum radiation with respect to the movement and direction of the sun. The absorbing unit can be wedge, tubular, flat, or bifacial. Because their concentration ratios are generally low, single or multi-reflectors may be used to boost the system's performance [28].

Evacuated Tube Collectors (ETC) have heat sensitive liquids changing state in the process of heat transmission at higher efficiencies. They comprise covered copper tubes located within a vacuum-packed cylinder. The cylinder is fixed onto dark copper projections filling the cylinder thus serving as the absorber-plate. Every tube has extended metallic tips at the upper side terminating at the enclosed pipe which is the condenser. Within the heat-pipe a trivial quantity of heat-sensitive fluid experiences a succession of evaporation-condensation processes under the influence of solar heat and in the process transfer heat to

the water. Another possibility is to use the ETC connected directly to a hot water storage tank with the tube metal tips hooked to a heat-exchanger [9].

Both the CPC and ETC use tubular absorber types with concentration ratios of less than 5 and indicative a temperature range of 50^oC -240^oC. However, more details of these collectors can be found in [12], [29] and [41]. Since this study focuses on flat-plate collectors it is prudent therefore to cover this type of collector in more detail for clear understanding.

In Flat-Plate Collectors (FPC), a large portion of solar radiation penetrating the translucent cover is absorbed by the absorber plate surface with superior absorptivity. The heat is then transferred to fluid circulating in tubes beneath the plate to a storage tank or for direct use. Conduction losses are minimized by insulating the underside of the absorber-plate.

The common design of a flat-plate collector typically consists of fluid tubes terminating in flat large-diameter header tubes on the extreme ends which have no serious problems of irregular flow delivery through numerous riser tubes as shown in figure 8 [38]. Alternatively, serpentine and coiled tube orientations are used in certain designs; however, they are ineffective in natural convection flow regimes, hence, limiting this approach to pumped circulation systems [8].

Solar collectors are designed to attain the highest possible thermal energy outputs. An optimised heat absorption and transfer mechanism is key to an effective and efficient thermal collector, depending on the purpose and conditions of application.
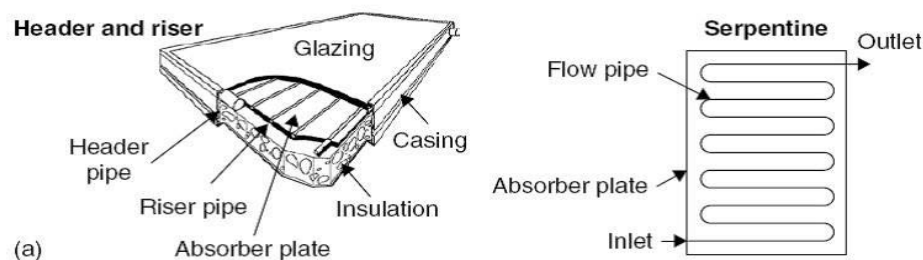
Figure 8: Typical pictorial cut-away view of a flat-plate collector

The major parts of a flat-plate collector, referred to in figure 8 are as follows:

- Top Cover: Single or multiple layers of transparent glass laid to lessen convection heat straying from the absorber-plate through the ceiling of the still-air sandwiched between the absorber-plate and glass cover.

29

- Heat removal fluid pathways: Tubing, projections, or hollow openings that conduct or guide the flow of heat-transfer fluid from the entry to exit.

- Absorber-plate: Level, wavy, or channelled plates to which the tubing, projections, or openings are fixed and which are normally covered with a black high-absorptance, low-emittance coating.

- Headers or manifolds: Pipelines and tubes to allow in and expel the fluid.

- Lagging: Used to minimize the heat loss from the back and sides of the collector.

- Frame: The covering enclosing all the other parts which shields them against dust, humidity and any additional destructive substance.

The different designs and configurations of solar flat-plate thermal collectors are shown in figure 9 [38]. The most common design is the standard single glazed type with air insulation layer between the top glass and absorber plate as shown in figure 10 (a). The unglazed collector design shown in figure 9 (b) is made of an absorber embedded with fluid-flow tubes. However, this design is prone to high heat losses and not recommended for freezing climates due to its direct exposure to the ambient environment.

The double glazed design shown in figure 9 (c) provides more thermal output but is also associated with greater optical losses due to refraction and reflections by the glass covers. Since air-layer insulation presents an avenue for convection and radiation loss, a number of interventions have been proposed to reduce these losses. Honeycomb insulation is designed to prevent or suppress convection losses through the top of flat-plate collectors and this design is shown in figure 9 (d). However, this design has an increased surface area which can increase conduction loss.

Another design that reduces the convective heat loss is the vacuum collector with pillars shown in figure 9 (e). Even though the supportive pillars guard against caving in of the cover due to low pressures, they immensely increase the surface area for conduction loss. The box channel absorber design shown in figure 9 (f) is commonly preferred in air heating systems, but is also used in water systems in isolated cases. In this design, due to the sharp corners of the box profiles, it is often characterised by high temperature and pressure build ups.

(a) Standard flat-plate collector   **(b) Unglazed collector**

(c) Double glazed flat-plate collector   **(d) Honeycomb insulated collector**

(e) Vacuum collector with pillars   **(f) Box channel collector**
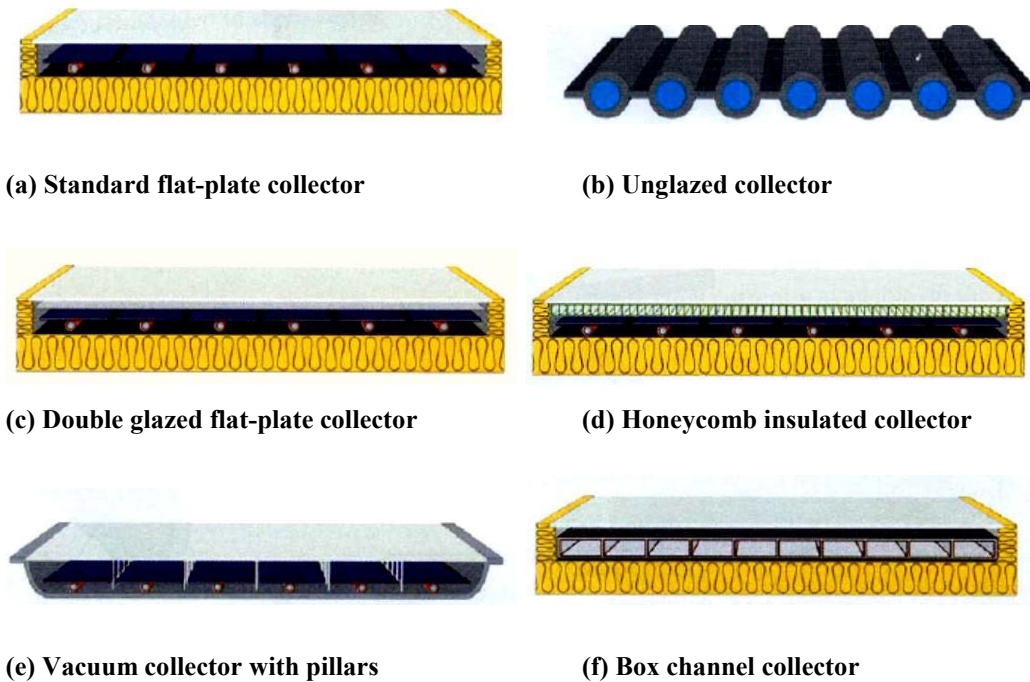
Figure 9: Typical solar thermal collector designs

Flat-plate collectors have the advantage of capturing and converting both direct and diffuse radiation, are cheap to manufacture and require fixed-position installation; hence, sun-tracking technology is not necessary. The optimal inclination angle of a collector is equivalent to the latitude of the location with a permitted variation in the range of $\pm15^0$, but this depends upon the use [28].

♦ **Single-axis tracking collectors**

For maximum collection of radiation energy, the collectors have to face the direct radiation for most of the active solar period. Therefore, for this to happen, the collectors may be equipped with the tracking mechanism so as to enable it turn in response to the change of position of the sun at different intervals of time. Single axis tracking collectors, as the name suggests, offer movement only in one axis and must be positioned to face the sun and the axis of movement must be aligned to the sun's track. Parabolic trough collectors and Fresnel collectors fall under this category.

Parabolic Trough Collectors (PTC), as the name suggests, are made using thin pieces of light-reflective materials formed into a parabola. The parabolic shapes are made in such a way that solar radiation is reflected to a common focal point on which a dark metallic tube receiver enclosed in a tubular glass to minimize heat loss is positioned. One major drawback of the glass-covered tube is that it adds a transmittance loss of around 0.9, but this loss can be reduced by applying an anti-reflective lining to increase transmissivity.
31

The focused heat on the receiver tube raises the temperatures of the fluid owing in it, consequently converting the radiant energy to valuable heat. The PTC are able to efficiently harvest heat at temperatures within the range of $50^{o}C$ - $400^{o}C$.

The receiver's exterior surface is usually coated with a preferably dark high-absorptance low-emittance lining to minimize heat-loss. Heat losses may additionally be reduced by evacuating the cavity amidst the glass-covered cylinder and heat-receiver which enhances the collector's output [39].

Fresnel Collectors are of two varieties: the Fresnel Lens Collector (FLC) constructed out of flexible material and formed to focus the sunlight to a centrally located receiver, and the Linear Fresnel Reflector (LFR) which depends upon a collection of lined mirror-stripes focusing sunlight to an aligned receiver. The stripes are alternatively fixed on ground surface and focus sunlight to an in-line static receiver located on top of a pylon. The main advantage of this type of system over parabolic glass reflectors is the use of inexpensive plane or flexibly bowed mirrors. Additionally, structural requirements are minimized since they are installed near the ground surface. More details of this type of collector's performance challenges, advancements and set ups are found in [3], [6] and [12].

♦ **Two axis tracking collectors**

Two axis tracking systems have two degrees of freedom, that is, they allow movement about two axes, say x and y directions. This presents the advantage of harnessing the solar radiation with minimal human intervention other than initial positioning. The two axis tracking mechanism enhances the efficiency of radiation collection as compared to one axis systems. Under this category, there are parabolic dish reflectors and heliostats.

Parabolic Dish Reflectors (PDR) is a tracking two-axis common-point focusing collector concentrating solar radiation towards a receiver situated at a common pivotal position on the bowl which trails the sunrays and redirect them onto a heat receiver at all times. The receiver takes up radiant energy from the sun and translates it to heat energy in a flowing fluid. The heat energy may be transformed to electric power through a generator linked to the heat-receiver or relayed within a pipeline to a centralized power generation system. PDRs attain temperatures of over $1500^{0}C$. They typically give concentration ratios between 600 - 2000; hence the PDR is superior in terms of efficiency compared to other solar collectors because it faces the sun at all times [42].

32

Heliostat Field Collectors (HFC) are composed of multiple plane mirrors, also known as heliostats, mounted on optimized platforms to redirect normal-to-surface radiant energy against a collective point for elevated levels of radiation absorption. For steam generation applications, small curved-mirror fragment heliostats may be used to produce great quantities of heat energy focused at the crater of a steam-generator giving vapour at elevated temperatures and pressures. The intensified thermal energy taken in through the receiver is conveyed to a flowing fluid for power production. A centralized receiving point has numerous merits, notably, gathering solar radiation and transmitting it to a solitary receiving element and as a result, reducing thermal energy movement needs. They have high collection and conversion efficiencies because they generally attain concentration-ratios of 300 - 1500. They are capable of expediently accumulating thermal power for delayed application. Their outputs are commonly above 10 *MW*, fairly big and therefore economical to operate [39] [42].

2.2.3 Hybrid photovoltaic/thermal (PV/T) systems

Hybrid PV/T systems consist of a combination of PV and heating units that generate thermal energy and electricity concurrently attaining a greater energy conversion capability from captured sunlight. The heating unit has provisions for circulating a heat removal fluid which may be water or air. In the process, the PV unit is cooled as the heated air or water is distributed for use at points of need [28].

Electricity production is given first priority in PV/T system applications; as a result, it is absolutely preferable to keep PV unit operating temperatures as low as possible to maintain their electrical efficiencies at satisfactory levels. PV/T systems give more power yield compared to normal PV units, hence, are economical because expenditure on thermal components is reduced.

The collector of a hybrid PV/T may be of flat-plate and concentrated PV/T types with thermosiphon of pumped circulation depending on the application, even though the latter is the most commonly used. The thermosiphonic PV/T technology is a relatively new concept in the field of PV/T and is more preferable than the ordinary thermosiphonic solar water heating systems [39].

As illustrated in figure 10, flat-plate hybrid PV/T collectors are categorized as water-based, air-based and water-air combination (dual) collectors depending on the kind of

cooling fluid used. The configuration of a Flat-plate PV/T collector comprises a clear glass cover, solar cells, encapsulation and an absorber-plate. The absorber-plate serves a very significant role in lowering the PV cell temperatures, at the same time, gathering heat energy accumulated for heating up the flowing fluid and as this action happens, PV unit efficiency is increased [43].
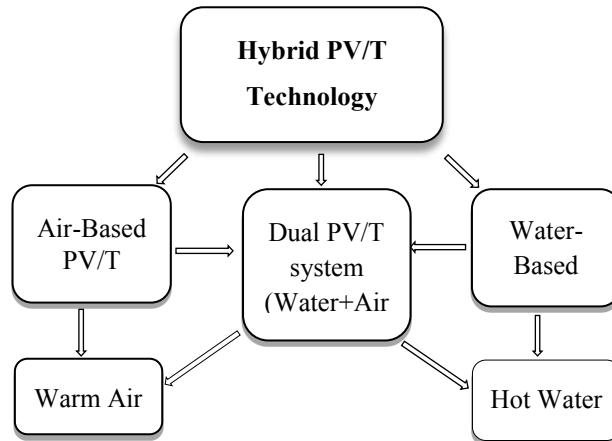
Figure 10: Classification of flat-plate collectors

2.2.3.1 Water-based PV/T systems

These systems are made from Si PV units and metal plate heat removal elements with water-flow tubes attached, to evade express contact between the flowing water and PV bottom surface. The absorber plate contacts the PV unit bottom face in a manner that permits conduction of heat and further transfer to the flowing fluid. The bottom of the absorber component and the module sides are lagged to prevent escape of heat to the surrounding atmosphere, as seen in figure 11 [31]. Water-based PV/T systems are convenient generally for household hot water needs and can serve efficiently at any time of year, mostly in low-latitude regions, because water in communal pipelines is typically below $20^{o}C$.

Numerous designs of water-based PV/T collectors exist but most common are: sheet-and-tube designs with an optional glass cover shown in figure 11 (a), box channel design where water circulates in rectangular or square tube mounted below the absorber plate with optional glazing shown in figure 11 (b). Channel designs in which water flows either below transparent PV or above PV designs are shown in figures 11 (c) and figure 11 (d) respectively.

34

Top glazing

Top glazing

(a) Sheet and tube design

(b) Box channel design

Front PV cover

Water in → *Water Channel* → Water out

(c) Channel below transparent PV design

Front glass cover

Water in → *Water Channel* → Water out

(d) Channel above PV design
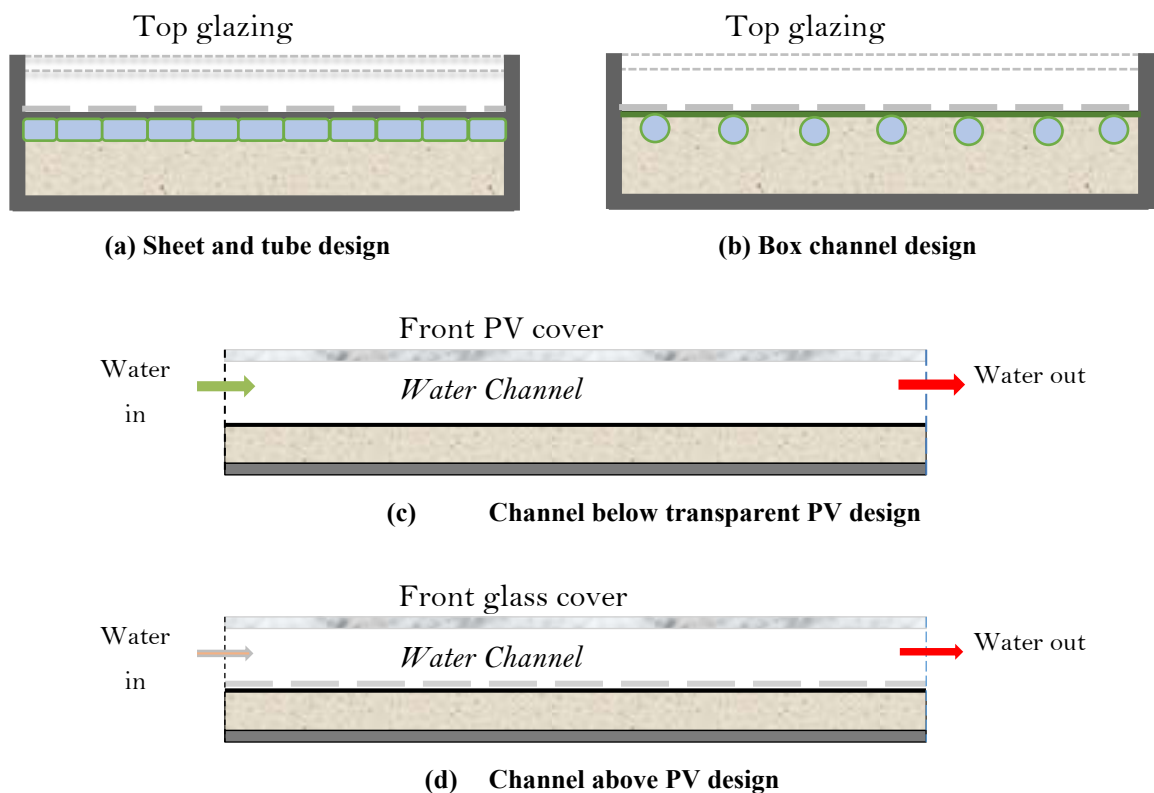
Figure 11: Cross sections of water-based PV/T designs

2.2.3.2 Air-based PV/T systems

In these systems, residual heat is removed by passing air over or beneath the PV unit. Circulation of air can be achieved either naturally by convection where hot air rises and gives way for incoming cold air and the cycle continues, or forced, where a fan or pump is used to accelerate or suck air through the system to maintain continuous flow. The continuous stream velocity within the air canal is driven by resilient heat energy thus results in a free flow mechanism. The variation in inlet and exit pressures as a result of the confined air-current effect could as well help or resist the non-stop stream of air, but may be overlooked to avoid complication. The resilience or buoyancy of energy is a multifaceted task of design and involves functional factors such as normal solar radiation, dimensions, directions, ambient temperatures etc. Elevated air temperatures within the duct produce high resilience energy, which gives rise to bigger air flow speeds throughout the collector [44].

Air-based PV/T systems are less expensive compared to water-based ones and are appropriate for built environment functions within moderate or elevated-latitude regions. For the former case, the daytime normal atmospheric air temperatures are in

excess of 20 ^oC for nearly half of the year, restricting their use to a short period of optimal power generation. These systems may be of single flow, double flow or counter flow design as shown in figure 12.

Glazing

Cold

Air in

Insulation

Warm air

out

PV Module

(a)   Single flow design

Glazing

Cold Air in

Cold Air in

Insulation

Warm air out

PV Module

Warm air out

(b)   Double flow design

Glazing

Cold Air in

PV Module

Warm air out

Insulation

(c)   Cross flow design
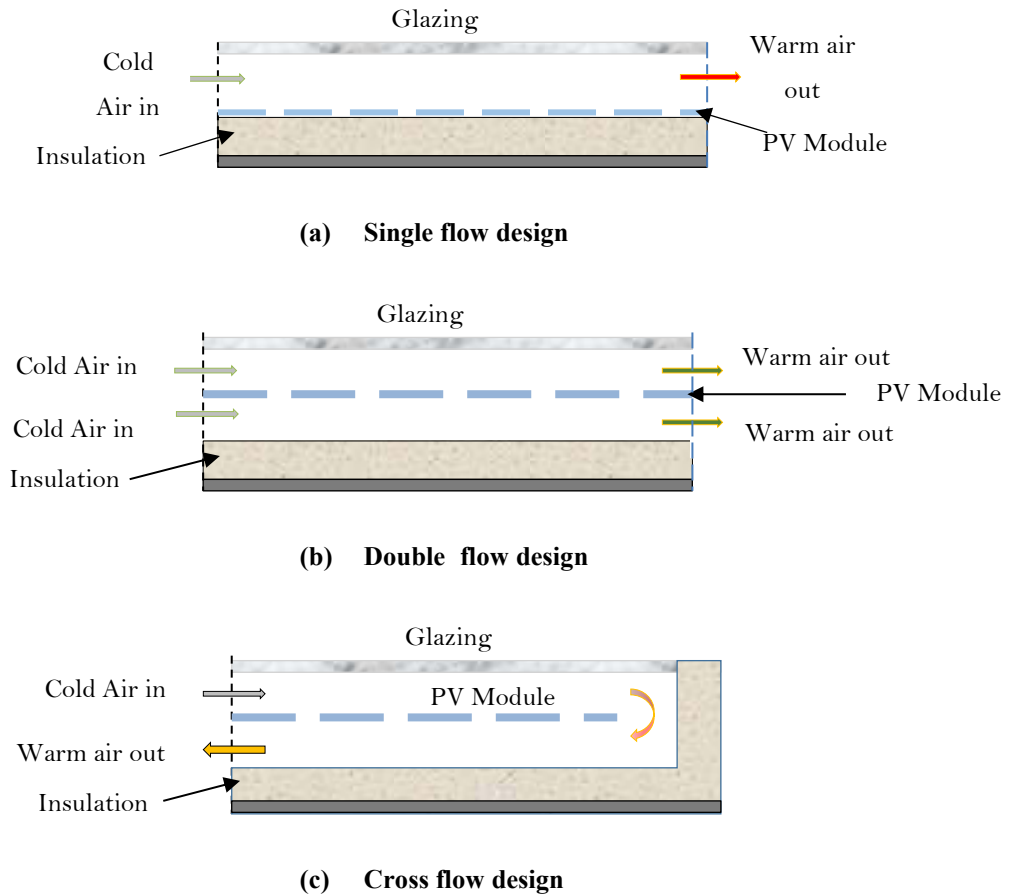
Figure 12: Cross sections of air-based PV/T designs

In both systems (air and water types) glazing is used; however, they can as well be without glazing, which is appropriate for use in extremely cold temperatures. The glazing significantly increases the heat conversion efficiency under varying working temperatures. However, the extra reflection and absorption caused by the glazing reduces the electric power yield from the PV/T system. For uncovered units, acceptable electrical power is attained in relation to the working environment but heating effectiveness is lowered for elevated working temperature, as a result of additional heat dissipation by the PV module's top face exposure to the surrounding atmosphere [45].

2.2.3.3 Dual collector PV/T systems

These systems involve a combination of water and air heating units incorporated in one system as shown in different modes in figure 13 [31]. This combined heat removal method in one system may perhaps prevail over the draw backs in individual designs and functioning of water-based and air-based systems.

The PV/T dual collector is normally flat in design and fits on house rooftops with little difficulty and is utilised in the industrial and agricultural sectors. The water-based heat removal section is suitable for the duration of elevated atmospheric temperatures, whereas the air-based section is suitable for when atmospheric temperatures go down to the extreme. A provision should be made for draining the water pipeline in cases where atmospheric temperature reduces past zero degrees or an antifreeze protection solution must be utilized. Otherwise, operating the system absolutely in air-flow mode could be beneficial, while in moderate climatic environments the two sub-systems function depending on the applicability [7] [46].
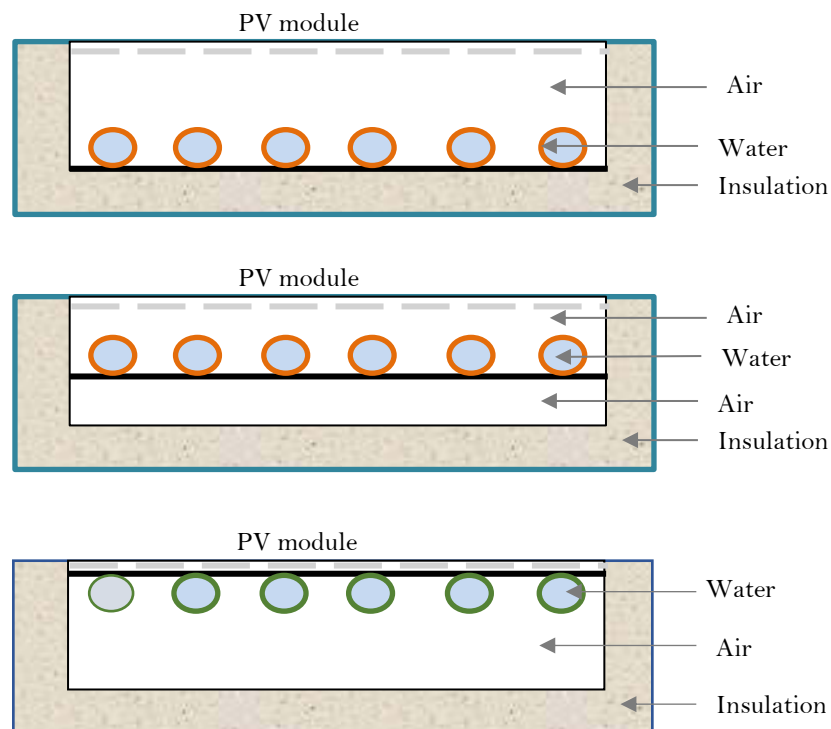
Figure 13: Alternative dual PV/T design modes

Concentrating PV/T collectors (CPV/T) collectors consist of sunlight concentrating and heating units operating on water, air, or both to remove the heat thereby cooling the PV unit. They concurrently produce electric power and heat energy, as in the case of flat-plate PV/T collectors; however, owing to attainable elevated fluid temperatures, these

37

components seek to be further realistic and economical. In CPVT systems, the PV component is significantly responsive to the degree of spread of sunrays and uniformity, whereas the thermal element is not affected as much because of the absorber's good heat conduction ability. The operational details, challenges and applicability strengths of CPV/T are given in [47] [48].

2.2.3.4 Application of photovoltaic/thermal collectors

Photovoltaic/Thermal collector technology is an emerging technology in its initial stages of implementation and has attracted immense attention. A review of literature shows extensive opportunity for application in different areas, notably, in industry and agriculture.

♦ **PV/T in industry**

Hybrid PV/T systems have enormous potential in numerous industrial processes such as sterilizing, cleaning, disinfecting, pasteurizing, aeration, steaming, refining, polymerization, etc. since most of these activities require both electric power and heat. Although a large physical foot print is required for PV/T modules to meet the power demands in industrial processes, they could be applied since electric power is, to a large extent, costly compared to heat energy. Just a minor fraction can be fulfilled particularly because the thermal and electricity demands are generally too high to be provided for only using solar energy systems.

Electricity requirements can be provided by PVs without difficulty, because they match definite voltages and rated powers. However, for heat energy, the working temperatures are of significant consideration, therefore the PV/T would be suitable only if it attains the required temperatures [6].

PV/T systems are suitable for numerous industrial processes operating under moderate temperature range($60^{o}C$- $80^{o}C$)and less than $50^{o}C$. For instance, water-based PV/T systems may well provide hot water suited for cleaning activities. Additionally, inexpensive reflectors and less costly non-concentrating reflectors may well improve the heat energy yield [12]. High efficiency may be achieved for water preheating because of low inlet temperatures for the solar device; hence, basic collectors can effectively serve when the necessary load delivery temperatures have an insignificant consequence on the solar system's output.

38

Solar plant application in industrial establishments is presently less than 1 % compared to their application in domestic households, restaurants and other commercial ventures. Much consideration should be given to the suitability of the system in deciding PV/T configurations to use for a particular purpose. Individual water or air based or dual systems operate the entire year. This justifies the applicability of PV/T systems for industrial activities compared to domestic dwellings in which the individual systems may not function throughout all spells especially air based PV/T [8].

♦ **PV/T in agriculture**

In the agricultural segment, PV/T collectors are used for providing the necessary thermal and electric power in conservatories, hatcheries, preservatories, aeration, saline water purification among other applications. The double function of PV/T collectors of absorbing solar heat and converting it to electric and heat energies justify their suitability to conform efficiently to agricultural operations. Greenhouses usually require warmth during winter and aeration in summer therefore PV/T collectors could provide these loads, whereas illumination controls in the interior is essential throughout most of the year and a combination of Fresnel lenses and linear PV/T collectors may well add value efficiently. Drying is another farming activity in which PV/T collectors have significant potential. Additionally, saline water purification and recovery to be used in irrigating land are further areas of potential PV/T collector application [49] [50].

2.2.3.5 Application of PV/T collectors in combination with other renewable energy sources

Energy generation through Renewable Energy Sources (RES) and saving initiatives in all sectors are the current measures taken by industrial and residential consumers to cut down on exorbitant energy costs. In several circumstances, a single energy source may be insufficient or uneconomical to meet the demand, hence, ought to be merged with supplementary resources. Solar thermal system combines well with geothermal power as well as biomass boilers to satisfy commercial and residential building energy requirements for heating or cooling. PV/T collectors provide novel prospects for efficient blending of solar powered heating and superficial well geothermal plants. For this situation, the fairly warm temperatures of underground water may be improved using PV/T collectors, while the electric power generated by the PVs can take care of electric load requirements [7].

Combined PV/T collector-biomass boiler systems provide a compatible and efficient pairing in terms of power outputs. The boiler meets the major heat demands while the PV/T preheats the boiler feed water to boost the steam generation rate in the boiler. Therefore, conventional fuel consumption is optimized and steam output maximized [7].

PV/T collectors when paired, mostly with low-scale wind turbines, reliably provide satisfactory energy yields. In PV/T/Wind Turbine system configurations the output from the solar element relies on the sunlight period while wind-turbine section productivity is largely determined by the prevailing wind speeds at all times (day and night). Hence, these subsystem combinations complement one another in meeting electric power demands while surplus heat energy heats water stored in tanks or is used directly for hot water needs [12].

2.2.3.6 Economic and environmental impacts of PV/T collectors

Hybrid PV/T system must rise above expenditure constraints for thermal and PV units in order to accomplish a balanced merger because price and associated expenditure concerns are highly relevant in energy-system decision making. The Cost-Payback Time (CPT) for ordinary PVs devoid of financial backing ranges from15 to 20 years. When PV/T system temperatures are kept low during operation, their CPT reduces to about 10 years while it is longer for elevated temperatures due to reduction in thermo-electric efficiency [13].

PV/T systems are generally known for large capital out lay but reduced running expenditure. A decision to use PV/T depends on the price of collectors, essential assembly components and supplementary traditional energy, which should be less compared to the expenditure for equivalent non-renewable energy resources to achieve a similar output. However, it is often difficult to weigh up a well-defined capital outlay against the indefinite expected running and maintenance expenditures of all components of the system. Other aspects such as duty, charges on loans, indemnity cover and salvage value attached to the components should be considered in relation to economic viability. Because of the discontinuous nature and randomness of solar radiation, it is normally unable to yield 100 % energy needs throughout the year. Careful consideration should be given to the fact that, under extreme running conditions, the solar energy system may be overrated thus raising costs further [51].

To evaluate the probable effects on the environment posed by manufactured goods or services offered throughout their entire existence, the Life Cycle Assessment (LCA) method is applied. LCA factors must be taken into consideration in the PV manufacturing process. In every part of the system, environmental parameters must be evaluated beginning with unprocessed material handling to discarding at the end of its existence. The major portion of the overall effects (up to 99 %) emanates from the PV unit itself, starting with the manufacture of every part, together with Balance of Systems (BOS). A detailed examination is essential for estimating the prospective gains from a controlled disposal scheme of PV/T collectors plus BOS, electric circuit, heat removal unit, and extra parts [13].

Krauter et al. [52] studied a CO_2 complete stability in a PV power unit life-cycle and established that the real PV system impact, in relation to residual CO_2 cutback, is the variation between the summation of electricity output associated with the neighbourhood distribution network and the cost of recovering, and the summation of the manufacturing needs and the transportation discharges.

Fthenakis and Kima [53] examined solar and nuclear electrical energy production technologies power generation life-cycle including CO_2 and other gases given off throughout the removal, generation and discarding of allied products. The researchers also evaluated greenhouse gas (GHG) release, specifically, Carbon dioxide, Methane, oxides of Nitrogen and CFCs as a result of resources and energy paths all through the life cycle phases of solar and nuclear electricity production machinery.

2.2.4 Performance assessment of hybrid PVT system

A PV/T collector principally combines the characteristics of a flat-plate solar (thermal) collector and those of a PV module. Therefore in assessing the performance of the PV/T, it is prudent to look at the two systems separately then, consider the overall combined effect.

2.2.4.1 Thermal performance assessment of flat-plate solar collectors

The thermal performance of the flat-plate solar collector was defined by the Hottel-Whiller-Bliss thermal efficiency equation [54]. The expression has gained widespread application in the design, modelling and simulation and performance assessment of solar systems as further documented in [3]. The arrangement in figure 14 is applied for analysis in this case.

41
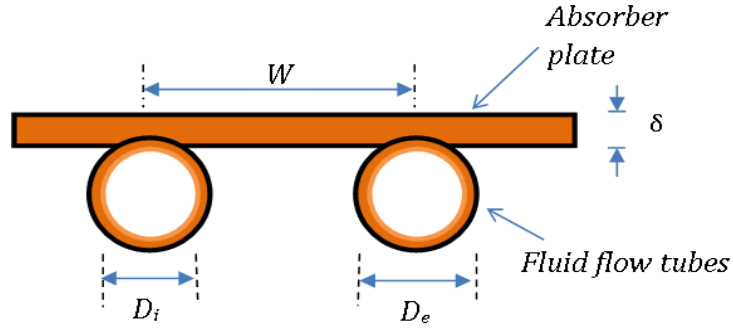
Figure 14: Cross section of the absorber plate and fluid tubes configuration

The rate of heat energy transferred to the working fluid $\dot{q}_u$ is conventionally expressed as the product of mass flow rate $\dot{m}$ specific heat capacity c_p of the cooling fluid and the temperature difference of the fluid at outlet T_{out} and inlet T_{in} as given in equation 2.1

$$\dot{q}_u = \dot{m}c_p \ (T_{out} - T_{in}) \tag{2.1}$$

Since the heat source is solar radiation, the useful energy Q_u absorbed by the collector was formulated by performing an energy balance on the collector. Hence the ensuing equation is given as:

$$Q_u = A_c[G(\tau\alpha) - U_L \ (T_{pm} - T_a)] \tag{2.2}$$

Where A_c is the collector area, $\alpha\tau$ is the transmittance-absorptance product of the absorber plate-glazing cover combination, U_L is the overall thermal loss coefficient, T_a and T_{pm} are ambient air temperatures and mean absorber plate temperatures respectively. The latter is an intricate function that depends on the collector design, solar insolation G and working fluid. Therefore, a modified Hottel-Whiller-Bliss thermal efficiency equation which excludes the heat energy converted into electrical energy Q_e comes into play as expressed in equation 2.3.

$$Q_u = F_R A_c[G(\tau\alpha) - U_L(T_i - T_a)] - Q_e \tag{2.3}$$

The substantial amount of heat converted to electrical energy is defined by:

$$Q_e = \eta_{el} G A_c \tag{2.4}$$

Where A_c is the collector area, τ is the transmittance of glazing cover, α is the absorptance of the glazing cover, U_L is the overall thermal loss coefficient; T_i and T_a are inlet water and ambient air temperatures respectively. The heat removal factor F_R is defined as:

$$F_R = \frac{GC_p}{U_L}\left[1 - \exp\left(-\frac{U_L F'}{Gc_p}\right)\right]$$ (2.5)

Where F' is the fin efficiency factor of the collector and varies with the type of working fluid flowing in the tubes of cross section shown in figure 14. For water, it is defined as:

$$F' = \frac{G/C_p}{W\left(\frac{1}{U_L[D_e+(W-D_e)F]}+\frac{1}{C_b}+\frac{1}{\pi D_i h_{fi}}\right)}$$ (2.6)

Where W is the separating distance between the central axes of the tubes, D_e and D_i are the external and internal diameters of the tubes respectively. C_b is the bond conductance between the tube and the fin expressed as a function of the thermal conductivity of the bond material k_b, bond width b_w and bond thickness γ_b as shown in equation 2.7.

$$C_b = \frac{k_b b_w}{\gamma_b}$$ (2.7)

h_{fi} is the heat transfer coefficient of the fluid inside the tubes, given as a function of the Nusselt number N_u, thermal conductivity of the surrounding air k_a and the tube internal diameter D_i by equation 2.8:

$$h_{fi} = \frac{N_u k_a}{D_i}$$ (2.8)

The fin efficiency F is given as:

$$F = \frac{\tanh\sqrt{(U_L/k\delta)(W-D_e/2)}}{\sqrt{(U_L/k\delta)(W-D_e/2)}}$$ (2.9)

Where δ and k are thickness and thermal conductivity of the absorber plate respectively.

The energy balance to the collector considers the amount of energy entering the system to be equal to that exiting, in the form of useful heat and losses. The losses are covered under the heat loss coefficient U_L which has three components; the top losses U_t, edge losses U_e and back losses U_b. Hence;

$$U_t + U_e + U_b$$ (2.10)

Where:

$$U_b = \frac{k_{back}}{l_i}$$ (2.11)

$$U_e = \frac{(UA)_{edge}}{A_p} \tag{2.12}$$

And,

$$U_t = \left[\frac{N}{\frac{c}{T_{pm}}\left(\frac{T_{pm}-T_a}{N+f}\right)^e}\right]^{-1} + \frac{\sigma(T_{pm}+T_a)(T_{pm}^2+T_a^2)}{(\varepsilon_p+0.005591Nh_w)^{-1}+\frac{2N+f-1+0.13\varepsilon_p}{\varepsilon_g}-N} \tag{2.13}$$

The terms f, e and c are constants imposed for simplicity and are expressed as:

$f = (1+0.089h_w\text{-}0.1166h_w\varepsilon_p)(1+0.07866N)$

$c = 520(1\text{-}0.000051\beta^2)$

$e = 0.430(1\text{-}100/T_{pm})$

h_w = Heat transfer coefficient of the wind $(W/m^{2o}C)$ = 2.8+3.0v

v = Wind speed (m/s)

N = Number of glass covers

β = Tilt angle of the collector (deg)

ε_g = Glass cover emittance

ε_p = Absorber plate emittance

T_a = Ambient temperature (K)

T_{pm} = Plate mean temperature (K) given by:

$$T_{pm} = T_{fi} + \frac{Q_u/A_c}{F_R U_L}(1 - F_R) \tag{2.14}$$

Transmittance-absorptance product.

Considering figure 15 [3], it can be seen that apportion of the solar radiation passing through the glass cover, an amount equivalent to $\alpha\tau$, is absorbed while a portion$(1-\alpha)\tau$ reflected back to the glass cover. However, the reflected portion is assumed to be unpolarised and is not fully lost since it is again partially reflected back to the absorber plate as $(1 - \alpha)\tau\rho_d$. The pattern continues and the intensity reduces as more and more

44

reflections occur. ρ_d denotes the reflectance of the glass cover for diffuse radiation striking it from below.
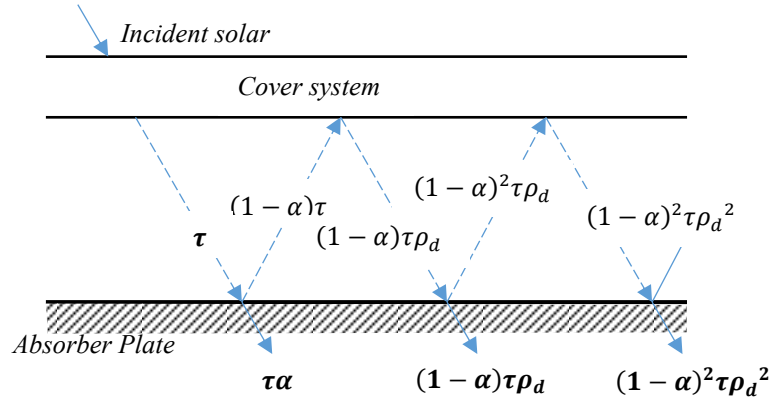
Figure 15: Solar radiation absorption by a glazed collector

From multiple reflections, the ultimate incident energy absorbed $\alpha\tau$ can be formulated for *n* number of covers as:

$$(\tau\alpha) = \tau\alpha \sum_{n=0}^{\infty}[(1-\alpha)\rho d]^n = \frac{\tau\alpha}{1-(1-\alpha)\rho d} \qquad (2.15)$$

The steady state thermal efficiency η_{th} of a flat-plate collector is expressed as the ratio of useful thermal energy, Q_u to the total solar irradiation calculated by:

$$\eta_{th} = \frac{Q_u}{A_c G} \qquad (2.16)$$

2.2.4.2 Electrical performance assessment of photovoltaic generator

The PV generator consists of a collection of solar cells connected either in parallel or series or a combination of both and connecting leads, guarding parts and supporting frame. When exposed to the photons of the sun, electrons are energized and released resulting in electron-hole pairs. When these two sides of the solar cell are linked by means of a load, flow of electric current (photon current I_p) is initiated provided it is exposed to sunlight. On the other hand, in the absence of sunlight, the solar cell is inactive and functions as a diode which when connected to a large external voltage source, produces a dark or diode current (I_d) [6].

The typical PV cell configuration can be represented diagrammatically in a circuit as shown in figure 16. As can be seen, there is a current source I_p, a diode and a series resistor

R_s equivalent to internal resistance of the cell. The shunt resistance represents the internal resistance of the diode.
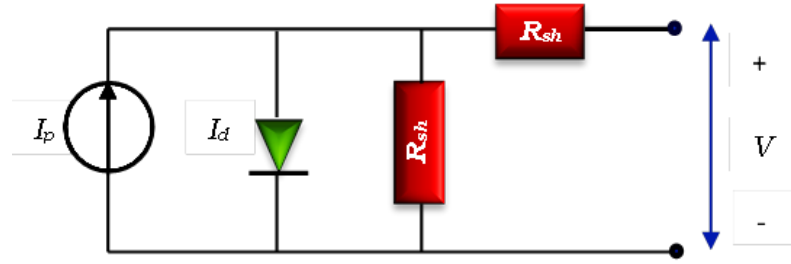
Figure 16: Solar cell circuit representation

The diode current I_d is given as:

$$I_d = I_o \left\{ exp \left(\frac{e(V-IR_s)}{\sigma T_c} \right) - 1 \right\} - \frac{V-IR_s}{R_{sh}} \tag{2.17}$$

Where I_o is the temperature dependent dark saturation current (A); e is the electronic charge (1.602 x 10^{-19} J/V); T_c is the cell absolute temperature (K); V is the voltage across the cell and σ is the Boltzmann's constant.

However, the load resistance is usually much less than the shunt resistance but much bigger than the series resistance, thus the power dissipated within the cell is negligibly small. Therefore, the series and shunt resistances can be ignored so the expression becomes:

$$I_d = I_o \left\{ exp \left(\frac{e(V-IR_s)}{\sigma T_c} \right) - 1 \right\} \tag{2.18}$$

The net current produced is the difference between I_p and I_d given as:

$$I = I_p - I_d = I_p - I_o \left\{ exp \left(\frac{e(V-IR_s)}{\sigma T_c} \right) - 1 \right\} \tag{2.19}$$

When the cell is short circuited, the short circuit current I_{sc} is maximum and the voltage across the cell is zero. While the circuit is open, the voltage V_{oc} is maximum and current is zero. The power dissipated is the product of current and voltage as follows:

$$P_{max} = I_{max} V_{max} \tag{2.20}$$

The maximum power point P_{max} as given in Equation 2.20 is ideal and is impossible to attain in practice therefore, fill factor (FF) comes into play. The FF is the ratio of the actual

areas of PV cells to the aperture area of the module. The new expression for P_{max} is given by:

$$P_{max} = I_{sc}V_{oc}FF \tag{2.21}$$

From which,

$$FF = \frac{P_{max}}{I_{sc}V_{oc}} = \frac{I_{max}V_{max}}{I_{sc}V_{oc}} \tag{2.22}$$

The correlation between short circuit current I_{sc} and I_o is obtained from equation 2.19 and can be formulated as:

$$\frac{I_{sc}}{I_0} = exp\left(\frac{eV_{oc}}{\sigma T_c}\right) - 1 \tag{2.23}$$

From which V_{oc} can be obtained as:

$$V_{oc} = \frac{\sigma T_c}{e} ln\left(\frac{I_{sc}}{I_0} + 1\right) = V_t ln\left(\frac{I_{sc}}{I_0} + 1\right) \tag{2.24}$$

Where V_t is the thermal voltage (V) expressed as:

$$V_t = \frac{\sigma T_c}{e} \tag{2.25}$$

The power output depends on the load resistance, R and can be expressed as:

$$P = I^2 R \tag{2.26}$$

Hence, equation 2.19 can be substituted in Equation 2.26 to give:

$$P = \left[I_{sc} - I_o\left\{exp\left(\frac{eV}{\sigma T_c}\right) - 1\right\}\right]V \tag{2.27}$$

Equation 2.27 can be differentiated with respect to V and equated to zero to obtain the external voltage, V_{max} that enables maximum output power from the cell. The resultant equation is given as:

$$exp\left(\frac{eV}{\sigma T_c}\right)\left(1 + \frac{eV_{max}}{\sigma T_c}\right) = 1 + \frac{I_{sc}}{I_0} \tag{2.28}$$

The load current that gives maximum power output can be found by substituting equations2.28 into equation 2.19 to obtain:

$$I_{max} = I_{sc} - I_o\left\{\frac{1 + \frac{I_{sc}}{I_0}}{1 + \frac{eV_{max}}{\sigma T_c}} - 1\right\} \tag{2.29}$$

47

This can be simplified to give:

$$I_{max} = \frac{eV_{max}}{kT_c + eV_{max}}(I_{sc} - I_0)$$ (2.30)

And P_{max} according to equation 2.20 becomes:

$$P_{max} = \frac{eV_{max}^2}{kT_c + eV_{max}}(I_{sc} - I_0)$$ (2.31)

Electrical efficiency of the PV panel is defined as the ratio of maximum electrical power output to the incident light power and is inversely proportional to the temperature i.e. it is reduced when the temperature increases [3]. This can be expressed as:

$$\eta_{max} = \frac{P_{max}}{P_{in}} = \frac{I_{max}V_{max}}{AG}$$ (2.32)

Where A = area of the cell (m^2).

To demonstrate this effect of temperature on the PV efficiency, Duffie [3] and Zondag [16] presented an expression written as:

$$\eta_{max} = \eta_{max,ref}\left[1 + \mu(T - T_{ref})\right]$$ (2.33)

Where $\eta_{max, ref}$ is the maximum power point efficiency of the PV collector at the reference temperature (T_{ref}), μ is the temperature coefficient of PV efficiency at reference conditions (normally a negative quantity), and T is the temperature of PV module. Equation 2.33 implies that, every PV module generates both electrical and thermal energy when struck by solar radiation. The maximum efficiency in this case is the electrical efficiency of the PV which is also designated as η_{el}. Substituting equation 2.32 into equation 2.33 we obtain:

$$\eta_{el} = \eta_{max} = \frac{I_{max}V_{max}}{AG} + \mu(T - T_{ref})$$ (2.34)

Therefore a reduction in temperature results in an increase in electrical efficiency of the PV module, as well as taking advantage of the resulting thermal energy to heat water for domestic or industrial applications. This constitutes the concept of a hybrid PV/T system.

2.2.4.3 Overall performance assessment parameters

The technical performance of the PV/T systems is usually assessed using several analytical parameters such as overall energy efficiency, overall exergy efficiency, primary-energy-saving efficiency, and solar fraction. The economic performance of the PV/T systems is

48

measured with Life Cycle Cost (LCC) and Cost Payback Time (CPT), and the environmental benefit of the system is justified using the Energy Payback Time (EPBT) and Greenhouse Payback Time (GPBT). These parameters are briefly described below:

♦ **Overall Energy Efficiency**

The ratio of collected electrical and thermal energy to incident solar radiation striking on the PV/T absorber gives the overall energy efficiency. The overall efficiency of a PV/T system can thus be calculated as the sum total of the electrical and thermal efficiencies expressed as:

$$\eta_o = \eta_{th} + \eta_{el} \tag{2.35}$$

In comparison, electrical efficiency of a PV/T module is inferior to its thermal efficiency. This fact implies that when the thermal energy conversion efficiency is increased the overall energy efficiency of the system is also improved. It is worth noting that the overall energy efficiency disregards or does not take into account the difference between heat and electrical energy qualities; hence, it is insufficient to completely warrant a good performance by PV/T systems and must be complemented by other parameters.

♦ **Overall Exergy Efficiency**

In contrast to the overall energy efficiency, the overall exergy efficiency encompasses thermal and electric energy quality difference by converting low quality heat energy into comparable high quality electrical energy using the theory of Carnot cycle. The overall exergy ex_o of the PV/T could be written as follows:

$$ex_o = ex_{th} + ex_{el} = (\xi_{th} + \xi_{el})G = \xi_o G \tag{2.36}$$

Where, ex_{th} and ex_{el} are the thermal and electrical exergy respectively; ξ_{th} and ξ_{el} are the thermal and electrical exergy efficiency; ξ_o is the overall exergy efficiency. The thermal exergy ex_{th} is expressed as:

$$ex_{th} = \eta_c Q_u = \eta_c \eta_{th} G = \xi_{th} G \tag{2.37}$$

Where η_c is the ideal Carnot efficiency [55] given by:

$$\eta_c = \left(1 - \frac{293K}{293K + (t_f - t_a)}\right) \tag{2.38}$$

49

And T_f is thermal temperature of the working medium while, T_a is the ambient temperature.

The electrical exergy is expressed as:

$$ex_{el} = \eta_{el}G = \xi_{el}G \qquad (2.39)$$

The sum total of the thermal and exergy efficiencies gives the overall exergy efficiency expressed as:

$$\xi_o = \eta_c\eta_{th} + \eta_{el} \qquad (2.40)$$

♦ **Solar fraction**

This is defined as the fractional ratio of primary energy savings that a PV/T system can obtain to overall energy demand [28] and is expressed as:

$$f = \frac{1}{2}\left(\frac{Q_{L,t}-Q_{Aux,t}}{Q_{L,t}} + \frac{Q_{L,el}-Q_{Aux,el}}{Q_{L,el}}\right) \qquad (2.41)$$

Where: $Q_{L,t}$ and $Q_{Aux,t}$ are the overall thermal load and auxiliary heat required respectively; $Q_{L,el}$ and $Q_{aux,el}$ are the total electrical load and auxiliary electricity needed respectively.

♦ **Primary-energy saving efficiency**

The principle of primary energy saving efficiency was introduced by Huang et al. [11], as a parameter that takes into account energy quality difference between heat and electricity. This is expressed as:

$$E_f = \frac{\eta_{el}}{\eta_{th}+\eta_{pgen}} \qquad (2.42)$$

Where: η_{pgen} is the electrical power generation efficiency for a conventional power plant usually considered to be 0.38. However, this value should be above 0.50, so as to be comparable to an individual conventional solar hot water system.

2.2.4.4 Economic and environmental indicators of PV/T systems

The economic indicators for evaluation of PV/T are the Life Cycle Costs and Energy Payback Time while the Greenhouse-gas Payback Time offers an indication in the environmental point of view. The details of these indicators are given below.

50

♦ **Life Cycle Costs**

Tripanagnostopoulos et al. [12] suggested Life Cycle Costing (LCC) as an economic and environmental assessment technique for PV/T systems. It accounts for the capital, installation, operation and maintenance costs for the entire life of the system. Other factors such as inflation, tax, degradation/wear and tear, discount rates etc. are also considered in the analysis [56].

♦ **Cost Payback Time (CPBT)**

The Time Cost Payback (CPBT) method is commonly applied in assessing economic worth of PV/T systems, however, it disregards the maintenance costs and time related quantities, thus weakens the accuracy of results.

♦ **Energy Payback Time (EPBT)**

Chow [56] defined EPBT as the ratio of the quantity of energy necessary to produce the PV/T in its production phase to its annual energy output, expressed as:

$$EPBT = \frac{\sum PVT + \sum BOS + \sum Mtl}{Q_{el} + Q_{th} + Q_{HVAC}}$$ (2.43)

Where $\Sigma PV T$, ΣBOS and ΣMtl are the energy required for the PV/T system production, the balance of system and the building materials respectively; Q_{el} is the annual useful electricity output; Q_{th} is the annual useful heat gain (equivalent), and Q_{HVAC} is the annual electricity saving of HVAC system due to reduction in thermal load.

♦ **Greenhouse-gas Pay Back Time (GPBT)**

GPBT as the ratio of the embodied Greenhouse-gas (GHG) or CO_2 equivalent of the PV/T in its production phase to equivalent annual reduction of GHG emission from the local power plant due to the PV/T operation energy output [56] given as:

$$GPBT = \frac{\Omega_{PVT} + \Omega_{BOS} - \Omega_{Mtl}}{Z_{el} + Z_{th} + Z_{HVAC}}$$ (2.44)

Where $\Omega PV T$, ΩBOS and ΩMtl represent the embodied GHG (or CO_2 equivalent) for PV/T, BOS and Materials respectively and Z_{el}, Z_{th} and Z_{HVAC} are the reduction of GHG emission from the local power plant due to the PV/T operation energy output with respect to electric, thermal and HVAC energy savings.

2.3 The physics of heat transport through the layers of PV/T solar collectors

To understand the heat transfer principles applicable to solar thermal collectors, it is important to consider the basic modes of heat transfer. Typically, thermal transport in matter takes the form of conduction, convection and radiation and their interactions for combined effects which is considered additive for simple evaluation [57].

2.3.1 Conduction

This involves transfer of energy between molecules; it involves movement of molecules and collision with each other within a material to transfer heat from one point to another. Conductive heat transfer can take place in gases, fluids and solids. The parts of solar PV/T where conduction takes place are the top, edges, PV cell-plate-tubes and bottom. The rate of heat flow per unit area (heat flux) $\dot{q}$through a conductive medium is given by Fourier's law expressed as:

$$\dot{q} = k\frac{\Delta T}{L} \tag{2.45}$$

Where: k is the thermal conductivity, ΔT is the change in temperature and L is the thickness of the conducting medium.

The heat conduction rate q through a medium of area A is given as the product of heat flux and area expressed as:

$$q = \dot{q}A \tag{2.46}$$

2.3.2 Convection

This is heat transfer mode by bulk movement of gaseous or liquid molecules. Usually occur when bulk air moves from an initial location in space to another point thus transferring thermal energy. In natural convective heat transfer which is usually the case in flat-plate solar collectors, a combination of three unit-less parameters are paramount. These are the Nusselt (Nu), Rayleigh (Ra) and Prandtl (Pr) numbers.

They are often evaluated at mean temperatures and are given as:

$$Nu = \frac{hL}{k} \tag{2.47}$$

$$Ra = \frac{\beta' \Delta T L^3}{v\alpha} \tag{2.48}$$

$$Pr = \frac{v}{\alpha} \tag{2.49}$$

Where: h is the heat transfer coefficient (W/m^2K), α is the thermal diffusivity (m^2/s), k is the thermal conductivity (W/mK), g is acceleration due to gravity (m^2/s), β' is the volumetric coefficient of expansion (for ideal gas $\beta = 1/T$) ($1/K$), ΔT is the change in temperature between plates and v is the kinematic viscosity (m^2/s).

Ra and *Nu* for angle of tilt of $0 < \theta.75$ as depicted in [3], are related by the expression:

$$Nu_{air} = 1 + 1.44\left[1 - \frac{1708(sin1.8\beta)^{1.6}}{Ra\ cos\beta}\right]x\left[1 - \frac{1708}{Ra\ cos\beta}\right]^+ + \left[\frac{Ra\ cos\beta^{0.333}}{1708} - 1\right]^+ \tag{2.50}$$

The (+) sign exponent implies that only the positive values of the terms enclosed in the brackets are applicable.

Convective heat transfer takes place in PV/T from the PV cell surface to air insulation layer, tube internal diameter to water, and glass cover surface to ambient air. The rate of convective heat flow q_{conv} is expressed by Newton's law of cooling given by:

$$q_{conv} = h(T_s - T_f) \tag{2.51}$$

Where T_s and T_f are surface and fluid temperatures respectively and convective heat transfer coefficient h is given by:

$$h = \frac{Nuk_f}{L} \tag{2.52}$$

2.3.3 Radiation

In this mode, heat energy is transferred by electromagnetic radiation as a result of temperature difference between two distinct bodies. Radiative heat exchange between two body surfaces depends on the surface temperature, properties and material positions but independent of air temperature.

The radiative heat transfer between a pair of two subjective surfaces of temperature T_1 and T_2 and area A is conventionally expressed as:

$$Q = Ah_r(T_2 - T_1) \tag{2.53}$$

Where h_r is the radiative heat transfer coefficient given by:

53

$$h_r = \frac{(T_2{}^2 - T_1{}^2)(T_2 - T_1)}{\frac{(1-\varepsilon_1)}{\varepsilon_1} + \frac{(1-\varepsilon_1)A_1}{\varepsilon_1 A_2}} \qquad (2.54)$$

In most cases A_1 and A_2 are often equal as in the cases of solar collectors hence the expression can be simplified further.

2.4 The concept and theory of vacuum insulation

In most common PV/T system configurations, air space has often been applied as an insulator between the glazing and the PV cells. In stagnant air, heat transfer is by radiation through gas, however, when the air is set in motion, convective mode of heat transfer sets in, replacing conduction; the effect of which result in higher thermal conductivity and subsequent high rate of heat loss. Air as an insulator has a thermal conductivity of 0.026 *W/mk* [58].

Materials with lower thermal conductivities than stagnant air can be developed by use of alternative gas such as noble gasses, inclusion of radiation scattering materials and evacuation of the air space. With these measures at hand, one or more of the heat transport mechanisms is suppressed i.e. conduction, radiation or convection.

A vacuum is a space from which air and gas has been removed. Even though this is a very difficult venture, the level of removal of air or gas depends on the application. Vacuum can be used to enhance thermal properties of most porous materials at different levels; most commonly applied in conjunction with core materials with small particles that allow for small points of contacts, limiting conductive heat transfer. Other conventional insulation material such as wool or glass fibre can be used as a core material for vacuum insulation. This is the concept widely used in energy management in built environment [40].

2.4.1 Heat transfer through a vacuum

The concept of vacuum insulation is comparable to double glazing of two sided glazing in which air filled space/envelope is evacuated to a low pressure, hence lowering the conduction and convection levels to negligible values, the residual heat transfer is mainly due to radiation which can be lowered by use of low emittance coatings. This concept can be applied to flat-plate solar collectors in order to improve thermal performance. The transparent evacuated insulation makes use of a vacuum envelope to reduce convection

and gas conduction. The insulation is such that, the space between the PV cells surfaces and the glazing is sealed and the space is evacuated of all gas to create a vacuum.

Heat transfer through a vacuum takes place only by radiation, however, infra-red waves (electromagnetic) waves do not require material medium to pass through. Heat energy is transmitted even through the vacuum in the form of infra-red waves; this is how we receive solar energy.

The two intermediate surfaces in question are two parallel plates separated by varying distances and in some cases supporting pillars. The radiative heat transfer between two parallel plates is independent on the separating distance; therefore, the spacing between the sheets can be varied to provide simple, compact and highly insulating system. To ensure negligible convection and conduction levels, it is important that a vacuum pressure of <0.1 *Pa* is attained and maintained between the two layers. The research in this area is still minimal with very few publications.

2.4.2 The edge seal

To maintain the vacuum at below $0.1Pa$, the envelope must have a substantial contiguous edge seal for the expected lifetime. However, the seal forms a conductive heat transfer path and affects the temperature of the glazing surface for a distance of approximately 75 *mm* from the edge seal itself. The effect of the edge seal on the vacuum glazed cavity is strongly hinged on the glazing and PV module areas. For the case of VIPV/T under study, the seal material used was a substantive heat resistant EPDM rubber.

2.4.3 Long wave radiative heat transfer

Owing to the narrow or close distance between the two parallel surfaces, the long wave radiative heat transfer in the glazing is possible to approximate. The values of emittance are seen to be decreasing in magnitude of untreated glass. Moreover, if the overall conductance of the glazing is to be less than 1, then, the input of edge seal heat transfer must be less than 0.74.

2.4.4 Thermal performance of the vacuum insulation

The most promising method of designing a vacuum glazing is based on the optimization of the minimal number of supports which may abate heat loss through conduction and a mechanism of bearing stress under intense atmospheric pressure on the glazing.

The overall heat transfer through the vacuum insulated collector has the following components:

- Heat flow from the ambient air to the glass cover exterior surface.
- Radiative heat flow within the vacuum envelope between the glass surface and the PV cells.
- Conduction through the PV cell, adhesive, thermal absorber, absorber-tube bond, fluid tubes and back insulation material.
- Convective heat flow from tube inner walls to the fluid.

The thermal resistance R_g associated with heat flow per m^2 due to conduction through the glass pane is formulated as:

$$R_g = \frac{l_g}{k_g} \qquad (2.55)$$

Where: l_g and K_g are thickness and thermal conductivity of the glass.

The thermal resistance R_v associated with the heat transfer per m^2 due to radiative heat transfer through the vacuum cavity is given by:

$$R_v = \left(\frac{1}{\varepsilon_c} - 1\right)\left(4\sigma T_c^{\,3}\right)^{-1} \qquad (2.56)$$

Where: ε_v is the hemispheric emittance of the collector, σ is the Stephan Boltzmann's constant and T_c is the collector mean surface temperature. It should however be noted that, since, the collector plate and PV cells are considered to be of same thickness and area; their conductive effects are lumped together for the simplicity of analysis.

The thermal resistance R_c associated with the heat flow per m^2 due to conductive heat transfer through the collector (absorber-plate + PV module) is given by:

$$R_c = \left(\frac{2l_c}{(k_p + k_{PV})A}\right) \qquad (2.57)$$

Where: l_c is the thickness of the collector, k_p and k_{PV} are thermal conductivities of the absorber-plate and PV cells respectively and A is the area of the collector.

The overall heat resistance is the sum total of the three components;

$$R_c + R_v + R_g \qquad (2.58)$$

Therefore, the thermal resistance associated with the heat flow per m^2 R_a and R_f at the ambient and in fluid respectively are the inverse of the surface heat transfer coefficients i.e. $R_a = 1/h_a$ and $R_f = 1/h_f$ Hence, the total heat transfer of the collector becomes:

$$h_{total} = \left(\frac{1}{R_f + R_o + R_a} \right) \qquad (2.59)$$

The total heat flow through the entire assembly is the sum of heat flow across the centre of the vacuum and heat flow through the edges including conductive heat transfer though the edge seal.

2.5 Chapter Summary

In summary, a hybrid PV/T is a novel piece of technology that maximises the conversion of solar incident radiation into electrical and thermal energies. PV/T technology combines PVs and solar thermal components into a unitary module to enhance the solar conversion efficiency and make economic use of the space.

Mechanisms of absorbing and transferring the residual heat dissipated as a result of exposure of solar cells to solar radiation have been designed in different configurations and dimensions optimized by different researchers. Studies in this area span across theoretical, modelling and simulation, experimental and combination of experimental and simulation studies which have been adequately reviewed.

Different types and configurations of PV/T technologies have been highlighted in order to give broad understanding. The theory of performance analysis has also been presented with relevant solar collector equations emphasised. To this end, none of the literature reviewed covered vacuum insulation applications in PV/T, therefore, it is comparatively clear that a model needed to be developed and verified experimentally to study the performance of a vacuum insulated PV/T (VIPV/T) which forms the basis of the next chapter.

CHAPTER 3

MODELLING AND SIMULATION

3.1 Introduction

Modelling involves simplification of a component and/or system by graphical or numerical representation to give close approximation to the actual system to enable analysis and prediction of their behaviours under different operating conditions. In graphical modelling, components are represented with pictorial objects interlinked to depict process flows from one stage to another. This enables interfacing of different compatible components of a system and studying the combined effects. On the other hand, in numerical modelling, objects are represented with the use of formula and mathematical functions. Simulation of a system involves the operation of the model to study the performance and infer the properties as a result of predefined input variables.

This study involved simulation of a graphical model of a modified hybrid Photovoltaic/Thermal (PV/T) by replacing the conventional air gap between the glazing and the PV cells embedded on absorber plate to make a Vacuum Insulated Photovoltaic/Thermal (VIPV/T) module. The system model was developed using predefined individual component models with pre-formulated numerical characterisation in TRNSYS software.

In this chapter, a brief overview of the Transient Systems Simulation (TRNSYS) Software is given, the model components identified from the inbuilt TESS library, described, numerically represented and graphically assembled in the TRNSYS simulation studio environment. Various parameters, input variables and expected outputs were inserted and studied in order to infer the systems behaviour under varying conditions. The simulation process is outlined in detail. The results of thermal and electrical energy outputs and conversion efficiencies were computed and compared for VIPV/T and PV/T from which the differences were identified to constitute the effects of the vacuum insulation.

3.2 Modelling and simulation software

Modelling and simulation studies are essential in cases where: (i) It is impossible or extremely expensive to observe certain processes in the real world, (ii) Mathematical

models can be formulated but analytical solutions are impossible (iii) It is impossible or extremely difficult or expensive to validate the mathematical model describing the system e.g. due to insufficient data. For these reasons, several system computer simulation software programs have been developed to simplify the process. One such program is Transient Systems Simulation (TRNSYS) which was selected for this study. However, in order to produce high quality graphical outputs, numeric results obtained were integrated into the Engineering Equations Solver (EES) software via the lookup table options for plotting. Brief descriptions of the software are presented in the following section.

3.2.1 Transient Systems Simulation (TRNSYS) Software

TRNSYS is a complete integrated successive transient simulation environment created in the University of Wisconsin, now widely utilized by technologists and scientists globally to corroborate innovative energy models, beginning with modest home water heating to conceptualization and modelling of commercial buildings and their appliances, together with controlling mechanisms, occupants' activities, and Renewable Energy Substitutes (RESs). It offers a comprehensive design platform containing hourly virtual realities of solar energy systems for the whole year. It can be applied in many other thermodynamic functions that require dynamic simulation by allowing for a system's model to be generated by connecting separate parts of models and solving the ensuing sets of simultaneous arithmetic expressions [59].

The software package holds FORTRAN subroutines for almost every component required for constructing solar energy systems including part simulations; either realistic or logical, and description of the component behaviour with arithmetic expressions. Additionally, TRNSYS combines with several supplementary application software, such as Ms Excel, MATLAB and COMIS without difficulty, in the synthesis and collaborative interactions throughout the simulation [60].

A TRNSYS assignment is normally constituted by joining parts of modules explicitly in the Simulation Studio environment. Every single module is designated an arithmetic expression in a simulation engine with sets of corresponding proformas in Simulation Studio window. These proformas have black-box explanations of components' inputs, variables, outputs and feedbacks. The Simulation Studio generates a deck file, which is a manuscript input to the simulation engine [60].

59

3.2.2 Engineering Equation Solver (EES)

Engineering Equation Solver (EES) offers the basic function of solving sets of numerical expressions, differential equations, complex variables equations, and optimization problems, regression analysis and plot graphs of superior quality. It routinely recognizes and categorizes expressions that need concurrent evaluation [61]. This feature makes the procedure simpler for the operator and guarantees that solver's nest efficiency. It offers several other in-built numerical and physical property functions suitable for scientific and engineering computations.

EES has an all-encompassing collection of calculated and physical characteristic functions and permits the operator to feed in own-formulated functional interactions in tabular form, user-written function modules, and dynamically-link peripheral functions and techniques compiled using high-level languages e.g. Pascal, C+, C++ and FORTRAN to EES [61]. This feature makes the EES to be very powerful software that can be applied in solving solar thermal and electrical problems both at design and in operation stages. It is predominantly valuable in design tasks where the impact of single or multiple factors require determination and also offers the ability to disseminate the ambiguity of experimental statistics in order to make available uncertainty estimations in calculated parameters. This function was useful to this study especially when determining the effects of the vacuum on the thermal and electrical efficiencies of the PV/T module and the overall performance assessment of the unit.

3.3 The TRNSYS model of the PV/T system

The hybrid PV/T system was represented by a TRNSYS model comprising a combination of several components interlinked by lines and arrows depicting the process and information flows. Each component was associated with a specific task and a combined effect of the components accomplished the intended larger task of the whole system. For each connection, there were accurately defined inputs, inbuilt parameters activated to influence the behaviour of a component in a desired manner and the expected outputs.

A TRNSYS assignment was constituted by joining part modules explicitly in the simulation studio environment. Every single module was designated an arithmetic expression in the simulation engine having sets of corresponding proformas in Simulation Studio window. These proformas had black-box explanations of components' inputs,

60

variables, outputs and feedbacks. The simulation studio generated a deck file, which was used as a manuscript input to the simulation engine. The simplified schematic representation of the model is shown in figure 17.
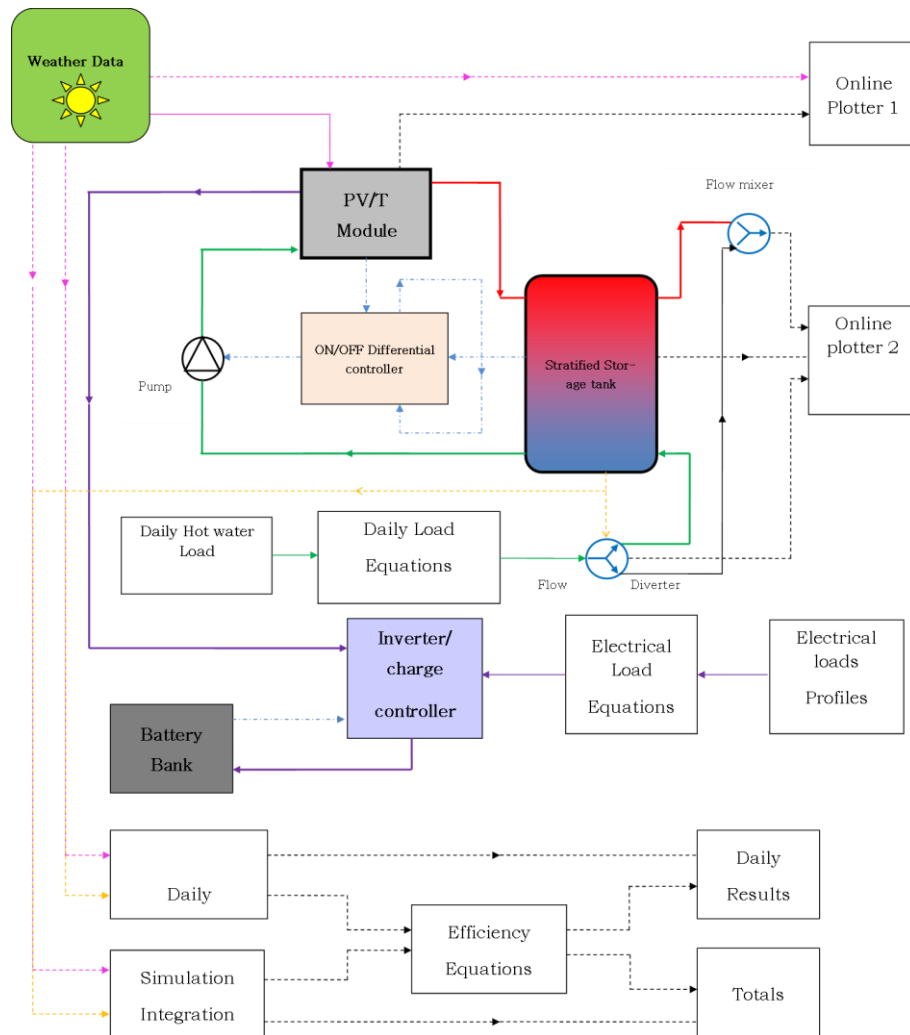
Figure 17: Schematic diagram of the TRNSYS model

In practice, there are always DC and AC isolators installed in the system to allow for maintenance and any adjustments that may be required from time to time. However, for the purpose of simplicity of the simulation model, these components were not included and anyway they are commonly manually operated.

A summary of the components used in the model is presented in the table 3. These components were selected from the TESS library and tested for compatibility by comparing individual inputs, parameters and expected outputs with respect to the proceeding counterparts before implementing them into the model.

The respective parameters and variables were obtained from the manufacturers' catalogues and design calculations.

Table 3: TRNSYS Model components

Model Part	Component	TRNSYS Types
Main Components	PV/T Collector	Type 50d
	Weather Generator	Type 15-2
Thermal Loop	Storage tank	Type 4c
	ON/OFF Differential controller	Type 2b
	Pump	Type 3b
	Flow Diverter	Type 11b
	Flow Mixer	Type 11h
Electrical Loop	Battery	Type 47
	Voltage Regulator/Inverter	Type 2b
Utility and Output devices	On-line Plotter	Type 65c
	Printer	Type 25c
	Integrator	Type 24
	Forcing functions(Load Pro les)	Type 14h

3.3.1 General system description of the PV/T model

The PV/T model is in four parts namely, the thermal loop and electrical loop, the individual and utility components. This section gives detailed description and configurations each part to enable clear understanding of the model. The numerical models implemented to predict the behaviours of the components are also are also formulated.

3.3.1.1 The thermal loop

More often than not the most commonly used hot water systems are categorized into active and passive systems. In the former, a pump is used to boost the flow of the fluid through the system while in the latter; the fluid flows naturally by convective currents. The pumped system was preferred for this study because of its flexibility in location of the storage tank and improved aesthetics of the system. The storage tank can be so designed to position the tank below or side by side with the collector, or in the plant room. For an effective system even during winter, an auxiliary heat exchanger and an antifreeze agent

62

were incorporated in the tank. The schematic diagram of the water loop active system used in the model is shown in figure 18.

The water loop/thermal side of the model is somewhat contrived. The solar pump (Type 3b) circulates cold water (represented by the green line) from the storage tank (Type 4c) to the VIPV/T or PV/T collector (Type 50d) array where it is heated. The hot water (represented by red line) then leaves the collector into the tank for storage and further to the hot water loads. The ON/OFF differential controller (Type 2b) senses the set lower and higher limits of VIPV/T or PV/T temperatures and triggers the solar pump accordingly. The controller also causes the tank to be emptied through the flow mixer (Type 11h), by a predefined load and is refilled by make-up water when it reaches a low volume limit. The storage tank is equipped with an auxiliary heater that carries the heating load when there is no sunshine.
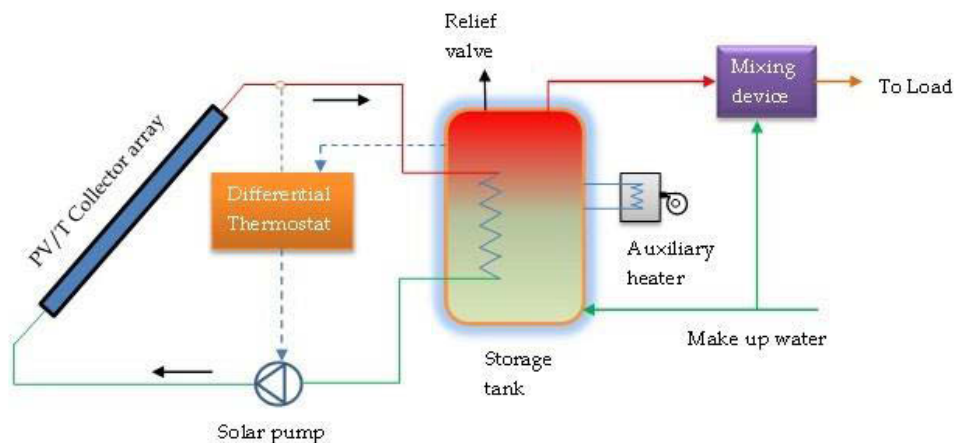
Figure 18: Schematic diagram of the water loop/thermal side of the PV/T model

3.3.1.2 Electrical loop

The schematic configuration of the electrical loop is presented in figure 19. The electrical power output from the PV/T (Type 50) array is passed through the inverter/charge controller (Type 48). This electrical output is compared by the inverter/charge controller with a predefined electrical load (set by a combination of Type 14, Type 41 and an equation). The charge controller, depending on its settings, then determines whether the electrical generation should be used to meet the load or charge the battery (Type 47). Types 47 and Type 48 were used in matching modes i.e. the battery bank mode parameter

63

and the inverter/charge controller mode parameters must be compatible with each other in order to provide the desired outputs.
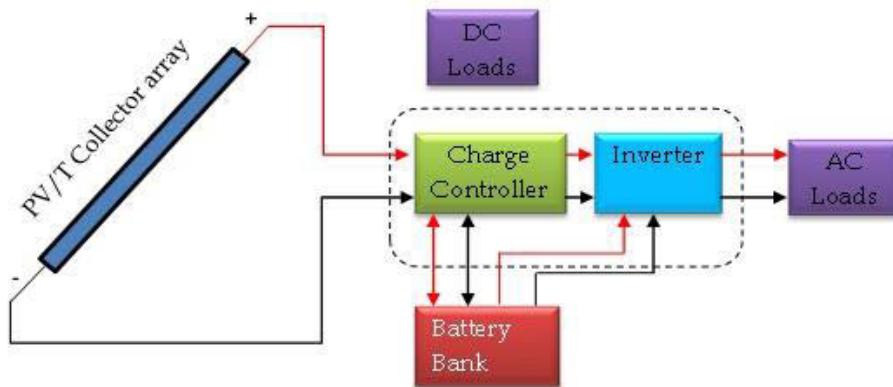
Figure 19: Schematic diagram of the electrical loop/side of the PV/T model

3.3.2 Individual component models

This section deals with optical and energy balance models for the PV/T and VIPV/T units, thermal models for the storage tank, internal auxiliary heater, on/off differential controller, water pump. The energy flow models for the battery and regulator/inverter units have been provide as well. The weather generator has also been modelled to provide the meteorological data and energy source.

3.3.2.1 VIPV/T and PV/T collector model

The PV/T collector is so denoted because it harnesses and converts the solar radiation exposed to it into thermal and electric energy simultaneously within the same unit. The structural configuration of the PV/T collector typically comprises a PV module mounted on a heat sensitive material known as the absorber whose principal function is to conduct away the heat absorbed by the PV cells to a circulating heat removal fluid usually water, air, water-air(dual) or refrigerant. Ducts or tubes are provided either under or above the absorber plate to provide passage for the fluid, depending on the configuration [56].

The water type PV/T collectors are characterised by higher efficiencies than the air types. In the water based PV/T, sheet and tube configuration is the most commonly used because it is reliable, cheap to construct and most promising notwithstanding its slightly lower efficiency compared to other configurations. The collector may also be glazed (glass covered) or unglazed. The former has been shown to attain the highest thermal efficiency compared to the latter, and has been recommended for domestic sanitary water

64

applications [16]. For the purpose of this study, the application is in the domestic domain, hence the glazed, sheet and tube design was chosen for simulation.

The PV/T collector was modified to include a vacuum envelope between the glazing and PV cells to constitute a Vacuum Insulated Photovoltaic/Thermal (VIPV/T) collector. Type 50 which is a modified Type 1 (Solar collector) with a PV module added to it was used to model both the VIPV/T and PV/T systems because it simulates a hybrid collector and combines both the analysis and operation of flat-plate collectors functioning at peak power, and analyses the I-V curves of the PV cells (or array) to solve for peak power or for current output at some forced voltage. For this simulation, the TYPE 50d was chosen because it provides for energy loss as a function of temperature, wind speed and solar radiation and provides for temperature as a function of collector angle i.e. Energy loss = *f(t,w,s,g)* and *t = f(angle)* parameters which were easily definable in the input file.

Since the VIPV/T collector was the main subject of study in this research, it was modelled as a Type 50d but with modified heat loss characteristics due to the vacuum insulation on the top part of the module between the PV cells and the glazing. These modifications were made to encompass the radiative, convective and conductive heat flow characteristics discussed in Chapter 4. The technical specifications of the module are summarized in table 3 in Chapter 4. The PV/T collector was modelled both in the optical and energy balance domains as highlighted in the following subsection.

♦ **Optical model**

The optical model describes a hybrid PV/T according to Fresnel's law which takes into account the various collector parameters related to solar radiation components and their reliance on the angle of incidence. The collective transmittance-absorptance (*τα*) product of the glazing and the absorber components was obtained from [31] and formulated as expressed in Equation 3.1.

$$(\tau\alpha) = \frac{\tau\alpha}{1-(1-\alpha)\rho_d} \tag{3.1}$$

♦ **Energy balance models**

According to Zondag et al [31] and[62] one-dimensional models achieve more acceptable levels of precision than the multifaceted ones when calculating the energy balance. In this regard, Da Silva et al [31] developed a transient model by upholding the principle of

65

conservation of energy on each individual layer of the collector, the results of which were sets of non-linear transient first order differential equations. Based on this model, the energy balance was formulated for both PV/T and VIPV/T. Figure 20 shows the cross sections of both PV/T and VIPV/T, showing the heat flows across the respective layers.

For PV/T in figure 20 (a) the temperatures for ambient air T_a, top T_{Tglass} and bottom $T_{bTglass}$ of glass cover, encapsulation glass $T_{PV\,glass}$, PV module T_{pv}, thermal plate absorber T_{abs} , bond T_b and water T_{water} in the tubes were denoted as T_a, T_1, T_2, T_3, T_4, T_5 T_6 and T_7 respectively, while for VIPV/T in figure 20 (b), T_a, T_{Tglass}, T_{bglass}, T_{pv}, T_{abs} , T_b and T_{water} also denoted as T_a, T_1, T_2, T_3, T_4, T_5 and T_6 respectively. With these annotations, energy flows and balance equations were formulated for each layer.
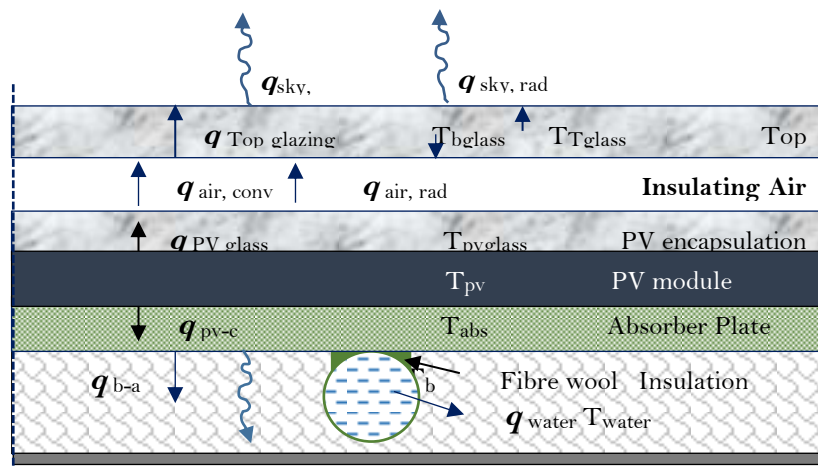
(a)   Conventional air insulated PV/T
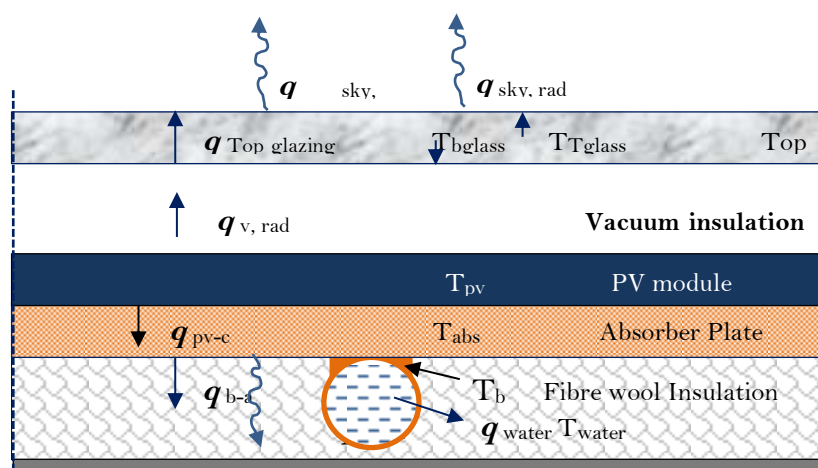
(b)   Vacuum Insulated PV/T

Figure 20: The heat flow and temperature distribution diagrams for PV/T and VIPV/T modules

For simplification of the heat flow processes, thermal network and equivalent interface resistance analogy diagrams were drawn as shown in figure 21. The PV/T collector with

66

top glazing and glass encapsulation is represented by figure 21 (a) while figure 21 (b) shows a glazed VIPV/T collector.

(a) Conventional air insulated PV/T   **(b) Vacuum insulated PV/T**
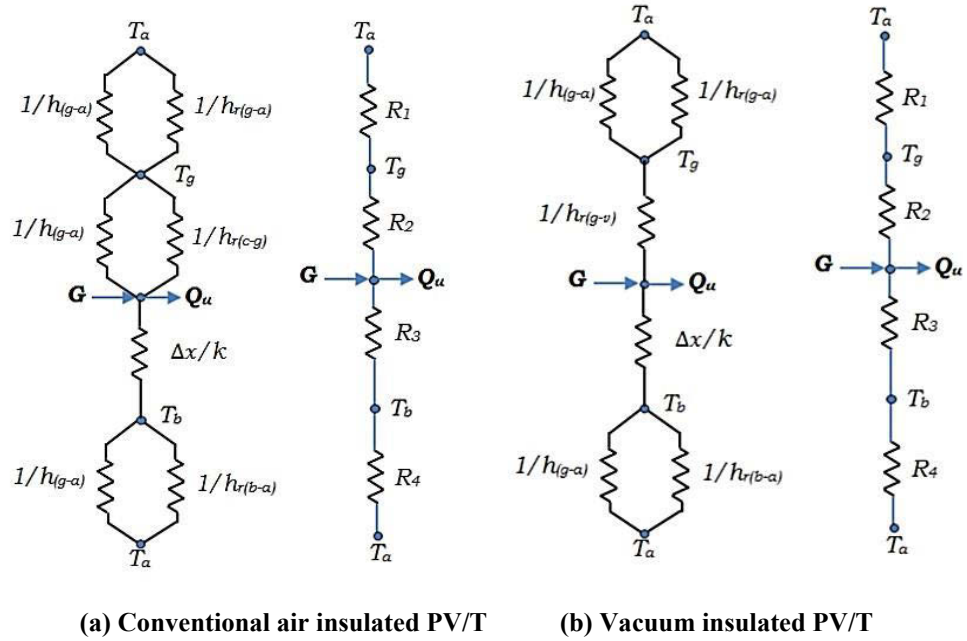
Figure 21: Thermal network and interface resistance diagrams for PV/T and VIPV/T

♦ **Energy balance model for PV/T**

For the single glazed PV/T collector with glass-encapsulated PV cells, the heat flow equations were formulated using figure 20 (a) as follows:

The heat flow to the water inside the tube q_{water}:

$$q_{water} = q_{pv-c} - q_{b-a} (3.2)$$

The heat flow through the PV module to the collector plate q_{pv-c}:

$$q_{pv-c} = (\tau\alpha - \tau_{pv}\eta_{el})G - q_{pvglass}(3.3)$$

The heat flow to the PV encapsulation glass $q_{PV\,glass}$:

$$q_{pvglass} = q_{air,conv} + q_{air,rad}(3.4)$$

The heat flow to the top glass cover (glazing) $q_{Topglazing}$ is two-fold;

$$q_{Topglazing} = q_{air,conv} + q_{air,rad}(3.5)$$

Or

$$q_{Topglazing} = q_{sky,wind} + q_{sky,rad} \text{(3.6)}$$

Since the PV module is attached to the absorber plate using an adhesive layer, the heat flow between the absorber-plate and PV module was modelled as follows:

$$q_{pv-c} = h_{pv-c}\left(T_{pv} - T_{abs}\right) = h_{pv-c}(T_4 - T_5) \text{(3.7)}$$

$$q_{b-a} = h_{b-a}(T_{abs} - T_a) = h_{b-a}(T_5 - T_a) \text{(3.8)}$$

To achieve better thermal performance, resistance to heat flow to the ambient via the top cover must be maximised and the resistance to heat flow from the collector to the water must be minimised. Therefore, for this pair of panels, a thin layer of highly conductive adhesive (tedlar and Ethyl Vinyl Acetate (EVA) of k = 0.85 *W/mK*, 0.2 *W/mK* and thickness δ = 50μm, 0.1 *mm* and 0.5 *mm* respectively) were used. These values were obtained from the manufacturer and were in agreement with the recommendations of Krauter [52].

Using the above data, the combined heat resistance for the PV-laminate was calculated thus:

$$h_{pv-c} = \frac{1}{R_{EVA} + R_{tedlar} + R_{glue}} = 500 \ W/m^2 K \text{(3.9)}$$

Using the temperature distribution schematic in Figure 21(a), Hottel-Whiller equation as given in [3] was applied to obtain T_{abs} as follows:

$$T_{abs} = T_a + \frac{(\tau - \tau_{pv}\eta_{el})G}{U_{loss}} + cosh(m)\frac{T_b + T_a - (\tau - \tau_{pv}\eta_{el})G/U_{loss}}{cosh[m(W-D_e)/2]} \text{ (3.10)}$$

Where:

$$m = \sqrt{\frac{U_{loss}}{k\delta_{abs}}} \text{(3.11)}$$

The heat loss coefficient U_{loss} and T_b are expressed as:

$$U_{loss} = \frac{q_{sky,rad} + q_{sky,wind} + q_{b-a}}{T_{PVglass} - T_a} = \frac{q_{sky,rad} + q_{sky,wind} + q_{b-a}}{T_3 - T_a} \quad \text{(3.12)}$$

$$T_b = T_{water} + \frac{q_{water}}{h_{tube}} = T_{water} + \frac{T_{water}D_e}{Nu_{water}k_{water}} = \left(\frac{T_i + T_o}{2}\right) + \frac{\dot{m}c_p(T_o + T_i)D_e}{Nu_{water}k_{water}} \text{(3.13)}$$

Where: $Re < 2300 \rightarrow Nu_{tube} = 4.3$ and $Re > 2300 \rightarrow Nu_{tube} = 0.023Re^{0.8}Pr^{0.4}$ In terms of temperatures, the individual heat fluxes were found as follows:

$$q_{water} = \dot{m}c_p(T_o - T_i)(3.15)$$

$$q_{sky,rad} = F_{sky}\varepsilon_g\sigma\left(T_{Tglass}{}^4 - T_{sky}{}^4\right) + F_{ground}\varepsilon_g\sigma\left(T_{Tglass}{}^4 - T_a{}^4\right)(3.16)$$

$$= F_{sky}\varepsilon_g\sigma\left(T_1{}^4 - T_{sky}{}^4\right) + F_{ground}\varepsilon_g\sigma\left(T_1{}^4 - T_a{}^4\right)(3.17)$$

$$q_{sky,wind} = h_{wind}\left(T_{Tglass} - T_a\right) = \frac{Nu_{wind}k_{air}}{l_c}(T_1 - T_a)(3.18)$$

$$Nu_{wind} = 0.56(Ra_{crit}sin\beta)^{0.25} + 0.13(Ra^{0.333} - Ra_{crit}^{0.333})(3.19)$$

$$Ra = Pr\frac{g\beta(T_{Tglass}-T_a)l_c^3}{v^2} = Pr\frac{g\beta(T_1-T_a)l_c^3}{v^2}(3.20)$$

Where: $Ra_{crit} = 10^8$

$$q_{air,rad} = \frac{\varepsilon_g\varepsilon_{PV}}{\varepsilon_g+\varepsilon_{PV}-\varepsilon_g\varepsilon_{PV}}\sigma\left(T_{PVglass}^4 - T_{bglass}^4\right) = \frac{\varepsilon_g\varepsilon_{PV}}{\varepsilon_g+\varepsilon_{PV}-\varepsilon_g\varepsilon_{PV}}\sigma(T_3^4 - T_2^4)(3.21)$$

$$q_{air,conv} = h_{air}\left(T_{PVglass} - T_{bglass}\right)\frac{Nu_{air}k_{air}}{l_{ins}}(T_3 - T_2) \quad (3.22)$$

Where:

$$Nu_{air} = 1 + 1.44\left[1 - \frac{1708(sin1.8\beta)^{1.6}}{Ra\ cos\beta}\right]x\left[1 - \frac{1708}{Ra\ cos\beta}\right]^+ + \left[\frac{Ra\ cos\beta^{0.333}}{1708} - 1\right]^+ (3.23)$$

According to Duffie et al,. [3] the terms raised to plus (+) signs only have values when positive, otherwise zero.

$$q_{PVglass} = \frac{k_g}{\delta_{PVglass}}\left(T_{PV} - T_{PVglass}\right) = \frac{k_g}{\delta_{PVglass}}(T_4 - T_3)(3.24)$$

$$q_{Topglazing} = \frac{k_g}{\delta_{Topglazing}}\left(T_{bglass} - T_{Tglass}\right) = \frac{k_g}{\delta_{Topglazing}}(T_2 - T_1)(3.25)$$

Taking the energy balance for the top glass cover we obtain:

$$M_1c_{p1}\frac{dT_1}{dt} = \frac{Nu_{air}k_{air}}{l_{ins}}(T_3 - T_2) + \frac{\varepsilon_g\varepsilon_{PV}}{\varepsilon_g+\varepsilon_{PV}-\varepsilon_g\varepsilon_{PV}}\sigma(T_3^4 - T_2^4) - \frac{Nu_{wind}k_{air}}{l_c}(T_1 - T_a) -$$

$$F_{sky}\varepsilon_g\sigma\left(T_1{}^4 - T_{sky}{}^4\right) + F_{ground}\varepsilon_g\sigma\left(T_1{}^4 - T_a{}^4\right)(3.26)$$

The energy balance to the air insulation layer is given by:

$$M_2 c_{p2} \frac{dT_2}{dt} = \frac{k_g}{\delta_{PVglass}}(T_4 - T_3) - \frac{k_g}{\delta_{Topglazing}}(T_2 - T_1) \quad (3.27)$$

The energy balance to the PV encapsulation glass is given by:

$$M_3 c_{p3} \frac{dT_3}{dt} = (\tau\alpha - \tau_{pv}\eta_{el})G - \frac{k_g}{\delta_{PVglass}}(T_4 - T_3) - \frac{Nu_{air}k_{air}}{l_{ins}}(T_3 - T_2) -$$

$$\frac{\varepsilon_g \varepsilon_{PV}}{\varepsilon_g + \varepsilon_{PV} - \varepsilon_g \varepsilon_{PV}}\sigma(T_3^4 - T_2^4) \quad (3.28)$$

The energy balance to the PV module is given by:

$$M_4 c_{p4} \frac{dT_4}{dt} = h_{pv-c}(T_4 - T_5) - \frac{k_g}{\delta_{PVglass}}(T_4 - T_3) \quad (3.29)$$

The energy balance to the absorber plate is given by:

$$M_5 c_{p5} \frac{dT_5}{dt} = h_{abs}(T_4 - T_5) - h_{b-a}(T_5 - T_a) - h_b(T_5 - T_6) \quad (3.30)$$

The energy balance to the absorber plate and tube joints is given by:

$$M_6 c_{p6} \frac{dT_6}{dt} = h_{abs}(T_4 - T_5) - h_{b-a}(T_5 - T_a) - \dot{m}c_{pb}(T_o - T_i) \quad (3.31)$$

Finally, the energy balance to the fluid flowing in the tubes is given by:

$$M_7 c_{p7} \frac{dT_7}{dt} = h_b(T_6 - T_7) - \dot{m}c_{pb}(T_o - T_i) \quad (3.32)$$

Where: T_7 is taken to be the fluid mean temperature given by:

$$T_7 = \left(\frac{T_{in} + T_{out}}{2}\right) \quad (3.33)$$

♦ **Energy balance model for VIPV/T**

The thermal energy flow throughout the layers constituting the VIPV/T were analysed in the same manner as the PV/T. Referring to figure 20 (b), the heat flow schematics are presented enabling an energy study. The major difference between the two scenarios is that the air insulation layer has been replaced with a vacuum insulation layer and the PV glass encapsulation removed. This option eliminates the $q_{air,conv}$ and $q_{PV\ glass}$ terms; hence equation 3.4 does not apply. The heat flow equations were thus formulated as follows:

The heat flow to the water inside the tube q_{water} remained unchanged as given in equation 3.2.

The heat flow through the PV module to the collector plate q_{pv-c} was formulated as:

$$q_{pv-c} = \left(\tau\alpha - \tau_{pv}\eta_{el}\right)G - q_{v,rad} \tag{3.34}$$

The heat flow to the top glass cover (glazing) $q_{Topglazing}$ is the same as given in equation 3.6, however, for heat balance we obtain:

$$q_{v,rad} = q_{sky,wind} + q_{sky,rad} \tag{3.35}$$

Where: $q_{sky,rad}$ and $q_{sky,wind}$ are as defined in equations 3.17 and equation 3.18 respectively while $q_{v,rad}$ also formulated as:

$$q_{v,rad} = \frac{\varepsilon_g\varepsilon_{PV}}{\varepsilon_g+\varepsilon_{PV}-\varepsilon_g\varepsilon_{PV}}\sigma\left(T_{PV}^4 - T_{bglass}^4\right) = \frac{\varepsilon_g\varepsilon_{PV}}{\varepsilon_g+\varepsilon_{PV}-\varepsilon_g\varepsilon_{PV}}\sigma\left(T_3^4 - T_2^4\right) \tag{3.36}$$

The heat flow between the absorber plate and PV module and from the back of the collector to the ambient remained as formulated in equations 3.3 and equation 3.8.

The heat transfer coefficient for the PV module to the collector h_{pv-c} also as shown in equation 3.9.

Taking the energy balance for the glass cover we obtain:

$$M_1 c_{p1} \frac{dT_1}{dt} = \frac{\varepsilon_g\varepsilon_{PV}}{\varepsilon_g+\varepsilon_{PV}-\varepsilon_g\varepsilon_{PV}}\sigma\left(T_3^4 - T_2^4\right) - \frac{Nu_{wind}k_{air}}{l_c}\left(T_1 - T_a\right) - F_{sky}\varepsilon_g\sigma\left(T_1{}^4 - T_{sky}{}^4\right) +$$
$$F_{ground}\varepsilon_g\sigma\left(T_1{}^4 - T_a{}^4\right) \tag{3.37}$$

The energy balance to the vacuum insulation layer was formulated as:

$$M_2 c_{p2} \frac{dT_2}{dt} = \left(\tau\alpha - \tau_{pv}\eta_{el}\right)G - h_{pv,}\left(T_4 - T_3\right) - \frac{k_g}{\delta_{Topglazing}}\left(T_2 - T_1\right) \tag{3.38}$$

The energy balance to the PV module is given by:

$$M_3 c_{p3} \frac{dT_3}{dt} = h_{pv-c,}\left(T_3 - T_4\right) - \frac{\varepsilon_g\varepsilon_{PV}}{\varepsilon_g+\varepsilon_{PV}-\varepsilon_g\varepsilon_{PV}}\sigma\left(T_3^4 - T_2^4\right) \tag{3.39}$$

The energy balance to the absorber plate, plate-tube bond and water flowing in the tube remained unchanged as given in equation3.30, equation 3.31 and equation 3.32 respectively.

71

These energy equations were implemented in the simulation for both PV/T and VIPV/T.

3.3.2.2 Storage tank model

Provision should be made for storage of water in cases where hot water produced is not used immediately or when the application is continuous, therefore it is always necessary to include a storage tank in the system. However, the tank must be able to guard against heat losses and in some instances, an auxiliary heater is incorporated to compensate for non-sunshine hours. For most domestic solar plants a stratified thermal storage tank is preferred because of its low cost, simplicity in construction, modular design and high level of stratification [62]. For these reasons, the stratified hot water tank was chosen for simulation in this study.

The stratified storage tank Type 4 with variable inlets and uniformly distributed loses was chosen to model the tank. This Type models a thermally stratified fluid filled functional energy storage tank, assuming that there are N fully-mixed fragments with equal volumes also known as nodes. The stratification level is determined by the value of N. When N equals to 1, the storage tank is modelled as fully-mixed and hence no stratification effects; however, the node sizes in this instance need not be equal. For this simulation, Type 4c was used because it models a stratified-tank with variable inlet locations ensuring that the temperature of entering fluid into the tank is as close as possible or equal to the temperature inside the tank. For maximum stratification the tank was segmented into six ($N = 6$) equal volumes of height of $0.15m$ each, which was found to be sufficient. The concept of stratification is shown in figure 22.
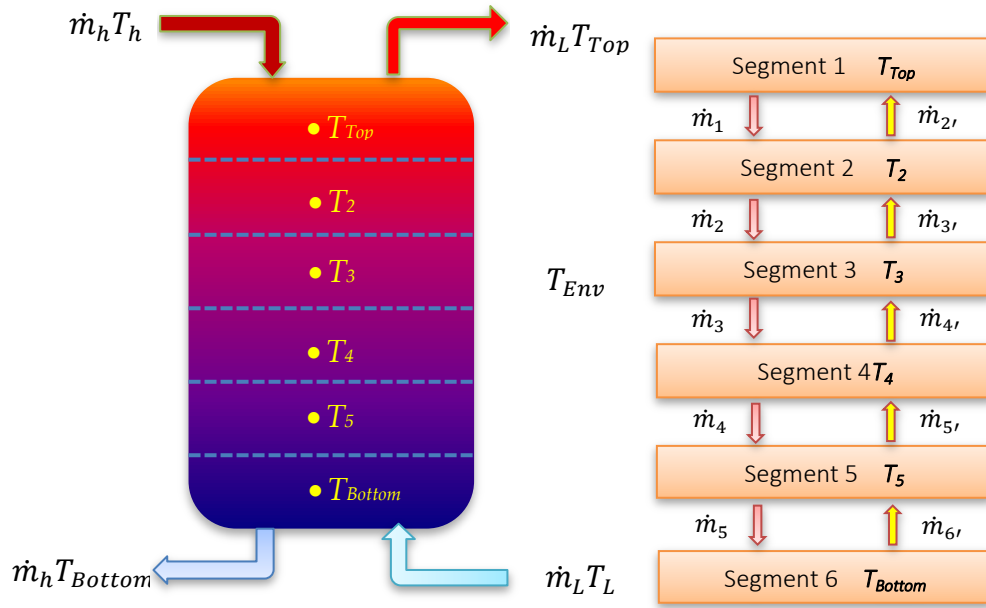
(a) Stratification in the tank   **(b) Flow regime**

Figure 22: Stratified fluid storage tank

To simplify the model, it was assumed that:

- The losses from each tank node were equal and the heat losses to the flue gas of the auxiliary heater were not calculated while the losses to the surrounding via the top and bottom and axial walls were included.

- The water flow inside the tank was unidirectional; this was true for most parts of the tank except for the inlet and outlet portions.

- The advective energy transfers were considered negligible since they tend to overate in the periods of non-flow in the order of double magnitudes.

- The convective heat transfer between the tank and the heat exchanger was modelled using empirical correlations obtained from the manufacturer.

- The diffusive turbulence at the entry zone was considered since its effect on the performance of the tank is in the order of 3 % and above [31].

Therefore the general energy balance equation of the tank was formulated as:

$$\rho c_p \frac{\delta T_1}{\delta T} = K \frac{\delta^2 T}{\delta x^2} + \frac{U_{int}P}{A_t}(T_m + T_t) - U\rho c_p \frac{\delta T_1}{\delta x} - \frac{U_{ext}P}{A_t}(T_t - T_{amb}) \qquad (3.40)$$

Further, an exploded nodal energy flow diagram as shown in figure 23 was adopted to analyse the energy balance for each node as follows:
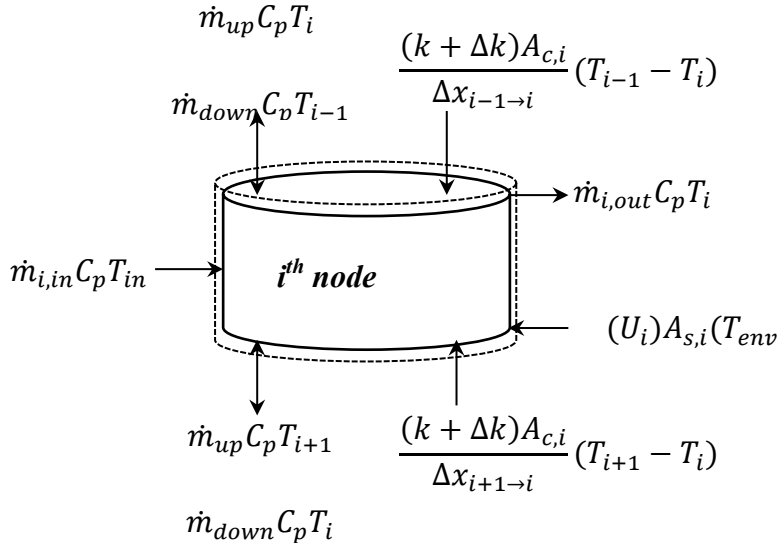
Figure 23: Stratified water storage tank nodal energy flow

$$M_i c_p \frac{dT_i}{dt} = \frac{(k+\Delta k)A_{c,i}}{\Delta x_{i+1\to i}}(T_{i+1} - T_i) + \frac{(k+\Delta k)A_{c,i}}{\Delta x_{i-1\to i}}(T_{i-1} - T_i) + (U_i)A_{s,i}(T_{amb} - T_i) +$$

$$\dot{m}_{i,in}c_p T_{in} - \dot{m}_{i,out}c_p T_i + \dot{m}_{i,up}c_p T_{i+1} - \dot{m}_{i,down}c_p T_i + \dot{m}_{i,down}c_p T_{i-1} - \dot{m}_{up}c_p T_i \quad (3.41)$$

Where: $\dot{m}_{up}$, $\dot{m}_{down}$, $\dot{m}_{i,in}$, $\dot{m}_{i,out}$ are the water flow rates up, down, in and out of the tank respectively; $A_{c,i}$ and $A_{s,i}$ are the cross-sectional and surface area of node i respectively; k and Δk are the tank fluid thermal and the de-stratification conductivities respectively, U_i is the node heat loss coefficient per unit area; T_{i+1}, T_i, T_{i-1}, $T_{w,in}$, $T_{w,out}$ and T_{amb} are the temperatures located below, at and above node i, the inlet and outlet water and the ambient respectively; and $x_{i+1\to i}$ and $x_{i-1\to i}$ are the distance between centres of node i and the adjacent nodes, respectively.

Node 1 housed the hot water inlet and outlet from the VIPVT collector and to the load respectively. The thermal energy due to the incoming and outgoing water was considered and because there was no preceding node to node 1, all the terms that refer to node zero are ignored hence, the energy balance for node 1 (*Top*) was given by:

$$M_1 c_p \frac{dT_1}{dt} = \frac{(k+\Delta k)A_{c,1}}{\Delta x_{2\to i}}(T_2 - T_1) + (U_1)A_{s,i}(T_{amb} - T_1) + \dot{m}_{1,in}c_p T_{in} - \dot{m}_{1,out}c_p T_1 +$$

$$\dot{m}_{up}c_p T_2 - \dot{m}_{down}c_p T_1 - \dot{m}_{up}c_p T_1 \quad (3.42)$$

Energy balance for node 2:

$$M_2 c_p \frac{dT_2}{dt} = \frac{(k+\Delta k)A_{c,2}}{\Delta x_{3\to 2}}(T_3 - T_2) + \frac{(k+\Delta k)A_{c,2}}{\Delta x_{1\to 2}}(T_1 - T_2) + (U_2)A_{s,2}(T_{amb} - T_2) +$$

$$\dot{m}_{up}c_p T_3 - \dot{m}_{down}c_p T_2 + \dot{m}_{down}c_p T_1 - \dot{m}_{up}c_p T_2 \qquad (3.43)$$

Energy balance for node 3:

$$M_3 c_p \frac{dT_3}{dt} = \frac{(k+\Delta k)A_{c,3}}{\Delta x_{4\to 3}}(T_4 - T_3) + \frac{(k+\Delta k)A_{c,3}}{\Delta x_{2\to 3}}(T_2 - T_3) + (U_3)A_{s,3}(T_{amb} - T_3) +$$

$$\dot{m}_{up}c_p T_4 - \dot{m}_{down}c_p T_3 + \dot{m}_{down}c_p T_2 - \dot{m}_{up}c_p T_3 \qquad (3.44)$$

Energy balance for node 4:

$$M_4 c_p \frac{dT_4}{dt} = \frac{(k+\Delta k)A_{c,4}}{\Delta x_{5\to 4}}(T_5 - T_4) + \frac{(k+\Delta k)A_{c,4}}{\Delta x_{3\to 4}}(T_3 - T_4) + (U_3)A_{s,4}(T_{amb} - T_4) +$$

$$\dot{m}_{up}c_p T_5 - \dot{m}_{down}c_p T_4 + \dot{m}_{down}c_p T_3 - \dot{m}_{up}c_p T_4 (3.45)$$

Energy balance for node 5:

$$M_5 c_p \frac{dT_5}{dt} = \frac{(k+\Delta k)A_{c,5}}{\Delta x_{6\to 5}}(T_6 - T_5) + \frac{(k+\Delta k)A_{c,5}}{\Delta x_{4\to 5}}(T_4 - T_5) + (U_5)A_{s,5}(T_{amb} - T_5) +$$

$$\dot{m}_{up}c_p T_6 - \dot{m}_{down}c_p T_5 + \dot{m}_{down}c_p T_4 - \dot{m}_{up}c_p T_5 \qquad (3.46)$$

Since node 6 was the bottom-most node and contained the feed water inlet from the mains and outlet to the collector, the energy transfers due to the incoming and outgoing water were included. However, the components that related to node 7 were ignored and therefore the energy balance equation became:

$$M_6 c_p \frac{dT_6}{dt} = \frac{(k+\Delta k)A_{c,6}}{\Delta x_{5\to 6}}(T_5 - T_6) + (U_6)A_{s,6}(T_{amb} - T_6) + \dot{m}_{6,in}c_p T_{in} - \dot{m}_{2,out}c_p T_6 +$$

$$\dot{m}_{down}c_p T_5 - \dot{m}_{up}c_p T_6 \qquad (3.47)$$

♦ **Internal Auxiliary Heater**

The auxiliary heater is an integral part of the stratified storage tank. The tank model was fitted with two electric resistance heating elements, subjected to temperature and/or time control, which enabled the supply of electric energy to the tank under specified periods and conditions e.g. off-peak hours.

The heaters were set to operate in a master/slave mode where the bottom element is activated only when the top element is satisfied. Therefore, at no point were the two heaters operating simultaneously. This mode is the most popularly applied in domestic water heating since it allows for economic monitoring of electricity use.

The model further assumed that the segment in which the heater was located retained the heat energy supplied until its temperature equalled that of the segment above it and once this condition was met, the heat energy then flowed equally to the subsequent upper segment. It was established that this assumption generally yielded higher degree of stratification and the results obtained agree well with the experimental results.

To obtain the temperature of each of the N segments their time-step derivatives were integrated and at the end of each time-step temperature inversions were excluded by sufficiently mixed adjacent nodes. The energy flows and variation in internal energy were then calculated as follows;

The rate of energy loss from the tank to the ambient environment Q_{amb} is given by:

$$Q_{amb} = \sum_{i=1}^{N} UA_i \left(T_i - T_{amb} \right) + \gamma_f \sum_{i=1}^{N} (UA_i)_{f,i} \left(T_i - T_f \right) \qquad (3.48)$$

Where: γ_f is the control function defining if auxiliary heater is ON or OFF, $(UA)_{f,i}$ is the conductance for heat loss to gas flue for node i and T_f is the average temperature of exhaust flue when the heater is OFF.

The sensible heat removal rate from the tank to the supply load Q_s is given by;

$$Q_s = m_L c_p (T_i - T_L) \qquad (3.49)$$

The heat energy input rate to the tank from hot fluid stream Q_{in} is given by:

$$Q_{in} = m_h cp (T_h - T_N) \qquad (3.50)$$

Where: T_N is the temperature of the node at the inlet of the tank.

3.3.2.3 ON/OFF Differential Controller model

Given the nature of unpredictability of solar radiation, there has to be provision for temperature controls to take care of the extreme heat. As the name suggests, this type of temperature controller monitors the temperatures and operates on the ON/OFF mode by producing a control function γ_0 whose value is either 1 or 0.

At any instance, the value of γ_0 is taken as a function of the temperature difference between the set upper and lower limits T_H and T_L respectively in comparison to their respective dead-band temperature differences ΔT_H and ΔT_L. The hysteresis effect is provided by connecting the input (γ_i) to the output (γ_0) control signal of the controller set to a higher

76

limit cut out for safety concerns. Irrespective of the dead-band situation, the control function was set to zero so long as the defined high limit condition is exceeded. This is the situation most suited for domestic hot water systems where the pump stops if the temperature of the tank reaches a predefined limit. For this simulation, the Type 2b controller for temperature based on solver 0 (successive substitution) control strategy was used since it applies unit descriptions of degrees Celsius (^{o}C), a condition that gives it a thermostatic effect.

3.3.2.4 Pump model

The PV/T system under study is an active type which requires the use of a pump to boost circulation of water. A variable speed pump was considered suitable because under the control strategy, the mass flow rate of the fluid was varied and calculated using variable control function which was set to lie between 0 and 1, with a fixed user specified maximum flow. For this simulation, Type 3b was chosen because it calculates the power consumption as a linear function of mass flow rate. In this case the outlet and power consumed were set to zero or at their maximum values.

The outlet temperature T_o was calculated from;

$$T_o = T_{in} + \frac{P x f_{par}}{m c_p} (3.51)$$

Where; T_{in} is the inlet fluid temp, P is the power consumption of the pump; f_{par} is the fraction of pump power converted to fluid thermal energy.

The outlet mass flow m_o calculated from;

$$m_o = \gamma m_{max} \qquad (3.52)$$

Where γ is the control function whose value lies between 0 and 1.

3.3.2.5 Battery model

The battery offers storage for electrical power generated from the PV array in DC form. This can be distributed for use by DC appliances or channelled through the inverter for conversion to AC and onward consumption or fed to the grid. A lead-acid storage battery that connected to the PV array (power source) and power conditioning equipment was modelled using Type 47 because it specifies the variation of battery state of charge over

time, at defined rates of charge or discharge. For simplicity of the simulation, Type 45a with power as input was used because it was found to be based on a modest battery energy balance as opposed to other modes with current as input. However, this mode neither computes nor outputs any values of current or voltage and its compatibility with the regulator/inverter Type 48 mode used in the simulation was taken into consideration.

Mathematically the battery was modelled according to the following expressions, taking into account even very low currents.

During discharge, the voltage V is:

$$V = V_{oc} - V_{zp} - g_c H + I r_{qc} \left(1 + \frac{m_c H}{Q_c/Q_m - H}\right) \quad (3.53)$$

During charging, the voltage is:

$$V = V_{oc} + V_{zp} - g_c H + I r_{qc} \left(1 + \frac{m_c H}{Q_c/Q_m - H}\right) \quad (3.54)$$

Where: $V_{zp} = \frac{1}{k_{zp}} ln\left(\frac{|I|}{I_{zp}} + 1\right)$ \hfill (3.55)

and

$$V_{oc} = \frac{1}{2}(e_{qd} + e_{qc}) \quad (3.57)$$

Where: V_{oc} is the open circuit voltage at full charge, V_{zp} is the additional voltage term in Hyman model, g_c is a small value coefficient of H, $H=(1-F)$, F is fractional state of charge (Q/Q_m), I is current, r_{qc} is the internal resistance at full charge, m_c is the cell type parameter used to determine the shape of the I-V-Q characteristics, Q_c and Q_m are the rated cell capacity and capacity parameters on charge respectively, K_{zp} and I_{zp} are parameters used to calculate V_{zp}. e_{qc} and e_{qd} are open circuit voltages at full charge, extrapolated from I-V curves on charge and discharge respectively.

3.3.2.6 Regulators/Inverter (Type 48)

Power conditioning is necessary in PV systems due to the intermittent nature of the primary energy source i.e. solar radiation. The power conditioning components used in these systems are the inverter and voltage regulator or controller. The inverter converts direct current (DC) to alternating current (AC) and passes it on to the AC loads for use

78

while the regulator allocates DC power from the solar module array to and from the battery bank for storage. When the battery attains full charge capacity excess power is either discarded or uncollected by shutting off power generation from the modules. For this simulation, Type 48 was used because it models both the regulator and inverter at the same time, and was operated in mode 1 (Type 48b) for Peak-power tracking collector, battery and state of charge monitoring. To ensure that all the load requirements were met, the inverter was characterised and sized according to the maximum load required. The inclusion of the inverter was necessitated by the fact that not all domestic appliances use electricity in the form of direct current (DC) as generated by the PV systems, but also alternating current (AC) and hence, the inverter therefore, allowed for conversion from DC to AC for application in AC appliances.

3.3.2.7 Weather generator

This element reads and interpolates statistics at fixed time intervals from a peripheral weather data file. All the weather characteristics required can be generated with this component, most notably: solar radiation both for horizontal and tilted surfaces at predefined time intervals of less than one hour. It also computes many other useful parameters such as the mains water temperature, the effective sky temperature, and the heating and cooling season forcing functions. For this simulation, the Metronome TM2 weather data for Durban South Africa was used specified as ZA-Durban-685880.tm2 and fed as an external file input.

3.4 The model simulation

Prior to alterations of an existing system or building a new system, it was necessary to optimize system performance through simulation studies. This made it possible to minimise the chances of failure to meet specifications, eliminate unforeseen bottlenecks and prevent under or over utilization of resources. To evaluate the performance of a proposed VIPV/T system under different configurations of interest and over prolonged periods of real time, a simulation model consisting of the system parameters, input variables, performance measures functional relationships and outputs was developed. The details of the simulation process control, time step and time range were defined in the global info window via the control cards icon.

The time-step of each component reaction was defined for a detailed representation of the whole system. The simulation was run in an interval of 0.25 hours (15 minutes) and integrated to daily and annual proportions to give the prospective projections of actual performance of the VIPV/T and system.

The simulation run time range considered for this study was in the order of a few seconds to several hours which gave an output in the medium-term range. Therefore, a simulation run of 24 hour cycle was considered appropriate for the system analysis. For purposes of comparison with the experimental results, the simulation time range considered was 07:30 - 17:30 hours.

3.4.1 Simulation assumptions

For simplicity of the simulation study, there were a range of assumptions made as itemized here:

- The accuracy of the simulation relied on the mathematical definition of the TRNSYS Types used in the model whose performances were further assumed to be optimised. This was done by selecting the appropriate simulation parameters (inputs and desired outputs) before running the simulation.
- The components behaviour lasting for milliseconds were not taken into account.
- The heat losses from the edges and back surface were considered negligible in the simulation.
- Only two dimensional (2D) heat transfer flow regime was considered for the collector in the simulation.
- The focus of this simulation study was on the power flows, temperature distributions and controls in the hybrid PV/T system.

The components were defined by sets of mathematical expressions in the form of algebraic and differential equations solved using successive substitution (solver 0) when the simulation runs are performed. The solver allowed for calculation of outputs from given inputs for each unit and passed as inputs to the other units for as long as there was no convergence but became tricky with systems having little or no capacitance and rapidly changing discrete states. These challenges were overcome by defining and increasing the number of iterations in the algorithm. On the other hand, there was an option for using Powell's method (solver 1), which generated and solved an input-output matrix of simultaneous equations; however, this solver had difficulties with components involving

80

fluid flows and internal storage. The successive solution and modular approach strategy involved the solution of the larger problem by solving several smaller subsystem problems, thus provided a high degree of flexibility.

The model was run by activating the run button from which graphical outputs were displayed to see the behaviour of the system. All the specifications and procedures of the simulation were registered in the list (.lst) file and recorded in a deck file.

For numeric outputs, the deck file was opened and run in the TRNEdit environment. This generated the sets numeric data corresponding to the results which were accessed via the window menu. The sets data obtained were then linked to the lookup tables in the EES program to produce the plots presented in Section 1.5.

3.5 Simulation results and discussion

The research sought to make use of solar energy to generate electric and thermal power by way of simulation studies of a glazed solar PV/T flat plate collector with vacuum insulation between the glazing and the solar cells (VIPV/T). The variation of global solar radiation and ambient temperature for a typical meteorological year in Durban, South Africa was taken as the basic input parameter of this study. The model developed in TRNSYS software was simulated and very interesting results were obtained which are further presented and discussed.

3.5.1 The VIPV/T and PV/T system model

Transient Systems Simulation (TRNSYS) software was used to develop the PV/T system model. The program was chosen because it consists of subroutines that model sub-systems. Various components were identified and connected or linked to form a system; each component was assigned mathematical and arithmetic functions and operations. As set out in the objectives, a TRNSYS model was developed and constructed using various components as listed in table 1. The simulation was run and desired results obtained thus proving its functionality. The diagram of TRNSYS model is shown in figure 24.
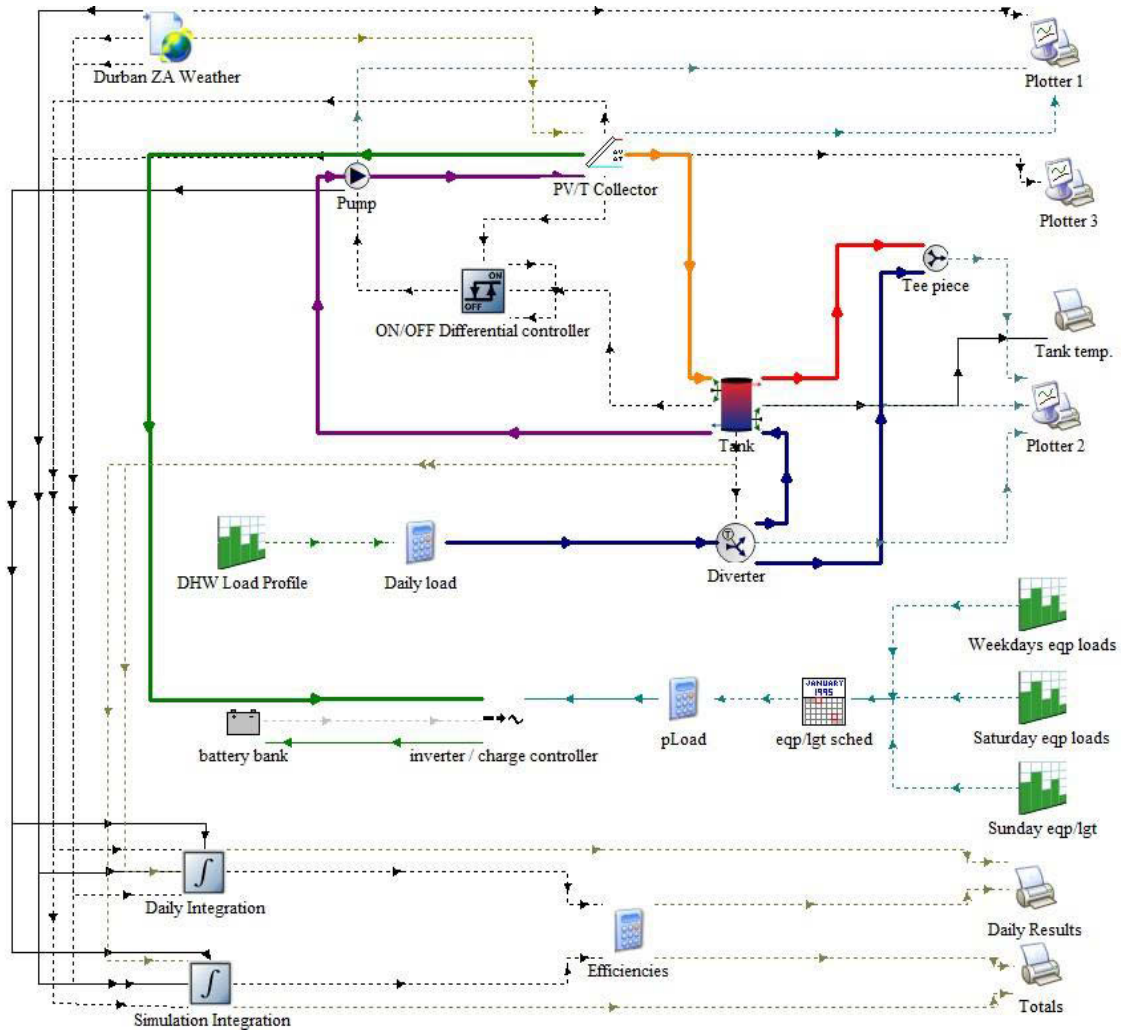
Figure 24: The TRNSYS graphical model of VIPV/T system

Combinations of different components were identified from the TESS library, both with predefined properties and user specified in the deck file. The input parameters were defined for each component and desired outputs obtained. The flexibility of the model allowed for change of component parameters like the manufacturer's geometric and operational specifications which were run to simulate the expected performance subject to the South African weather conditions.

A series of problems were encountered during the construction of the model, such as inappropriate input-output connections, unit specifications and compatibility issues, which were shown as a series or chain of errors listed in the *.lst* file automatically generated during the simulation runs. These errors prevented the model from producing the desired results and were progressively eliminated by modifying the component geometrical configurations, analytical parameters and running compatibility tests.

By altering the weather characteristics of the intended geographical location of installation and the geometrical dimensions of the PV/T collector module, the model is capable of giving out the results of thermal and electrical performance. Although the loads may vary, flexibility in alteration of the various schedules as per location is also provided. The user has the option of altering the desired outputs to be plotted, but basically the most critical ones have been included in this model. Therefore, the first objective of the study is adequately achieved.

3.5.2 The optimum collector slope

In order to determine the angle of tilt at which the VIPV/T and PV/T collectors could be installed to give optimum output, a detailed parametric study was conducted on the model. The collector slope was varied and thermal energy outputs and efficiencies computed over the entire simulation period.

The results obtained in TRNSYS were integrated into EES parametric table environment via the look-up table option and plotted as shown in figure 25. From the graph, it was established that the angle corresponding to the highest thermal output and efficiencies for Durban was 35°. This was adopted for this study as the optimum angle of tilt and was found to be in line with other researchers' findings which proposed a tilt angle defined by the altitude of location in consideration, plus 5° (Altitude + 5°)
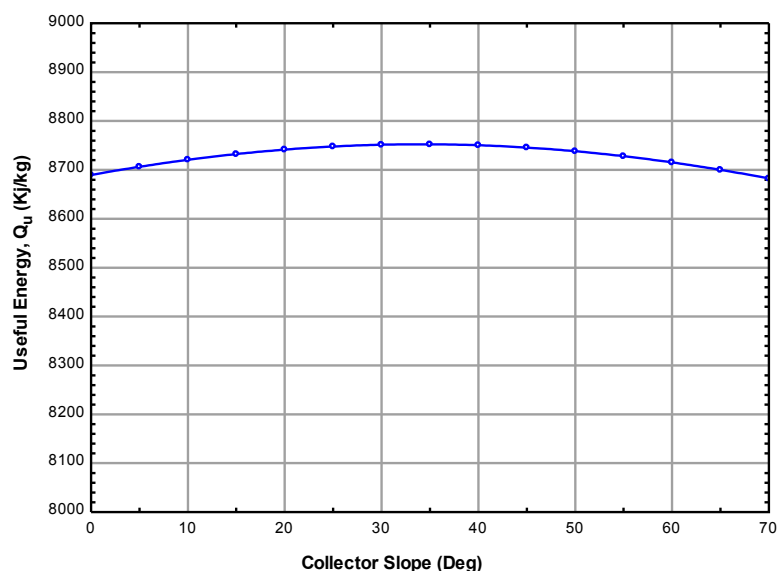
Figure 25: The effect of collector slope on the thermal efficiency

3.5.3 Daily performance analysis

To provide a basis for comparison with experimental results, the daily simulation studywas conducted on22[nd] August 2014 and produced data on which the experimental analysis was based. The results obtained are presented in the following section.

3.5.3.1 Thermal Energy

The variation of useful energy obtained from the VIPV/T and PV/T during day under analysis is shown in figure 26. The amounts received were 5385*J/kg* and 4662*J/kg* for VIPV/T and PV/T respectively which represented an average increase of about 16.5 %. The maximum instantaneous values recorded for the former and latter were 208.87*J/kg* and 183.12*J/kg* respectively. The difference was noted to have been as result of reduced convective losses due to application of the vacuum insulation layer.
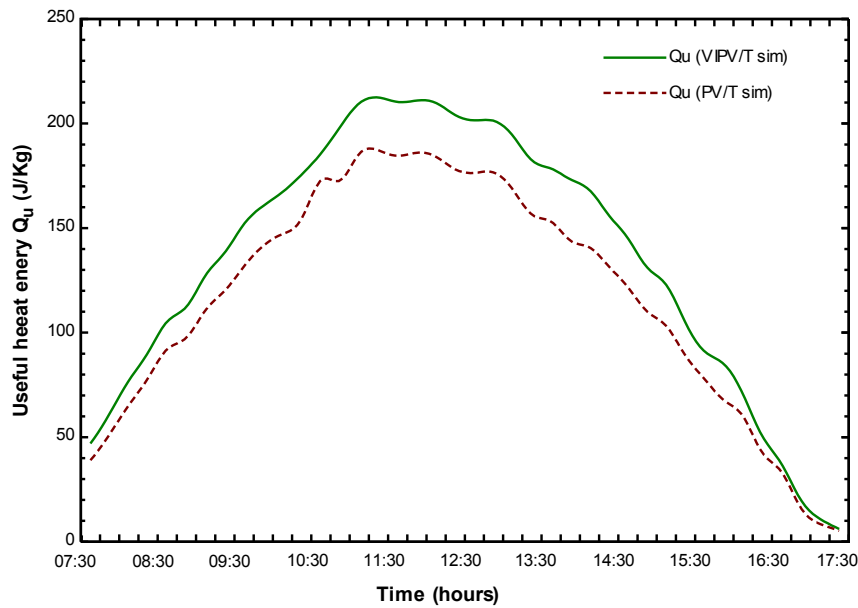
Figure 26: Useful heat *Qu* as a function of time of the day

As an input to the PV/T unit, the mains water temperature set at default ambient conditions of 20^oC was set as inlet while the outlet water temperature which is an indicator of heat gain was recorded at the respective intervals. The maximum daily outlet water temperatures recorded were 51.82^oC and 62.31^oC for PV/T and VIPV/T respectively; this implied an average increase of 12.9 % in hot water temperatures during the simulation times. These were extracted to have occurred in the months of June and February respectively. This can be seen in figure 27.

84

An average hot water temperature of about 40^oC is considered a standard requirement for domestic applications such as hot water sanitation, bathing, and washing among other activities [39]. The average water temperature was 42^oC for VIPV/T which was above the acceptable range hence the system could satisfy the hot water needs of an eight person residence without auxiliary heating on a sunny day.
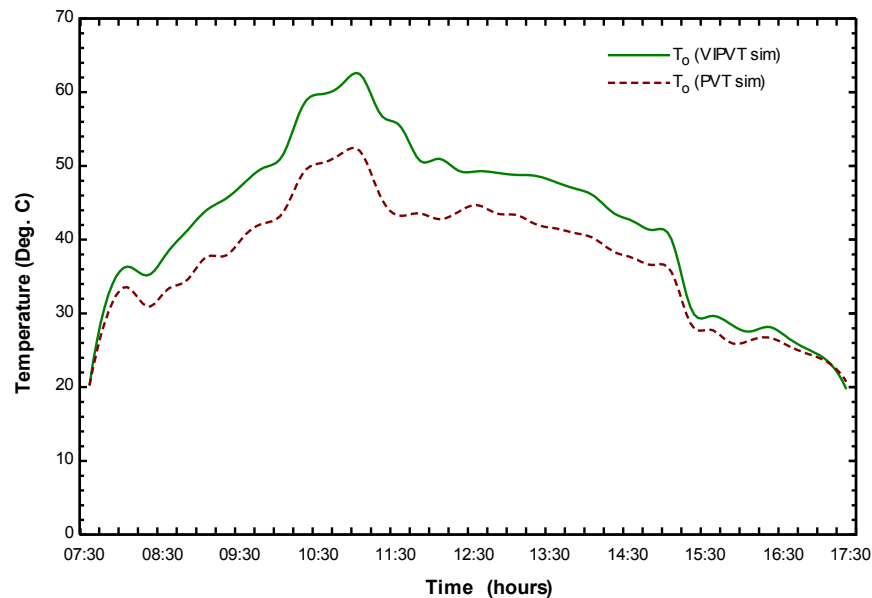
Figure 27: The variation of outlet water temperature with time of the day

3.5.3.2 Average PV cell temperatures

The average PV cell temperature was recorded directly from the VIPV/T and PV/T collector units in the simulation model. The variation of average PV cell temperatures is shown in figure 28. The VIPV/T and PV/T recorded maximum PV cell temperatures of 179.88^oC and 179.64^oC, occurring at 12:00 and 11.30am respectively. There was an average variation to the tune of 5.4 % above PV/T values. This is the reason for marginal reduction in electrical efficiency as will be seen in the next section. Electrical efficiency was found to be decreasing with an increase in average cell temperatures and the converse was also true, subject to the prevailing varying solar radiation levels. This has proved the fact that a heat removal and cooling mechanism was essential to keep the electrical efficiency as high as possible, hence, the need for water circulation for hot water generation.
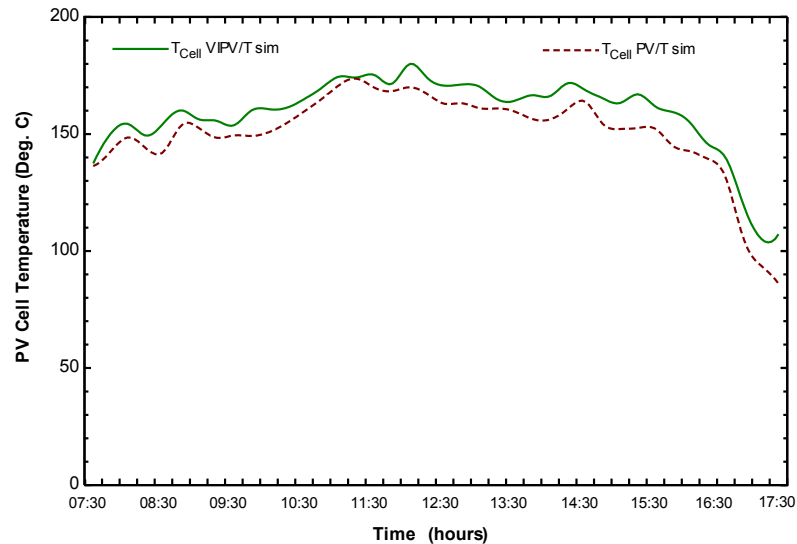
Figure 28: The variation of average cell temperatures with time

3.5.3.3 The temperature variation in the storage tank

The stratified hot water storage tank was simulated with two variable inlets at the bottom and one auxiliary heating element located in the topmost node, where the hot water outlet is also located. The initial temperature of the water was set to 20^oC, which is the mean temperature of the municipality water mains at the inlets. The variation of the water temperatures across the tank nodes with and without auxiliary heating were recorded and plotted.

With auxiliary heating shown in figure 29, it can be seen that in the non-sunshine hours i.e. between 00.00 and 01:00 hours, the auxiliary heater was triggered to heat the top most node to about 60^oC. The heater was located at the top node where hot water outlet to the load was also situated. However, the stratification gap was wide due to the constant water draw to the load which was set to run automatically. When the sun rises and solar radiation sets in at around 08:00 hours, the temperatures of other nodes starts rising due to continuous solar heating until the peak is reached at around 16:00 hours.

Without auxiliary heating, figure 30, the temperatures start to rise steadily at about 8:00 hours when the sun rises and peaks at 16:00 hours when the intensity reduces as it approaches sunset. The highest temperatures attained with and without heating are 90.1^oC and 85.97^oC respectively. There was a time lag of about 1.45 hours between the top most and the bottom most nodes to reach a given temperature and with temperature difference of about 12^oC. There was high temperature concentration on the top because of the location of the hot water inlet at the top side. The cold water inlet is at the bottom. In addition to

86

that, the auxiliary heater is also located close to the top node, so when on, heats the top first before mixing takes place with the adjacent nodes.

However, the annual solar fraction was evaluated using Equation 2.41 and the average values obtained for this PV/T system was S %with the high values of H %occurring during the month of February and Lows of L %in the month of June.
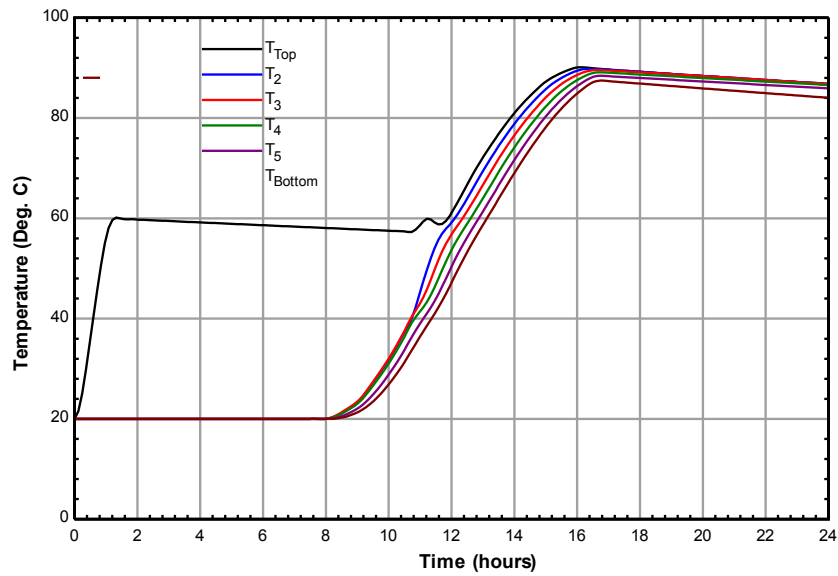
Figure 29: The nodal water temperature distribution in the tank with auxiliary heating
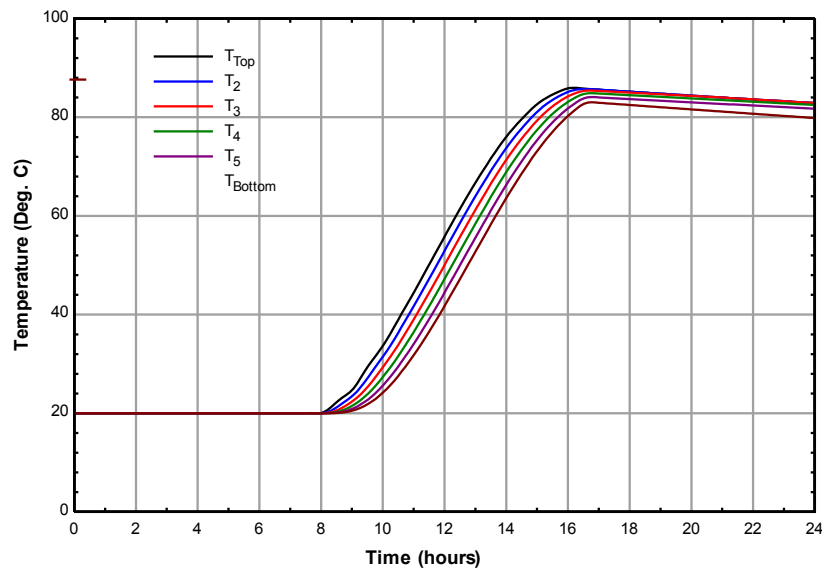
Figure 30: The nodal water temperature distribution in the tank without auxiliary heating

It was comparatively important to evaluate the average water temperature distribution in a fully mixed scenario. This was plotted as shown in figure 31. The maximum mean

temperature attained was 84.81^oC. The value was high because it was as a result of the two collectors
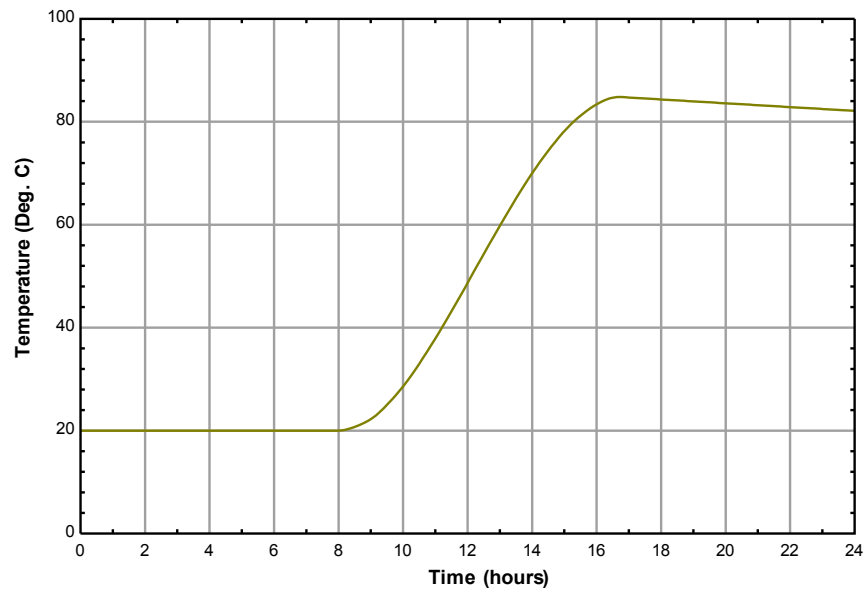
Figure 31: Average water temperature in the tank

3.5.3.4 Electrical Energy

Figure 32 gives the daily variations of the voltage and current outputs from the VIPV/T and PV/T collectors. From the voltages and currents obtained, the electrical power was calculated and values corresponding to the respective data points plotted as shown in figure 33. A total of 9885.90 *W* was realized from the two modules during the day under analysis. Individually, 4951.10 *W* and 4934.80 *W* were generated by the VIPV/T and PV/T systems respectively. An increase of 0.03 % on power generated was realized, a magnitude of which was negligibly small compared to the change realized in thermal energy.

88
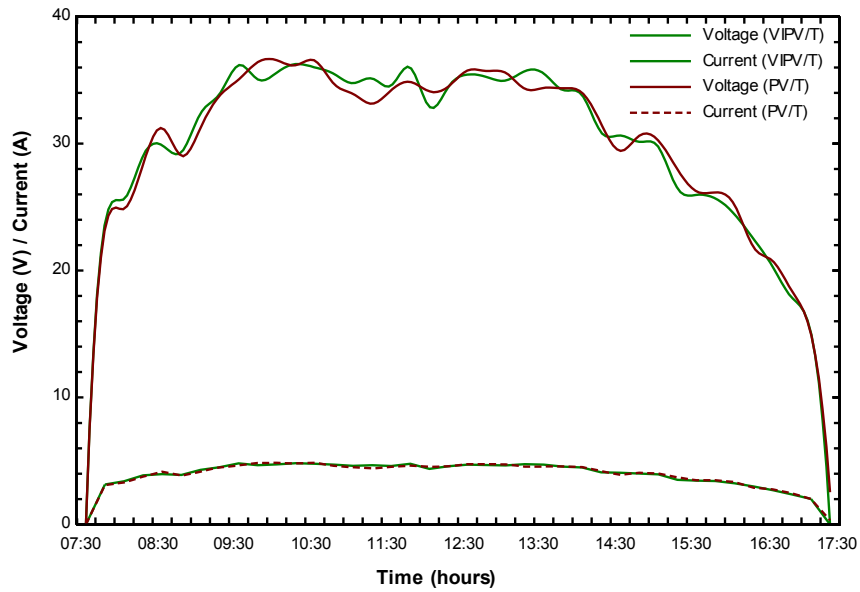
Figure 32: The variation of voltages and currents from the VIPV/T and PV/T collectors with time
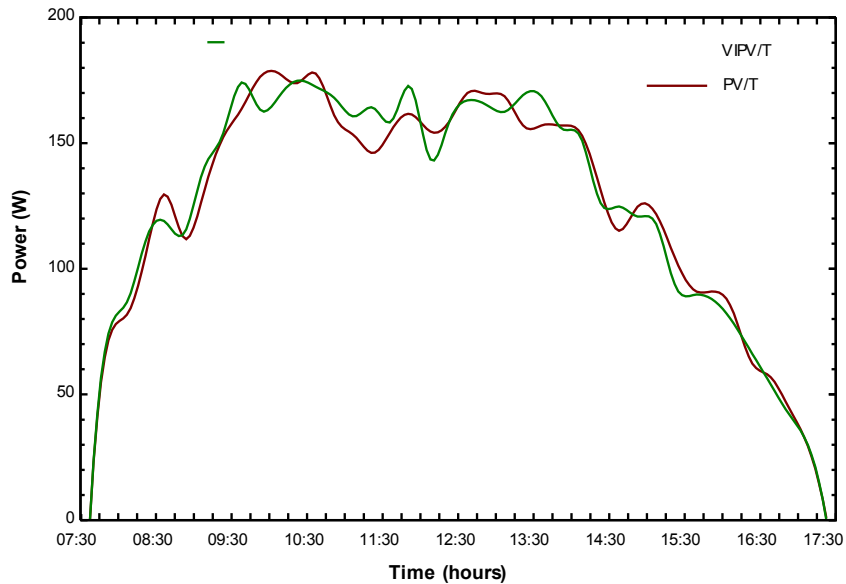
Figure 33: The variation of electrical power yield as a function of time

3.5.3.5 Efficiencies

In a PV/T system, electrical power generation is often given priority, while the thermal energy generation is an efficiency improvement strategy. Therefore, it is important to operate the PV unit at its near maximum efficiency possible by cooling. However, the cooling mechanism constitutes the thermal unit which must also operate efficiently to supply the heating loads. The efficiencies for the hybrid VIPV/T in comparison to the PV/T were evaluated and hourly results plotted as shown in figure 34.
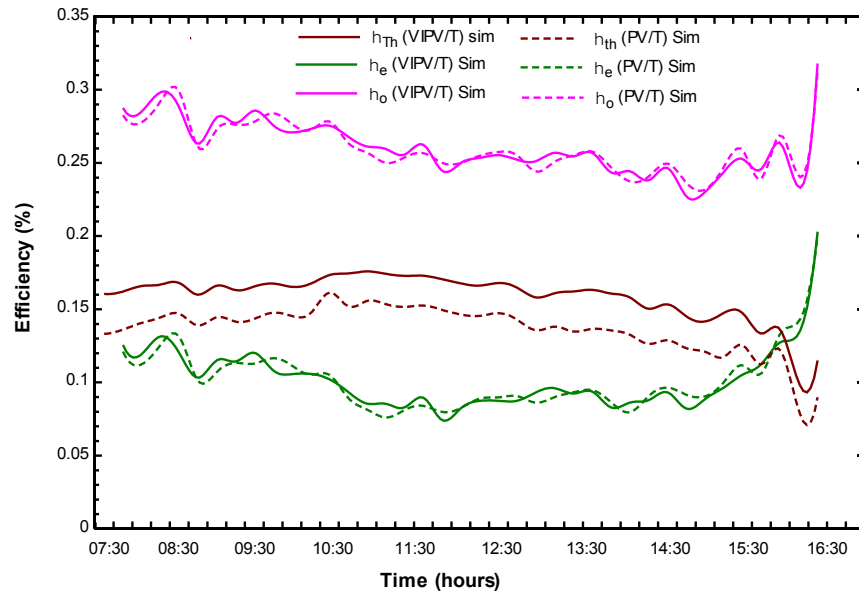
Figure 34: The variation of electrical power yield as a function of time

Based on the results obtained, the *Thermal efficiencies* were evaluated to be 15.74 % and 13.5 % for VIPV/T and PV/T systems respectively on a daily average. There was an increase of 16.8 % which was attributed to the inclusion of the vacuum insulation layer. However, this figure could go up or down depending on the prevailing irradiance of the day and region.

The mean daily *Electrical efficiencies* obtained were 9.75 % and 9.77 % for VIPV/T and PV/T respectively. Apparently, there was a reduction of 0.02 %. Even though the decrease was negligibly small, there was an indication that this was due to high temperature build-ups which may require stringent controls in the long term exposure to solar radiation.

The *Overall efficiency* was evaluated as the sum of the electrical and thermal efficiencies and was obtained as 25.49 % and 23.3 % for VIPV/T and PV/T respectively. Again an improvement of 9.51 % was realized.

To give a broader picture regarding the performance of the VIPV/T, the overall exergy efficiency and primary energy saving efficiencies were also evaluated to support the respective energy efficiencies.

Using the expressions given in equation 2.40, the *Overall exergy efficiencies* were evaluated as a function of Carnot efficiencies and found to be increased by an average of 1.82 % from 10.58 % to 10.94 % for PV/T and VIPV/T respectively.

The *Primary energy saving efficiencies*, on the other hand, improved by 4.08 % for VIPV/T at 19.01 % compared to PV/T at 18.18 %. A conventional energy power plant generation efficiency minimum of 0.38 % was assumed in the calculations, to give the minimum possible indication of performance improvement.

3.5.3.6 Effect of the vacuum insulation

In the PV/T system configuration, air space was applied as an insulator between the glazing and the PV cells. In stagnant air, heat transfer is by radiation through gas, however, when the air is set in motion, convective mode of heat transfer sets in, replacing conduction; the effect of which result in higher thermal conductivity.

From the approach and findings of this study, the vacuum envelope was introduced in place of air layer as insulation against the heat losses through the top of the flat-plate PV/T. The overall effect was found to be convection suppression thus, limiting heat loss to the radiative mode. This option resulted in an increase in thermal efficiencyof9.51 % while electrical efficiency negligibly reduced by 0.02 %. The PV glass encapsulation was removed since there were no chances of cell degradation due to direct air contact. Additionally, optical efficiency was improved by eliminating extra reflections by the encapsulation glass. However, the negligible indication of reduction in electrical efficiency was noted as a serious matter since it could escalate further depending on the prevailing meteorological conditions of the location and period of exposure, therefore high levels of control should be put in place to ensure PV temperatures are not raised. The edge and back losses remained the same and were not considered.

3.5.4 Annual performance analysis

To predict the long term performance of the VIPV/T, it was significant to simulate its annual performance as was outlined in figure 3 In the previous section, the daily performance was analysed weighed against the PVT/T, however, in this section only the VIPV/T module annual performance assessment is presented.

The annual energy output results are presented in figure 35. The VIPV/T module was subjected to a total annual irradiance of 6,590.26*MW*, out of which the *Useful heat Q_u* energy output of the module was found to vary from a low of 386.33*kJ/kg* during the winter month of June and a high of 673.65*kJ/kg* during the summer month of January. However, the total annual output was 6,092.03*kJ/kg*

91

The *actual heat* energy transferred to hot water Q_{DHW} was in the range of 528.3*kJ/kg* and 380.97*kJ/kg* also corresponding to the months of January and June respectively. The total and average outputs for the year were 40.89*MJ/kg* and 340.76*kJ/kg* respectively.

On the other hand, based on the hot water loads considered, a total of 34.81*MJ/kg* was required for use during the non-sunshine or low radiation periods. However, this figure would go up were it not for the solar energy intervention as will be demonstrated by the solar fraction in a later stage.

Based on the electrical loads considered for simulation, the *annual electrical* energy yield for the VIPV/T was found to be in the range of 423.37*KW* and 524.36*KW*; however, the total power generated for the year was 5,581.06*KW*. Considering the peak demand 850*W* of the domestic set up consideration, this energy was found to be adequate. Even though, in some instances, it went lower than required, this challenge could be met by adding more storage hours to supply the deficit or consider supplementing with grid power if available inthat instance.
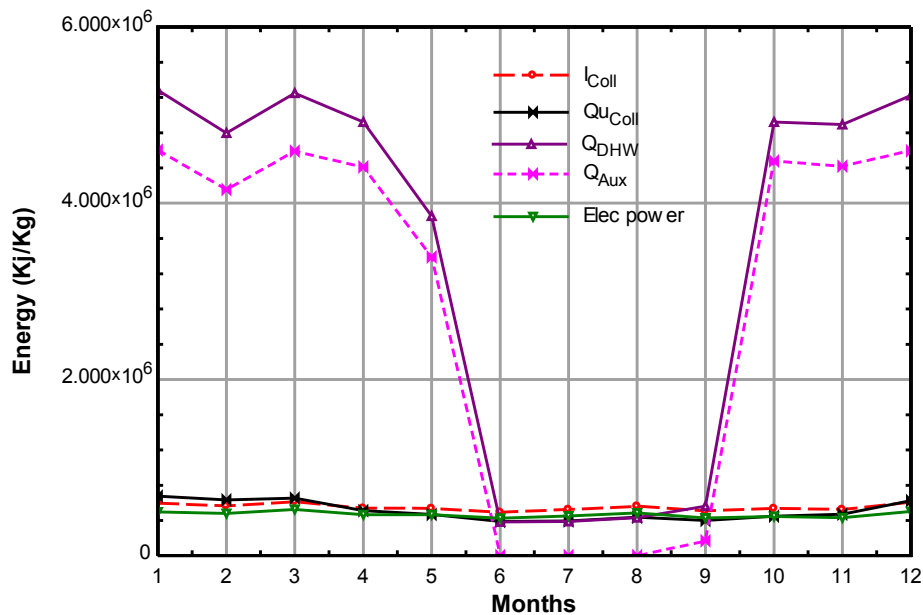
Figure 35: The annual variation of energy generated by the VIPV/T

The annual variations of efficiencies are as shown in figure 36. The mean thermal, electrical, exergy and primary energy saving efficiencies were found to be 18 %, 11 %, 29 % and 27 % respectively.

The overall energy efficiency was 29 % and solar fraction of 39 %. Most notably significant was the solar fraction which in some months between June and August was at

92

100 % during which the corresponding auxiliary energy required was zero. This was attributed to the fact that the skies were clear and less humid during this period allowing more direct and less diffuse radiation to reach the VIPV/T collector surface.
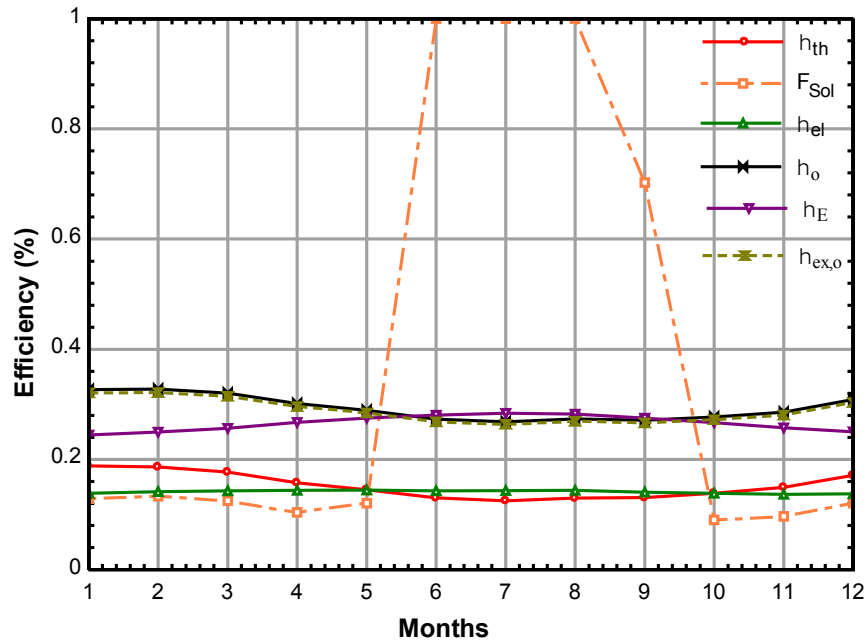
Figure 36: The annual variation of efficiencies of VIPV/T

3.6 Chapter summary

In summary, this chapter presented detailed simulation studies on the VIPV/T module compared to the PV/T counterpart inorder to establish the effect of the vacuum envelope insulation on the performance in terms of energy generated and efficiencies. The VIPV/T and stratified storage tank thermal models were developed and implemented in the system's simulation model in TRNSYS software based on an eight occupant residential building application. The simulation runs were performed on the model from which varying results were obtained and discussed in details. A sensitivity analysis was also performed to obtain the optimal collector inclination slope to be implemented in the experimental study.

In relation to these studies, the modelling and simulation results were then verified by conducting an experiment using the similar VIP/T and PV/T collectors connected with various components modelled as presented in the next chapter.

CHAPTER 4

EXPERIMENTAL STUDY

4.1 Introduction

The performance of solar systems varies as a function of the meteorological conditions of a particular location. In order to establish the actual performance characteristics of the hybrid Vacuum Insulated Photovoltaic/Thermal (VIPV/T) system, it was necessary to perform experiments and obtain real, reliable and practical data in comparison to the conventional hybrid Photovoltaic/Thermal (PV/T). These data were then further processed and used as a benchmark for simulation. In this Chapter, the experimental set-up is extensively covered, equipment and materials are categorically listed and described, procedures followed are stipulated, results obtained are analysed and conclusions drawn appropriately.

4.2 Aims and objectives of the experiment

The main aim of the experiment was to investigate the performance characteristics of a hybrid VIPV/T flat-plate collector compared to conventional Photovoltaic/Thermal (PV/T) with air-gap. In order to do this, the following were specific objectives:

- To measure the current and voltage outputs of the VIPV/T and PV/T at specified regular intervals during sunshine hours and determine the electrical power.
- To measure the temperatures of water at inlets and outlets of the VIPV/T and PV/T collectors, mean and nodal temperature distribution in the storage.
- To calculate and compare the thermal and electrical efficiencies for both the VIPV/T and PV/T collectors respectively.
- To assess the effect of vacuum insulation on the thermal and electrical performance of PV/T.

4.3 Materials and Equipment

The materials and equipment used in the experiment were: Vacuum Insulated Photovoltaic/Thermal (VIPV/T) conventional Photovoltaic/Thermal (PV/T), water storage tank, battery, charge controller, water circulation pump, Data logger, thermocouples and

multimeter. The detailed descriptions of these components are further described below in the following sections.

4.3.1 The Flat-plate Hybrid VIPV/T and PV/T collectors

The main component in this study was the PV/T collector used to convert solar radiation into thermal and electrical energy. Two hybrid PV/T collectors (PowerTherm brand, obtained from Solimpeks Corporation, Turkey) were used in the study: one conventional PV/T with air layer insulation and the other one, modified with a low pressure vacuum insulation envelope of $<1bar$, between the glazing and PV cells. The vacuum was created by use of a vacuum pump (vacuum cleaner) connected to a pressure gauge to monitor the pressure. To maintain the vacuum pressure and ensure no leakage, the edges were further reinforced with an extra EPDM sealing. This concept gave rise to a hybrid vacuum insulated photovoltaic/thermal (VIPV/T) module. The need for PV cells' encapsulation for the VIPV/T was eliminated due to the inclusion of the vacuum envelope, which formed the basis of this study. The other geometric, physical and operational parameters were identical. The basic structural configuration of the collectors is as shown in figure 37. The collectors consisted of PV module attached to a thin copper sheet-and-tube heat absorber plate. The tubes were of riser and header rail configuration of $12mm$ and $22mm$ respectively. The underside was insulated with fibre wool and encased in an aluminium frame. The technical specifications are detailed in table 4.
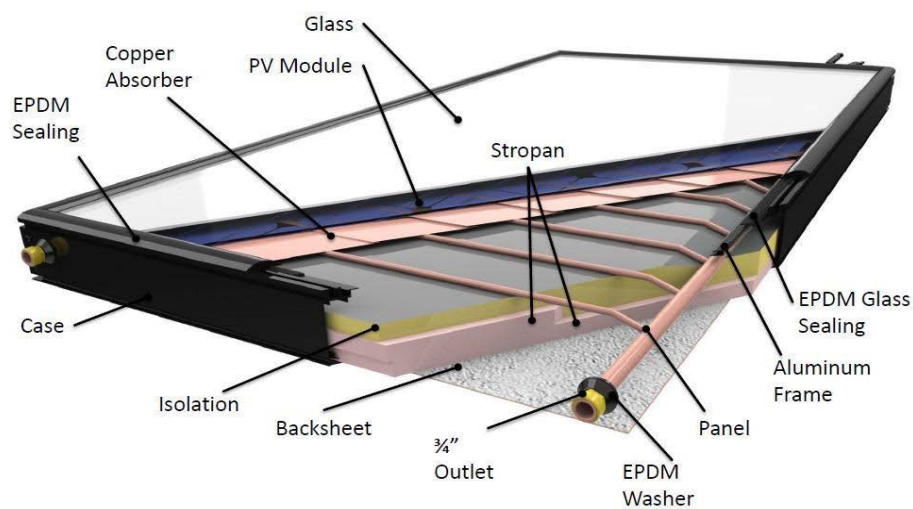
Figure 37: Cut way section of hybrid PV/T collector

95

Table 4: VIP/T and PV/T collector specifications

Collector Property	VIP/T	PV/T
Collector dimensions	1.640 m × 0.87 m × 0.105 m	1.640 m x 0.87 m x 0.105 m
Collector area	1.42 m^2	1.42 m^2
Collector slope	35°	35°
Absorber type	Sheet and tube	Sheet and tube
Absorber Plate thickness	0.001 m	0.001 m
Absorber Plate material	Copper	Copper
Internal piping	Copper	Copper
Riser tube diameter	0.012 m	0.012 m
Riser tube thickness	0.007 m	0.007 m
Header tube diameter	0.022 m	0.022 m
Header tube thickness	0.008 m	0.008 m
Number of tubes	14	14
Tube spacing	120	120
Sealing	EPDM rubber	EPDM rubber
Plate-tube attachment	Ultrasonic welding	Ultrasonic welding
PV module power	180 W	180 W
PV cell type	Mono-crystalline	Mono-crystalline
PV cell dimension	0.125 m × 0.125 m	0.125 m × 0.125 m
No. of cells	72	72
PV cell encapsulation	Non-encapsulated	Encapsulated (0.002 m glass)
Packing factor	1.0	1.0
Top insulation medium	Vacuum	Air
Bottom insulation material	Fibre wool	Fibre wool
Insulation thickness	0.05 m	0.05 m
Glass cover	0.004 m low iron tempered	0.004 m low iron tempered

4.3.2 Water storage Tank

The storage tank was necessary to hold hot water which was not required for immediate use. A 100l volume, 600 kPa dual tank from Kwikot was used because of its flexibility in mounting positions e.g. both horizontal and vertical. The tank was South African Bureau of Standards (SABS) approved 600 kPa pressure vessel fitted with pressure relieve valve, vacuum breakers, drain cock and multi-valve for regulating the flow and inlet water pressures. The inner cylinder was made of thermo-fused porcelain enamel for hygiene and high endurance. The outer surface was entirely insulated against heat loss using fibre wool.

4.3.3 The Battery

In a typical solar energy generation system, specialised batteries are used to store electrical energy for use in non-sunshine hours. The capacity, number and type of batteries used depend on the size and application of the system. For this study, the intended application of the solar system was to drive the circulation pump and light load domestic appliances which implied repeated charge-discharge cycles, therefore, 100Ah deep cycle type was preferred. A regulated valve sealed lead acid rechargeable battery shown in figure 38 (a) was used. During the experiment, the battery was secured on a wooden step beneath the frame as shown in figure 38 (b). The technical specifications are listed in Appendix C, table C.1.

(a) 100Ah battery   (b) Battery Installation

Figure 38: The solar battery and its installation

4.3.4 Circulation pump

A 12 volts DC light duty pump shown in figure 39 (a) was used in the experiment to circulate water through the system as set up in figure 39 (b). It was fitted with an inbuilt on/off operational control that prevented dry running and also regulated the water flow rates with respect to the varying PV module temperatures. The technical specifications are shown in Appendix C Table C.1.

(a) Pump   (b) Pump installation

Figure 39: The solar pump and its installation

4.3.5 Charge controller

The solar charge controller received the electrical energy output from the PV/T and VIPV/T array, regulated it and only permitted the proportionate amount to charge the battery. The TRISTAR-45 charge controller shown in figure 40 (a) was used in the experiment as connected in figure 40 (b) because, besides National Electric Code (NEC) and SABS compliant, it had full protection with automatic and manual recovery, up to seven charging or load programs chosen with DIP switches, with the ability to connect to a PC via an RS-232 port, perform self-testing with fault detection and a battery voltage sensor. Optional features include digital meter and remote battery temperature sensor. The technical specifications are shown in Appendix C Table C.1.

(a) Controller   (b) Controller connection

Figure 40: The TRISTAR solar charge controller and its installation

4.3.6 Thermocouples

Thermocouples are devices made of two dissimilar metals fused together configured to measure temperatures. They are self-powered temperature sensors standardized against a

98

reference value, usually 0^oC. The type-K thermocouples shown in figure 41 (a) were used in this experiment to measure temperatures at inlets, outlets and surfaces of VIPV/T and PV/T collectors in addition to internal temperatures of the tank because of their high sensitivity to slight changes in temperature, lower cost and connectivity to a data logger enabling continuous measurements. Their installation on horizontal, vertical and tanks are as shown in figure 41 (b), figure 41 (c) and figure 41 (d) respectively.

(a) Type-K thermocouple pipe   (b) Thermocouple on horizontal pipe

(c) Thermocouple on vertical pipe   (d) Thermocouple on water tank

Figure 41: The Type-K thermocouple and its installation for water temperature measurements

4.3.7 Data logger

A DT80 DataTaker digital data logger was used for data acquisition because of its robustness, low power consumption and capability of being used as stand-alone. It also provided a simple and straight forward interface with an in-built, 18-bit resolution digital display and USB port. It logged, scaled and returned temperatures, currents, voltages, resistances, frequencies, strains and stresses in engineering units using *dlogger 5* platform

99

in the dEX software. The configuration of the DataTaker is shown in figure 42 while the technical specifications are summarised in the Appendix C Table C.1.

Figure 42: DT80 DataTaker configuration

4.3.8 Weather station

The weather parameters were measured at the University of Kwazulu-Natal, Howard College weather station located on top of Desmond Clarence building. This station shown in figure 43 is South African Universities Radiometric Network (SAURAN) accredited and having instruments which are calibrated regularly. The parameters of interest to this experimental work were solar radiation (irradiance), wind speeds, air temperatures and relative humidity which were measured using the equipment listed in table 5.

Figure 43: The University of Kwazulu-Natal weather station

Table 5: The weather parameter measurement equipment

Parameter	Equipment	Sensitivity factor
Irradiance (W/m^2)	Thermopile SPN1 pyranometer	0.1
Wind speeds (m/s)	R. M. Young Sensor	0.75
Relative Humidity (%)	Campbell Scientific CS215 Sensor Inputs	
Air Temperatures (^oC)	Campbell Scientific CS215 Sensor	

Since solar radiation was the main primary source of energy for the system under study, the thermopile SPN1 sunshine pyranometer was further singled out for detailed description and specifications in order to ascertain the degree and accuracy of measurement.

4.3.8.1 Sunshine Pyranometer

Solar radiation was the primary source of energy for the system under study, therefore, it was important to monitor and record the respective radiation levels of the location for the duration of the experimental study. An SPN1 sunshine pyranometer installed on top of Desmond Clarence building, University of Kwazulu-Natal was used to measure both the direct and diffuse solar radiation. This type is comparably easy to install and use; needs no routine adjustment or polar alignment and works at any latitude with in-built heater, designed for long-term outdoor exposure. The pictorial representation is in figure 44 and the technical specifications are summarized in Appendix C Table C.1.

Figure 44: The SPN1 sunshine pyranometer

4.4 Experimental set up

The experiment was carried out under varying outdoor climatic conditions of the University of Kwazulu-Natal, Durban ($-29^o27^{'}S$, $30^o95^{'}E$, 8m), in the republic of South Africa in the month of August, year 2014 in accordance and compliance with ISO 9806-1:1994 standard for solar systems. This standard requires, among other provisions that:

101

- Solar radiation must be greater than 800 W/m^2
- Wind speed at the time of the experiment be within the range of 2-4m/s.
- Fluid flow rate be 0.02 kg/sm^2.
- To minimise errors, a temperature rise of at least 1.5K be attained between the logging intervals.
- Angle of incidence of direct radiation be within ±2 %of normal incidence angle.

To ensure complete adherence to the above provisions, the experiment was run for a period of 10 days under distinctively different weather conditions. The results for 22/08/2014 was found to perfectly match the stipulated requirements of ISO 98061:1994, hence were used for analysis. This period fell within the winter season and was suitably preferred due to the associated clearness of the sky. On this date, the sun rose at 06:23 hours and set at 17:38 hours, giving a total of 11.59 hours of sunshine.

The various components were assembled onto a mobile support frame for mobility and easy positional adjustment. The angle of inclination was fixed at optimum level of 35° previously established by the simulation in Chapter 5. The plumbing works were accomplished using 22 mm copper tubes and associated fittings with the hot water side lagged to reduce heat losses to the environment. The water storage tank was laid horizontally for ease of water draw and stability of support structure.

The VIPV/T and PV/T collectors were laid side by side and connected in parallel with their outlets discharging to the tank to ensure complete independence on each other. The temperatures at the inlets and outlets of the modules were measured by use of type-K thermocouples and logged on to the DataTaker DT80. The electrical terminals were connected via a combiner box to the charge controller. The currents and voltages from each panel was measured and logged separately. The data logged were transferred to the computer for storage and further analysis at the end of each day. A simplified schematic diagram showing the hardware components and their connections, the water flow, electrical terminals, temperature measurement points and controls is shown in figure 45.
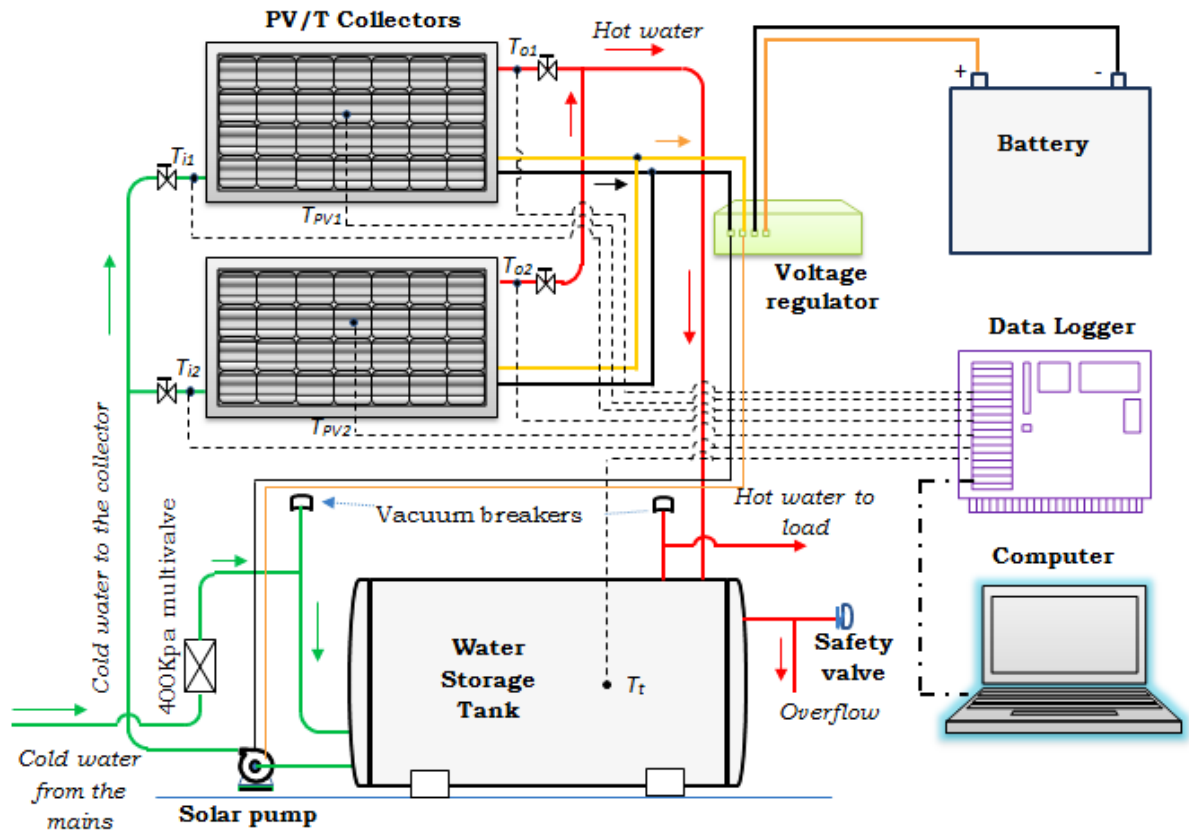
Figure 45: Schematic diagram of the experimental set up

The TRISTAR-45 charge controller was installed indoors and configured with an algorithm to charge and monitor the State of Charge (SOC) of the regulated valve lead acid deep cycle battery. A 300 *W* inverter was connected to the battery to convert DC to AC and supply power to the loads which would discharge the battery in readiness for another charge cycle.

In order to attain considerable difference in temperatures, the measurements were configured to be logged at intervals of 15 minutes; a time lag that was good enough for solar energy to make considerable change in temperatures. For voltages and currents, this interval was insignificant since they varied in the order of milliseconds but were logged at the same instances with the temperatures for assessment of efficiencies.

The pictorial representations of the front and rear views of the set up are as shown in figures 46 and figure 47 respectively.

Figure 46: The front view of the experimental set up

Figure 47: The rear view of the experimental set up

4.5 Experimental procedure

The experimental procedure was structured to include assembling the apparatus, calibrating the thermocouple and configuring the data logger. All the steps followed in conducting the experiment have been highlighted in this section.

4.5.1 Assembling the apparatus

The assembly of the experimental set-up was accomplished using the following procedures:

- The support frame was designed, fabricated and assembled by firmly tightening the bolts and nuts at each joint.
- The water storage tank was then mounted on the base as can be seen from figure 47 and figure 48.
- The VIPV/T and PV/T panels were mounted on the frame, cushioned with self-adhesive rubber sponge to avoid metal to metal contact. The VIPV/T was on the lower side and the PV/T on the upper frame.
- Plumbing works for the water circulation system was made using 22mm diameter copper pipes joined by removable compression elbow and tee fittings that could be easily removed when disassembling. The pump was also securely mounted and connected to the pipeline at this stage.
- Electrical cords were connected to the power distribution lines using male and female couplers. The power lines were connected to the voltage regulator power input terminals.
- The battery was connected to the voltage regulator via output terminals. A temperature sensor and battery SOC sensor were also connected in their respective ports. The circulating pump power cables were then connected to the battery's positive and negative terminals.
- The system was completely filled with water from the municipal mains.
- The DT80 data taker was configured as explained in the following section and then connected to the thermocouple probes, voltage and current relaying cables and power source.
- The calibrated type-K thermocouples were connected to the respective temperature measurement points on the water circulation pipes and storage tank.

- Once everything was connected and the system fully filled with water, the pump was started to cause circulation of water and the system was ready to function and log measurements as programmed.

4.5.2 Calibrating the thermocouples

To ensure accuracy of the thermocouples, it is always recommended that they be calibrated first before use to bring the probes to a common reference temperature and for setting their sensitivity levels.

To do this, a simple procedure outlined below was followed:
- The thermocouple probes were immersed in a container filled with water heated to 30^oC. The ends of the thermocouples were connected to multimeter leads from which a voltage of $1\mu V$ was measured for each.
- With the junctions of the thermocouples immersed in water, the voltage was allowed to stabilize and was recorded i.e. when there were no more voltage fluctuations.
- The water temperature was increased to 35^oC and the process repeated, for every 5^oC increase interval until 60^oC.
- The room temperature was measured using a mercury thermometer and the voltage for type K thermocouple at room temperature checked in the recommended thermocouple guide published by the National Institute of Standards and Technology (NIST).
- The voltages recorded at each temperature point were then compared to the thermoelectric voltages in mV provided by the NIST as shown in Table 6.

Table 6: Thermocouple calibration

Temperature (^{o}C)	Thermoelectric voltage (mV)		
	Measured voltage	NIST Ref. Voltage	% Error
30	1	1	0.00
35	1.406	1.407	0.071
40	1.612	1.612	0.00
45	1.816	1.817	0.055
50	2.021	2.023	0.099
55	2.231	2.230	-0.044
60	2.434	2.436	0.082
65	2.645	2.644	-0.038
70	2.852	2.851	0.035

4.5.3 Configuring the data logger

The DT80 DataTaker obtained from the Department of Mechanical Engineering of UKZN was upgraded to the latest series of firmware obtained from the manufacturer's website. To configure the DT80 DataTaker, the dEX family of software was first loaded on to a computer from which the logging was controlled. The dlogger d5 program was launched to access the properties through the connection menu. In the connection dialogue box, network tab was chosen where new connection name, IP address and port number were filled then accepted.

To check and confirm the status of the connection, the DataTaker menu was selected under which a self-test run was activated and status report given confirming the connection to the PC. Once connection was confirmed, the configuration and connection of the thermocouples, current and voltage sensor probes were then done.

The thermocouples were connected to the DataTaker analogue channels 1,2,3,4 and 5 and programmed to measure temperatures at 15 minutes intervals. The temperatures were designated names Temp 1, Temp 2, Temp 3, Temp 4 and Temp 5 for inlet 1, inlet 2, outlet 1, outlet 2 and tank temperatures respectively. The K-type, two-wire thermocouples with red and yellow probes were connected to the negative and positive terminals respectively of the DataTaker.

The logging window presented a default label value of R1, temperature chosen as signal type, default type as TK thermocouples and the respective channels chosen through wiring tab. Once this was done, the send-to-connection tab was activated via the program menu until a clicking sound was produced to show that it was ready to start logging.

4.6 Experimental results and discussion

During the experimental period, various values of data were obtained from measurements of weather parameters, temperatures, voltages as well as currents. These data were then analysed and used in evaluating performance characteristics of the VIPV/T compared to PV/T. The results are analysed and discussed in the following section.

4.6.1 The weather parameters

The climatic characteristics of a given location determine how much solar energy can be harnessed and converted into meaningful use. The most important parameter of this study was solar radiation which provided the primary energy source. However, its propagation is affected by parameters such as relative humidity, wind speeds and ambient air temperatures.

These parameters were logged and recorded at the University of Kwazulu-Natal weather station which is part of the South African Universities Radiation Network (SAURAN) and their profiles plotted to show the trend of variation during the test period.

The variation of solar radiation during the experimental period is presented in figure48from which it was observed that the maximum value recorded was 862.53 W/m^2 occurring at 12:00 (noon).
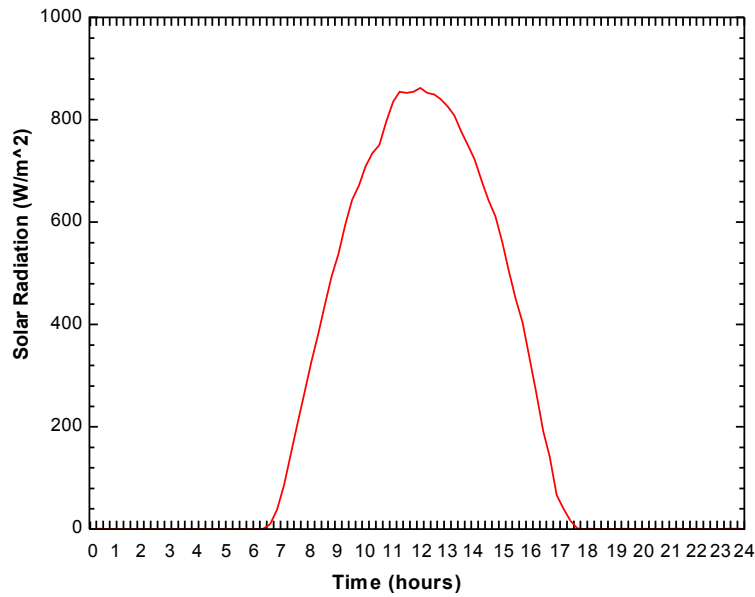
Figure 48: The variation of solar radiation during the test period 22nd August 2014

The environment in Durban is highly humid as can be seen in figure 49. The variation in relative humidity recorded on the day was 93.2 %maximum and 65.41 %minimum.
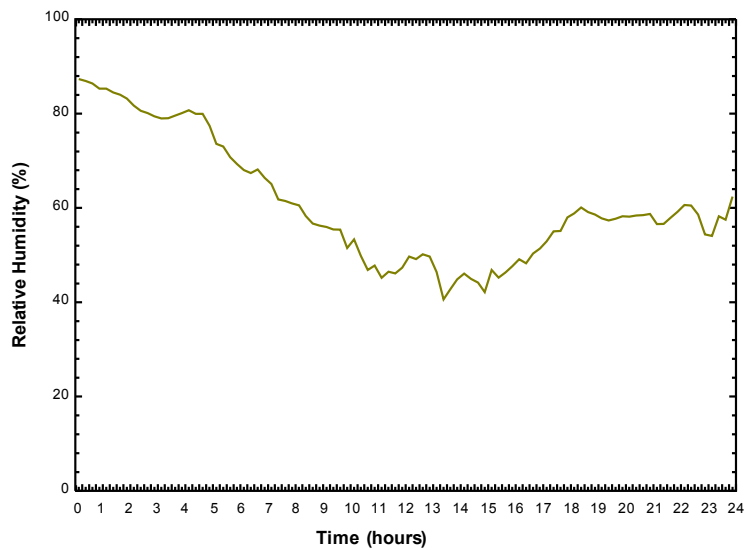
Figure 49: The variation of relative humidity during the test period 22nd August 2014

Ambient air temperature plays a crucial role in determining the conversion efficiency of the collector. The hourly variation of ambient air temperature is shown in figure 50from which it can be observed that maximum and minimum values were $23.46^{o}C$ and $17.78^{o}C$ respectively.

109
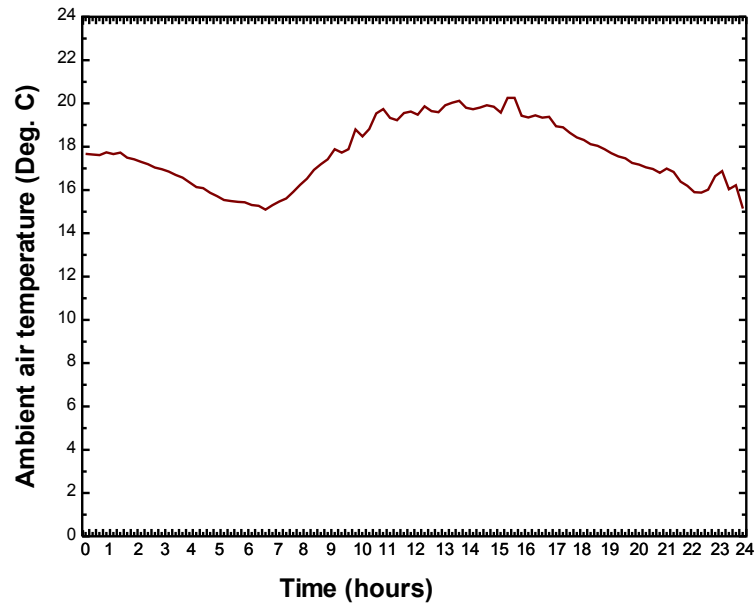
Figure 50: The variation of ambient air temperatures during the test period on 22nd August 2014

In order to evaluate heat losses through the top of the collector, the variation of wind speeds must be monitored. From the wind speed variation profile shown in figure 51, the highest and lowest values were 4.66 *m/s* and 0 *m/s* respectively while the mean speed was 2.17 *m/s* which is within the acceptable range as stipulated in Section 6.4.
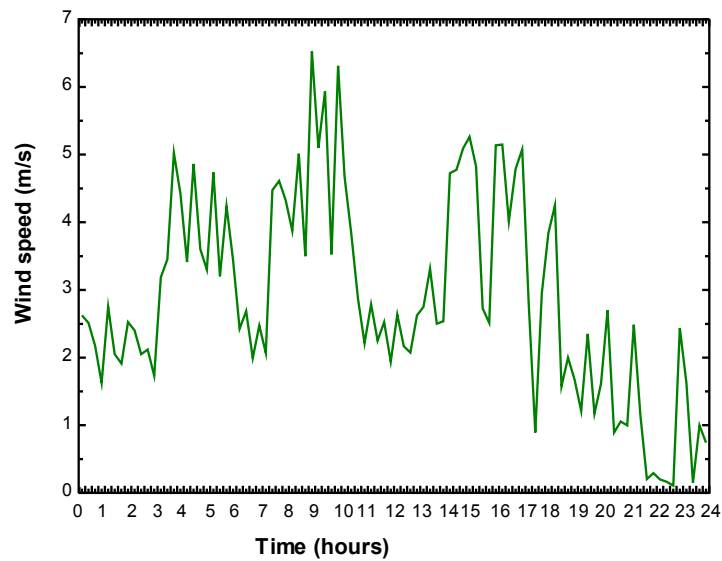
Figure 51: The variation of wind speeds during the test period on 22nd August 2014

It should be generally noted that these values were measured and recorded in a 24 hour daily interval. However, for experimental analysis, only values that corresponded to the sunshine exposure hours were considered, most notably, from 7.30am to 17.30pm.

110

4.6.2 The daily thermal performance

In evaluation of the thermal and electrical performance of the VIPV/T weighed against PV/T, a variety of constants, measured and calculated variables were used. The constants and measured variables are listed in tables A.1 and A.2 shown in Appendix A. The numerical formulas highlighted in Chapter 4 were applied in evaluating the various performance indicators. The useful heat energy, hot water temperature profiles, thermal and electrical efficiency curves for both modules were plotted and compared in the next section.

4.6.2.1 Useful energy

The thermal performance of a solar collector is greatly dependent on its ability to produce water at elevated temperatures. The rise in temperatures is as result of heat absorption which constitutes useful heat (Q_u) after all the losses have been accounted for. The variation of Q_u generated by the modules was evaluated and results plotted as shown in figure 52. The VIPV/T generated 16.09 % more useful heat energy than the PV/T counterpart with daily individual values of 5,376kJ/kg and 4,652.8kJ/kg respectively. The highest instantaneous values of Q_u attained for the day were 208.87kJ/kg and 183.12kJ/kg respectively. However, these values could vary depending on the solar radiation.
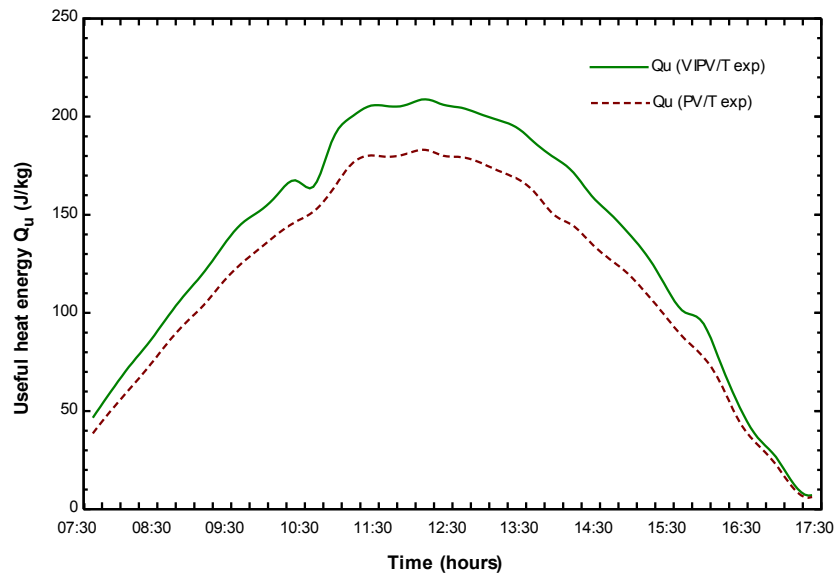
Figure 52: The hourly variation of useful heat

4.6.2.2 The water temperatures

The water temperatures were measured at both inlets and outlets of the modules in order to establish the change. The modules were fed through a common inlet at equal temperatures and discharged at different outlets to the storage tank.

♦ **Inlet and outlet water temperatures**

As can be observed in figure 53, while both modules had the same inlet temperatures, the VIPV/T and PV/T attained their maximum temperatures of 57.97^oC and 52.02^oC respectively at around 12.00 noon. On average, the former realised an additional 12.8 % increase in water temperature. The superiority of VIPV/T over PV/T can also be shown in terms of heating rates; for instance, a temperature of 45^oC was realised at around 9.00am and 9.45am for VIPV/T and PV/T respectively, an indicator that the former took shorter time to realise a higher temperature than the latter. At the end of the measurement duration, both the VIPV/T and PV/T discharge water at around equal temperature of 27^oC.
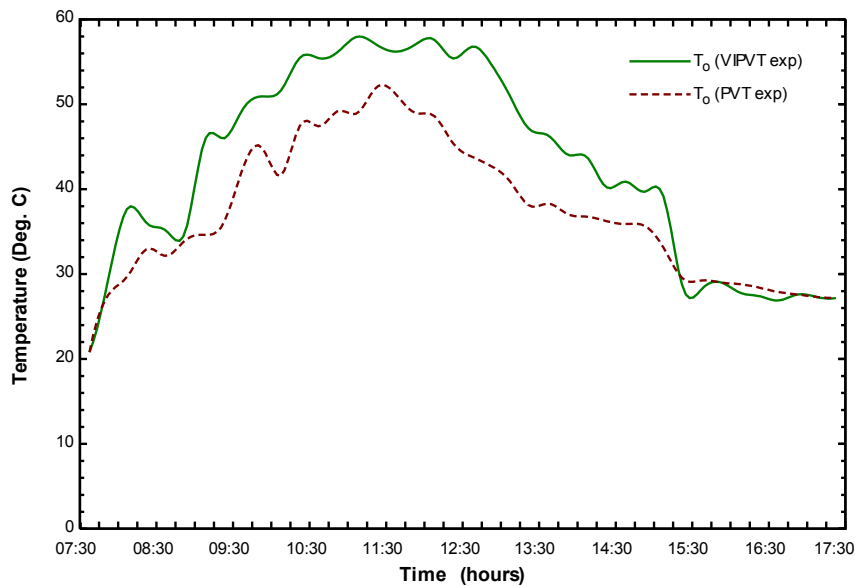
Figure 53: The water temperature profile for VIPV/T and PV/T

♦ **Average PV cell temperatures**

The main purpose of the absorber plate in a hybrid solar collector is to absorb the residual heat rejected by the PV cells. In the process, the plate temperatures rise and heat water circulating in the tubes attached beneath the plate. The plate temperature is a critical parameter in assessing the thermal performance of the modules, because this dictates the degree to which water is heated.

112

It is often tedious to measure the temperatures at every point on the plate; therefore, a mean value calculated using equation A.4 was used in the analysis. The variation of mean plate temperatures were plotted for both VIPV/T and PV/T as shown in figure 54.The maximum values obtained were 181.75^oC and 172.39^oC respectively. It was however noted that these temperatures could only heat water to59.91^oC and 56.02^oC respectively because only $8mm$ along the length of each tube was in contact with the absorber plate surface.

Since the PV cells were directly embedded on the top surface of the absorber plate, they were subjected to the same mean temperatures as the plate. These temperatures required high degree of controls to avoid high stagnation temperatures that would damage the cells. This necessitated the need to remove the cell encapsulation.
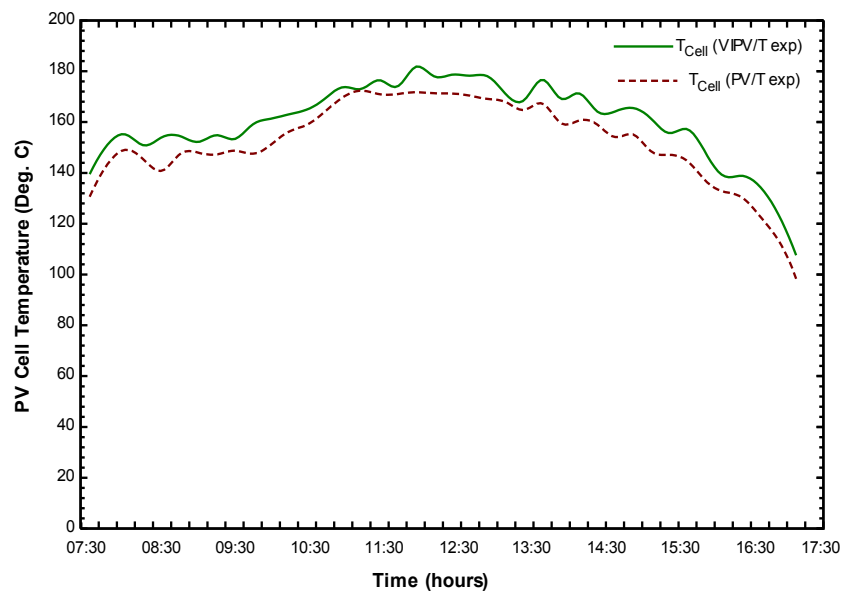
Figure 54: The variation of mean PV cell temperatures

♦ **The water storage tank temperatures**

The storage tank was mounted in a horizontal orientation at the base of the support frame as indicated in figures 56 and figure 57. Even though there could have been some degree of stratification, for the purpose of this experiment, the tank was considered to be fully mixed. Cold water inlet and outlets were located at lower levels than the hot water inlet and outlet as shown in figure 55. The tank was initially filled to capacity with water which was pumped to the inlets of the collectors and circulated back to the tank at raised temperatures. Both the VIPV/T and PV/T discharged hot water to a common tank inlet.

The tank water temperature T_t was measured at the centre of the tank and taken as the average. The temperature values were plotted as shown in figure 55, from which it can be seen that there was a steady increase in water temperature to a maximum of 56.95^oC at around 2.00pm before falling gradually due to the reduction in solar radiation intensity. Due to the properties of the tank described in Section 6.3, the tank was able to maintain water temperatures at about 49^oC by sunset at around 17.30pm, hot enough for domestic applications.
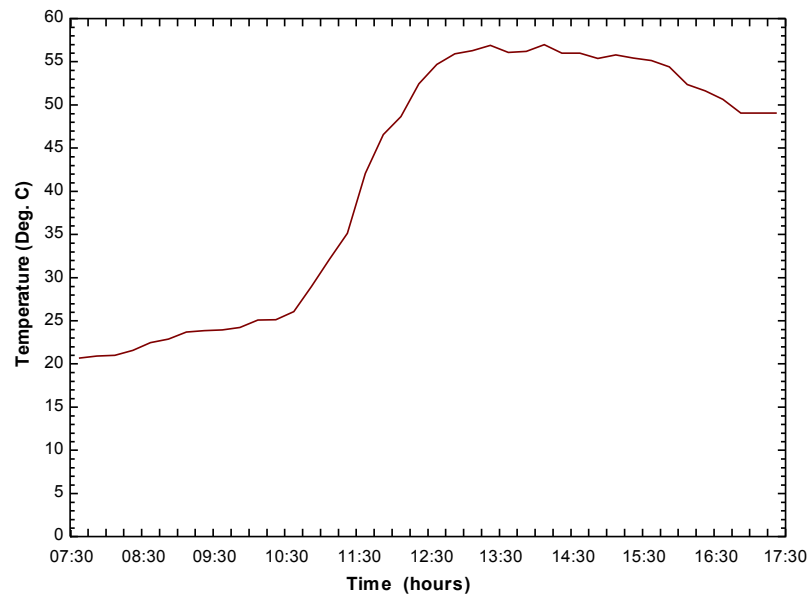
Figure 55: The water temperature profile for VIPV/T and PV/T

4.6.2.3 Efficiencies

The variations of thermal, electrical and overall efficiencies were plotted as shown in figure 56. It can be generally observed that the VIPV/T gave a superior thermal performance compared to the PV/T.

The mean thermal efficiencies were 15.91 % and 13.71 % for VIPV/T and PV/T respectively. This presented an increase in thermal efficiency of 16.01 %. These values demonstrated that the vacuum envelope inclusion positively affected the thermal performance. The difference in thermal efficiency was attributed to the fact that the vacuum envelope offered additional thermal resistance to the radiative heat loss through the top side of the module. There was also significant reduction in heat loss through the top as registered by the thermal loss coefficient for the top (U_t). However, it should be noted that the vacuum envelope geometry was kept constant during the study.
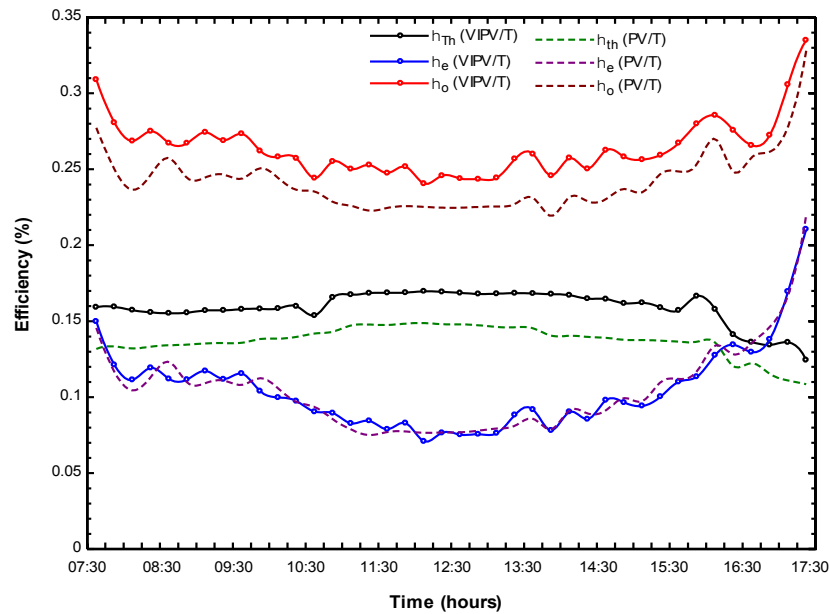
Figure 56: The variation of thermal and electrical efficiencies

The individual mean electrical efficiencies achieved for both the VIPV/T and PV/T were 10.53 % with a marginal increase of 0.28 %. The electrical efficiency curves were observed to be highest at the morning and evening, while sagging at around noon when solar radiation and subsequent rise in temperatures were at their highest. This demonstrated the temperature dependence on electrical efficiency. At sunset after 17:00 hours, the electrical efficiency was seen to shoot up beyond the maximum rated value for mono-crystalline cells. This was because the voltage regulator was drawing power from the batteries since there was no more solar energy. Values measured past this time, were approaching 100 %.

The overall efficiencies as defined by equation 2.35 were evaluated as 26.44 % and 24.25 % for VIPV/T and PV/T respectively, representing an improvement of 9.16 %.

The overall exergy, primary energy saving and Carnot efficiencies were evaluated and plotted as shown in figure 57. The mean overall exergy efficiencies as defined by equation 2.40 were evaluated to be 11.33 % and 11.59 % showing an increase of 2.74 % due to the variation of the Carnot efficiencies which highly depended on the temperature difference between the ambient air and the outlet water of the modules.

On the other hand, the mean primary energy saving efficiencies as defined by equation 2.42 were found to be 20.48 % and 19.63 % for VIPV/T and PV/T modules respectively. This meant that an improvement of 4.25 % was realized.

115

The conventional power generation was taken to be 0.38 %. The change was due to the thermal energy performance improvement which would result in savings of auxiliary energy required for water heating during the non-sunshine hours.

The solar fraction as defined in equation 2.41 was not evaluated since the experimental set-up did not include the measurement of energy used for auxiliary heating. In addition, the experiment was only run during the day when there was sunshine. However, it was included in the simulation as given in Chapter 5.

The Carnot efficiency is not one of the performance assessment indicators but was evaluated and used to assess the exergy efficiencies of the VIPV/T and PV/T modules. The mean values attained were 6.53 % and 5.61 % respectively. Their variations are shown in figure 57.
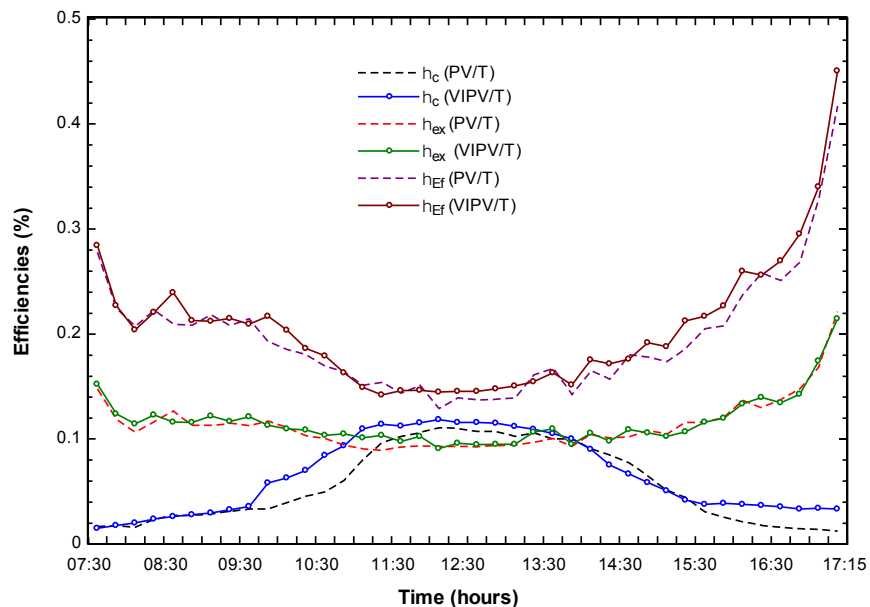
Figure 57: The variation of overall exergy, primary energy saving and Carnot efficiencies

4.6.2.4 Electrical power

To assess the electrical performance of the modules, voltages and currents were measured and logged at the same instances with temperatures. Electrical power generated was calculated for each module from which their efficiencies were deduced. The results of the electrical performance were plotted as shown in figure 58. The variation of voltage and current flows with time were as depicted in figure 58 (a) while power generated was plotted in figure 58 (b). The maximum voltages achieved were $35.44V$ and $35.74V$ for VIPV/T and PV/T respectively while maximum current flows were $4.71A$ and $4.75A$

116

respectively. This implied that the modules operated within 94 % to 90 % of their rated capacity of $36.16V$ and $4.98A$.
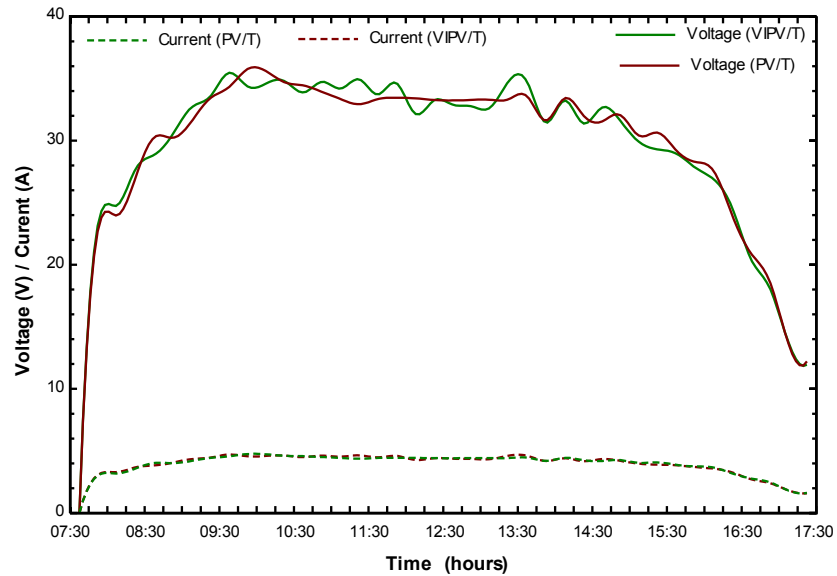
(a) The variation of voltage and currents over time
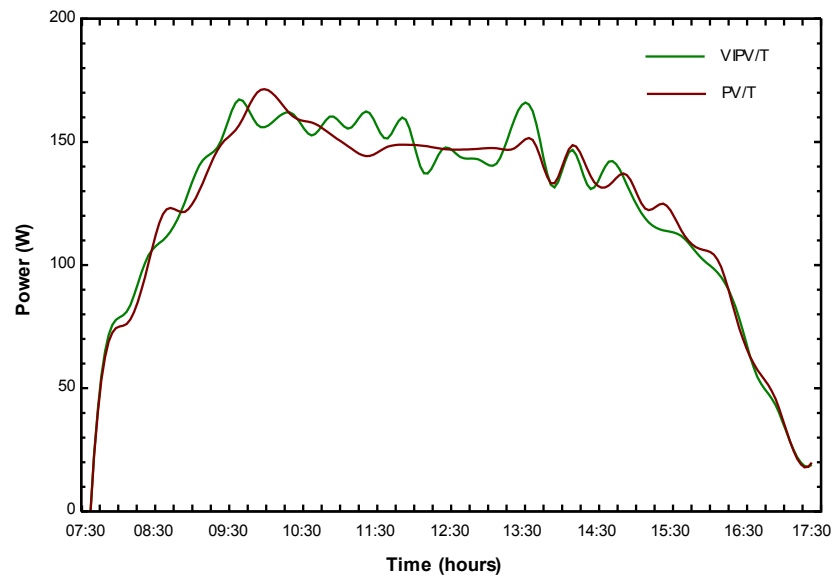
(b) The variation of electrical power generated

Figure 58: Electrical performance of the VIPV/T and PV/T modules

The maximum hourly power generated was $167.10W$ and $169.92W$ from VIPV/T and PV/T respectively while the modules rated power were both 180W. The total power generated within the 10 hour span was $4,851.90W$ and $4,835.66kW$ respectively. For the two modules, $9,687.56kW$ was realised which was adequate to power most of the domestic appliances. The power curves were similar to voltage profile except for the shift by a factor equivalent to the value of currents. It was observed that there was marginal change in electrical power generated.

117

4.7 Chapter summary

In summary, the experiment to assess the effect of vacuum insulation on thermal and electrical performance of the PV/T was largely successful. Placing the hybrid VIPV/T and PV/T modules side by side and subjecting them to the same meteorological conditions allowed for measurements of temperatures, voltages and currents used in evaluating power and heat flows. It was demonstrated that the VIPV/T gave a superior performance relative to conventional PV/T.

It was deduced that the vacuum inclusion resulted in thermal efficiency improvement by about 16.01 % while electrical efficiency remained largely the same with a difference of 0.28 % even when the PV cell encapsulation was removed. Consequently, the overall efficiency was improved by 9.16 %. The overall exergy and primary energy saving efficiencies also increased by 2.74 % and 4.25 % respectively.

The parameters used in the experiment were implemented in the simulation study in Chapter 5 as previously discussed. To develop an accurate and reliable standardized TRNSYS model for PV/T modules, the experimental results came in handy in validation of the simulation outcomes. In the next chapter, the experimental and simulation results are compared to confirm the degree of conformity or divergence from each other in order to determine the accuracy of the simulation model.

CHAPTER 5

VALIDATION OF SIMULATION AND EXPERIMENTAL RESULTS

5.1 Introduction

In the previous chapters, comprehensive modelling, simulation and experimental studies have been conducted on the hybrid VIPV/T and PV/T systems made of similar components. Simulation models provide results for virtual experiments used to predict performances of a system in a long-term duration; on the hand, experiments provide real results of the system's performance under actual prevailing circumstances. The experimental outcomes of the system were further used to re-tune the model in order to give results similar or close to the actual ones, hence, improve the validity. This chapter outlines the comparison between the simulation and experimental results of hybrid VIPV/T system to ensure functionality, validity and accuracy of the VIPV/T model developed.

5.2 Comparison of model and experimental results

The periods for comparison are based on the experimental hours between 07:30 hours and 17:30 hours of the 2nd August 2014. The most important performance characteristic parameters compared were:

- The thermal energy output, including the hot water and PV cell temperatures and useful heat energy generated.
- The efficiencies including thermal, electrical, overall energy, overall exergy and primary saving efficiencies.

5.2.1 Thermal energy outputs

The thermal outputs for the VIPV/T were compared in order to establish the performance in terms of useful heat output, out let (hot) water temperatures and the average PV cell temperatures which together had an effect of the performance, these quantities are analysed in the is section.

5.2.1.1 Useful heat

The comparison between the simulated and experimental useful heat were as shown in figure 59. The simulated results were represented by dashed lines. As can be seen, there was an average variation between simulated and experimental values of about 1.22 % and 1.53 % for VIPV/T and PV/T respectively. This deviation was within the acceptable limits of below 5 % as stipulated in the ISO 9806-1:1994 and compares well with the findings of Da Silva et al.,[31]. The maximum values attained for experimental and simulation studies were 208.87J/kg and 212.41J/kg for VIPV/T and 183.2J/kg and 187.17J/kg for PV/T respectively. However, the daily total values were almost the same for both systems at 5,376J/kg and 5,385.4J/kg (VIPV/T); 652.8J/kg and 4262.2J/kg respectively.
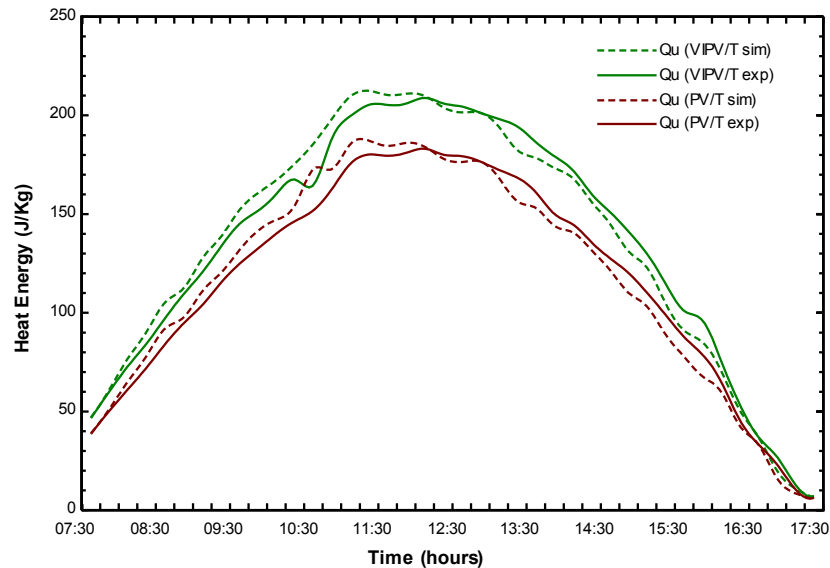
Figure 59: The variation of simulated and experimental useful heat energy transferred to hot water

5.2.1.2 Outlet water temperature

As an indicator of thermal energy output, the outlet water temperatures were measured from each module both in the experiment and in the simulation model. The variation of the outlet water temperatures for simulation (dashed lines) and experimental results were plotted as shown in figure 60. The maximum temperatures attained by VIPV/T during the experiment and simulation were 62.31^oC and 57.97^oC respectively while the PV/T attained 51.83^oC and 52.02^oC respectively. As can be seen, the maximum simulated values occurred at around 11:00 hours while experimental values peaked at around 12:00 hours. The shift was caused by the estimations of the TMY weather files used in the simulation as opposed to the actual measured data for the experiments. In general, the variations

120

between the simulated and experimental water temperatures were 0.4 % and 0.7 % for VIPV/T and PV/T systems respectively. The variation was less than 5 % and was found to satisfy the requirements of ISO 9806-1:1994, upon which Zondag et al., [24] also based his comparison.
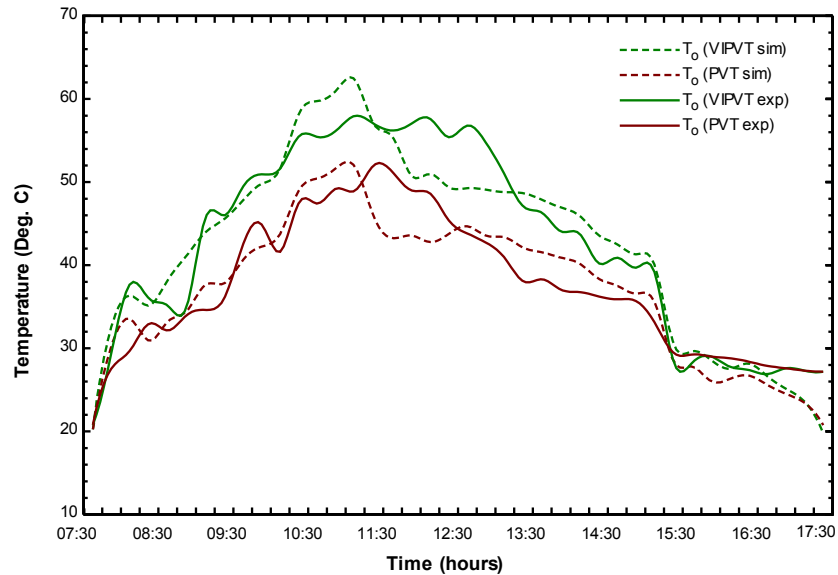
Figure 60: The variation of experimental and simulated outlet water temperatures

5.2.1.3 The average PV cell temperatures

The average PV cell temperature is a very important parameter in electrical performance analysis. It is an established fact that electrical efficiency reduces with increase in PV cell temperatures, therefore, a well-designed hybrid PV/T system must be able to ensure these temperatures are kept as low as possible to keep the efficiencies at sufficiently near maximum levels.

Figure 61 shows the variation of simulated (dashed lines) and experimental average PV cell temperatures for the hybrid VIPV/T as well as the PV/T collectors. The highest values attained by VIPV/T were $179.88^{o}C$ and $181.75^{o}C$ for simulation and experiment respectively, both occurring at 12:00 hours both for simulation and experiment. On the other hand, the PV/T achieved simulated and experimental values of $173.65\ ^{o}C$ and $172.39\ ^{o}C$ respectively occurring at 11:30 hours. Overall, the simulation tallied with the experimental results to the degree of 0.8 % and 1.05 % for the VIPV/T and PV/T respectively. This variation was due to the assumptions made and ideal scenarios used in the simulation which was not the case in the experiment. However, the provisions of ISO 9806-1:1994 standard set at not more than 5 % variation was satisfied.

121
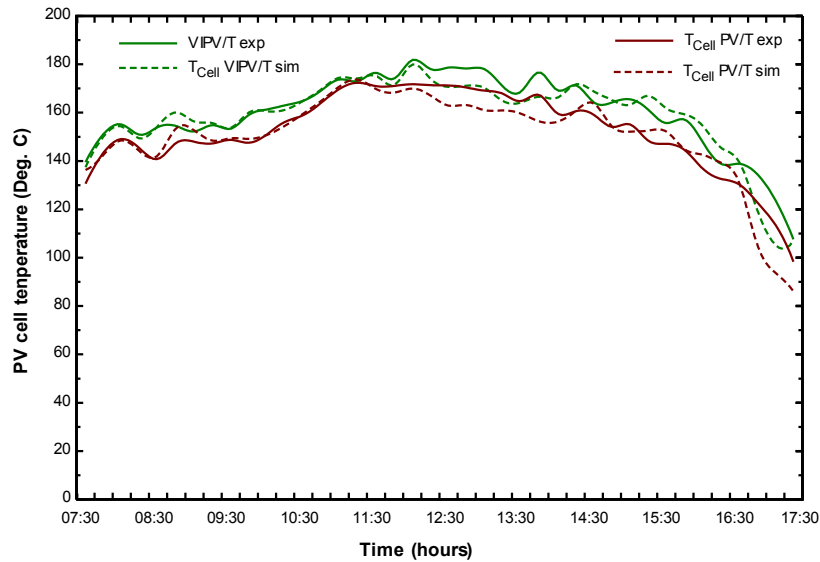
Figure 61: The variation of simulated and experimental average cell temperatures

5.2.2 Efficiencies

The efficiencies for hybrid VIPV/T module obtained by simulation and experiment were compared and plotted as shown in figure 62. The variation between the simulated (dashed lines) and the experimental thermal, electrical and overall efficiencies were 1.05 %, 1.29 % and 3.57 % respectively.
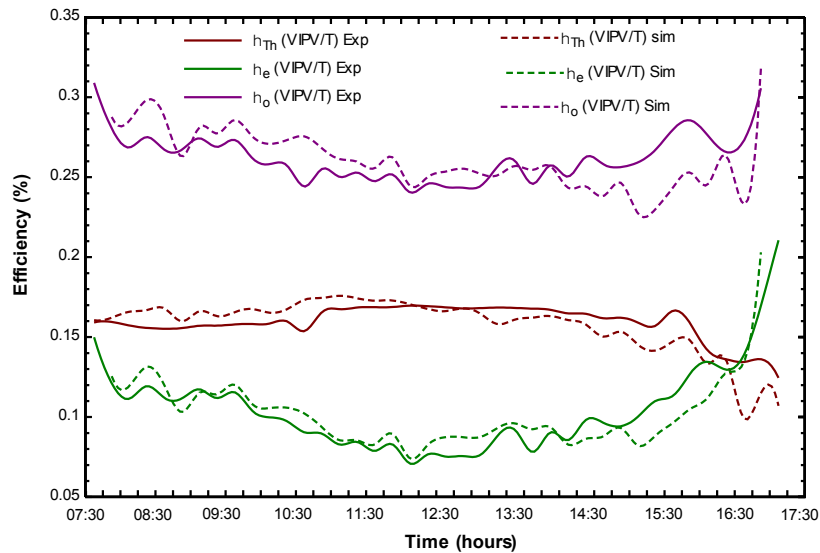
Figure 62: The variation of simulated and experimental thermal, electrical and overall efficiencies for VIPV/T module

The individual simulated average values were 15.7 %, 9.7 % and 25.5 % while experimental values were 15.9 %, 10.5 % and 26.4 % respectively. Again the variations between simulated and experimental efficiencies were within the allowable tallying limits.

122

Figure 63 presents the variation of exergy and energy saving efficiencies for the hybrid VIPV/T collector. As can be seen there was a narrow gap of 3.6 % and 2.8 % between the simulated (dashed lines) and experimental values for exergy and energy saving efficiencies respectively. The average values as obtained for exergy efficiency were 10.9 % and 11.7 %, while, energy saving efficiencies were 19.48 % and 20.48 % by simulation and experiment respectively.
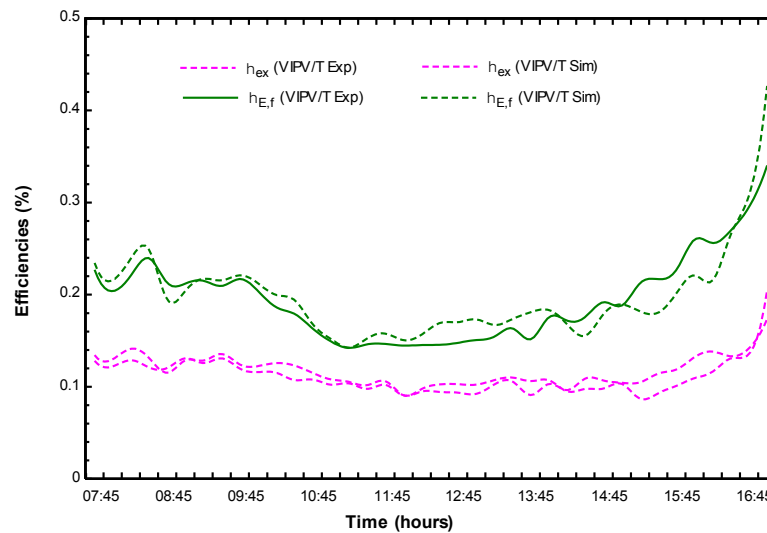
Figure 63: The variation of simulated and experimental exergy and primary energy saving efficiencies for VIPV/T module

5.3 Chapter summary

In summary, the results of the simulation and experimental studies have substantively been compared and analysed with relevant observations in this chapter. The variation deviations between the respective simulated and experimental results have been shown to vary in the range of 0.4 % to 3.6 %. These were attributed to the various assumptions made for simplification of the simulation. Additionally, the major contributor to the deviations was the difference between the predicted (TMY weather data) and the actual (measured weather data) file used for simulation and experiment respectively. However, these variations were well within the acceptable limits of 5 %as stipulated in ISO 9806-1:1994 standard. It was also found to be comparable to the findings of Zondag et al., [16] [24] and Da Silva et al., [31] .It was concluded that the simulation and experimental results tallied satisfactorily to show the functionality, accuracy and validity of the model developed.

Based on these and other results discussed in the previous Chapters, relevant conclusions were drawn and recommendations made as shown in Chapter 6.

CHAPTER6

CONCLUSIONS AND RECOMMENDATIONS

6.1 Conclusions

Hybrid Photovoltaic and Thermal technology is a novel idea that originated in the 1970's, and has undergone several efficiency improvement modifications. One such modification is the inclusion of vacuum insulation between the glass cover and the PV modules in order to cushion against top side heat loss to the ambient atmosphere. This study has provided an in-depth performance analysis of a hybrid VIPV/T module in comparison to conventional PV/T with air insulation layer by computer simulation and experimental studies. The conventional PV/T with air insulation layer was used as a basis of the study.

Prior to alterations of an existing system or building a new system, it was necessary to optimize the system's performance through simulation studies. This made it possible to minimise the chances of failure to meet specifications, eliminate unforeseen bottlenecks and prevent under or over utilization of resources. To evaluate the performance of a proposed VIPV/T system under different configurations of interest and over prolonged periods of real time, a simulation model consisting of the system parameters, input variables, performance measures, functional relationships and outputs was developed.

The VIPV/T system's numerical energy balance equations were formulated and implemented in TRNSYS software. A TRNSYS assignment was constituted by joining part modules explicitly in the simulation studio environment. Every single module was designated an arithmetic expression in the simulation engine with sets of corresponding proformas in the simulation studio window. These proformas had black-box explanations of respective components' inputs, variables, outputs and feedbacks. The simulation studio generated a deck file, which was used as a manuscript input to the simulation engine. The details of the simulation process control, time step and time range were defined in the global info window via the control cards icon. The simulation runs were performed on the model from which varying results were obtained and discussed in details. A sensitivity analysis performed on the collector slope revealed an optimum collector inclination angle of 35° which was implemented in the experimental study.

The model so developed was able to accept weather data from any location, geometrical dimensions for any PV/T, physical and control information for the respective components constituting the system depicting its flexibility and applicability to different scenarios. To this end, the requirements outlined in the first objective were successfully achieved.

It was imperative that actual solar collection output varied from analysis but dependable and resolute sets of data were essential to forecast the tendencies arising from design changes. The performance of VIPV/T system against conventional PV/T was evaluated experimentally. To perform this study an experimental rig was developed and measurements of temperature, voltage and current taken over a Medium-term period of daily cycles. The system was evaluated under varying environmental conditions of different days. The experiment to assess the effect of vacuum insulation on thermal and electrical performance of the PV/T was largely successful. Placing the hybrid VIPV/T and PV/T modules side by side subjected to the same meteorological conditions allowed for measurements of temperatures, voltages and currents used in evaluating power and heat flows. It was demonstrated that the VIPV/T gave a superior performance relative to conventional PV/T.

From the results of the daily simulation, it was ascertained that the inclusion of the vacuum insulation gave rise to improved thermal efficiency by 16.8 %; correspondingly, the useful heat generated also increased by 16.8 %. The electrical efficiency marginally reduced by 0.02 % due to increased average PV cell temperatures of about 5.4 %. Most importantly, the overall efficiency improved by 9.51 %, in addition to increases of 3.36 % and 4.08 % in overall exergy and primary energy saving efficiencies respectively.

In the annual simulation scale, the hybrid VIPV/T attained average values 18 %, 11 %, 29 % and 27 % thermal, electrical, exergy and primary energy saving efficiencies respectively. The overall efficiency was 29 % while annual solar fraction of 39 % was also registered.

It was deduced from the experimental results, that the vacuum inclusion resulted in thermal efficiency improvement by about 16.09 % while electrical efficiency remained largely the same with a downward difference of 0.28% even when the PV cell encapsulation was removed. Consequently, the overall efficiency was improved by 9.16 %. The overall exergy and primary energy saving efficiencies also increased by 2.74 % and 4.25 % respectively. The hot water and average PV cell temperatures were

125

increased by 12.8 % and 5.3 % respectively. The later was undesirable and gave rise to marginal decrease in electrical efficiency, an indication that it could escalate further.

The results of the simulation and experimental studies were substantively compared and analysed with relevant observations. The deviations between the respective simulated and experimental results were shown to vary in the range of 0.4 % to 3.6 %. These were attributed to the various assumptions made for simplification of the simulation. Additionally, the major contributor to the deviations was the difference between the predicted (TMY weather data) and the actual (measured weather data) file used for simulation and experiment respectively. However, these variations were well within the acceptable limits of 5 % and therefore, in relation to objective four, it was concluded that, the simulation and experimental results tallied satisfactorily well to show the functionality, accuracy and validity of the model developed.

6.2 Recommendations

The model of VIPV/T and PV/T developed in TRNSYS has produced satisfactory and realistic results and is therefore recommended for adoption by manufacturers, designers and installers to predict performance before actual implementation.

The use of a Typical Meteorological Year (TMY) weather data file in TRNSYS and actual measured weather data in experiments gave rise to some variations in trends of the parameters compared. TRNSYS software does not easily accept actual meteorological data but only conditioned sets specifically designed for its use. Therefore, it is recommended that same sets of weather data be used for both cases in order to achieve better comparison.

The analysis of the experimental study carried out on the VIPV/T and PV/T systems presented in this work was based on measurements for one day. To establish a trend of system's behaviour under varying weather conditions, measurements for prolonged periods could be conducted to cover the thermal behaviour during night hours.

Based on the results obtained from this study, the VIPV/T offers an improved thermal energy output as well as efficiencies. However, it has shown a possibility of elevated PV cell temperatures which results in reduced electrical efficiencies. In order to check these temperatures, the use of thermostatic controls is recommended.

The economic and financial benefit analysis has not been included in the current study. However, since the targeted application of the system is in the domestic domain, this needs to be done. This may provide more incisive information on investment decision making with regards to VIPV/T *vis a vis* PV/T by potential consumers.

REFERENCES

[1]   Joshi A. S., Tiwari A., Dancer I. Tiwari G. N., and Reddy B. V. Performance evaluation of a hybrid photovoltaic thermal (pave/t) glass-to-glass system. *International Journal of Thermal Sciences*, 48:154–164, 2009.

[2]   Daghigh R., Ruslan M. H., and Sopian K. Advances in liquid based photovoltaic/thermal (pv/t) collectors. *Renewable and Sustainable Energy Reviews*, 15:4156–4170, 2011.

[3]   Duffie J A and Beckman W, editors Solar Engineering of Thermal Processes, volume 4th edition of Encyclopaedia of Mathematical Sciences. John Wiley & Sons, Hoboken, New Jersey, 2013.

[4]   ESKOM. Solar water heating. http//www.eskom.co.za/sites/idm/Residential Technologies/pages/Solarwaterheating, 2013. Online; Accessed on 28/02/2014.

[5]   Howells M. Baseline and greenhouse gas mitigation options for bulk energy supply, South African country study on climate change. *Technical report*, Draft Energy Research Institute, University of Cape Town, 1999.

[6]   Kalogirou S.A. and Tripanagnostopoulos Y. Industrial application of PV/Solar energy systems. *Applied Thermal Energy*, 27:1259–1270, 2007.

[7]   Tripanagnostopoulos Y. Photovoltaic solar collectors. *Comprehensive Renewable Energy*, 3:255–300, 2012.

[8]   Sadness B. and Rekstad J. A photovoltaic/thermal (pv/t) collector with a polymer absorber plate-experimental study and analytical model. *Solar Energy,* 72:63–73, 2002.

[9]   Chow T. T. Performance analysis of photovoltaic collector by explicit model. *Solar Energy*, 75:143–152, 2003.

[10]   Huang B. J., Lin T. H., Hung W. C., and Sun F. S. Performance evaluation of solar photovoltaic/thermal systems. *Solar Energy*, 70:443–448, 2001.

[11]   Tripanagnostopoulos Y., Nousia T. H., Souliotis M., and Yianoulis P. Hybrid photovoltaic/thermal solar systems. *Solar Energy*, 72:217–234, 2002.

[12]   Tripanagnostopoulos Y., Souliotis M., Battisti R., and Corrado A. Energy cost and LCA results of PV and hybrid pv/t solar systems. *Progress in Photovoltaics: Research and Applications*, 13:235–250, 2005.

[13]   Agrawal B. and Tiwari G. N. Life cycle cost assessment of building integrated photovoltaic thermal (BIPVT) systems. *Energy and Buildings*, 42:1472–1481, 2010.

[14]   Elswijk M. J., Jong M. J. M., Braakman J. N. C., de Lange E. T. N., and Smit W. F. Photovoltaic/thermal collectors in large solar thermal systems. *In 19th EPSEC, 2004.*

[15]   Zondag H. A., De Vries D. W., and Van Helden W. G. J. The yield of different combined pv-thermal collector designs. *Solar Energy*, 74:253–269, 2003.

[16]   He W. Chow T. T. and Ji J. Hybrid photovoltaic-thermal water heating system for residential applications. *Solar Energy*, 80:298–306, 2006.

[17]   Erdil E., Ilkan M., and Egelioglu F. An experimental study on energy generation with a photovoltaic (PV)/solar thermal hybrid system. Energy, 33:1241–1245, 2008.

[18]   He W., Chow T. T., Ji J., Lu J., Pei G., and Chan L. Hybrid photovoltaic and thermal solar-collector designed for natural circulation of water. *Applied Energy*, 83:199–210, 2006.

[19]   Robles O B., Ruiz V. E., Canseco S. H., Cornejo M. R.C., Trapaga M. G., and Garcia R. F. J. Photovoltaic/thermal solar hybrid system with bifacial PV module and transparent plane collector. *Solar Energy Materials and Solar Cells*, 20:1966–1971, 2007.

[20]   Florschuetz L. W. Extension of the Hottel-Whillier model to the analysis of combined photovoltaic/thermal flat plate collectors. *Solar Energy*, 22:361–366, 1979.

[21]   Hendrie S D. Evaluation of combined photovoltaic/thermal collectors. *In The International conference ISES*, volume 3, pages 1865–1869, Atlanta GA, USA, May-June, 1979.

129

[22]   Joshi A. S. and Tiwari A. Energy and exergy efficiencies of a hybrid photovoltaic-thermal (PV/T) air collector. *Renewable Energy*, 32:2223–2241, 2007.

[23]   Zondag H. A., De Vries D. W. Van Helden W. G. J., Van Zolingen R. J. C., and Van Steenhoven A. A. The thermal and electrical yield of a pv-thermal collector. *Solar Energy*, 72:113–128, 2002.

[24]   Jones A. D. and Underwood C. P. A thermal model for photovoltaic systems. *Solar Energy*, 70:349–359, 2001.

[25]   Meir M., Rekstad J., Peter M., L. Henden, and Sandness B. Determination of the performance of solar systems with the calorimetric method. *Solar Energy*, 73:217–234, 2002.

[26]   Charron R and Athienitis A K. Optimization of the performance of double façades with integrated photovoltaic panels and motorized blinds. *Solar Energy*, 80:482 –491, 2006.

[27]   Kalogirou S. A. Use of TRNSYS for modelling and simulation of a hybrid PV/T solar system for Cyprus. *Renewable Energy*, 23:247–260, 2001.

[28]   Kalogirou S. A. and Tripanagnostopoulos Y. Hybrid PV/T solar systems for domestic hot water and electricity production. *Energy Conversion and Management,* 47:3368–3382, 2006.

[29]   Bergene T. and Lovvik O. M. Model calculations on a flat-plate solar heat collector with integrated solar cells. *Solar Energy*, 55:453–462, 1995.

[30]   Da Silva R M and Fernandes J L M. Hybrid photovoltaic/thermal (pv/t) solar systems simulation with simulink/matlab. *Solar Energy*, 84:1985–1996, 2010.

[31]   Raghuraman P. Analytical prediction of liquid and air photovoltaic/thermal Flat-plate collector performance. *Solar Energy Engineering*, 103:291–298, 1981.

[32]   Anderson T.N., Duke M., and Carson J. K. Designing photovoltaic/thermal solar collectors for building integration (BIPVT). *Solar Energy: Research Technology and Applications*, pages 403–426, Hamilton, New Zealand, 2008.

[33]   Tiwari A. and Sodha M. S. Performance evaluation of solar pv/t system: an experimental validation. *Solar Energy*, 80:751–759, 2006.

[34]   Mattei M., Notton G., Cristofari C., Muselli M., and Poggi P. Calculation of the polycrystalline PV module temperature using a simple method of energy balance. *Renewable Energy*, 31:553–567, 2006.

[35]   Jie J., Lu. J., Chow T. T., He W., and Pei G. A. Sensitivity study of a hybrid photovoltaic/thermal water heating system with natural circulation. *Applied Energy*, 84:222–237, 2007.

[36]   Dubey S. and Tiwari G. N. Thermal modelling of a combined system of photovoltaic/thermal (pv/t) solar water heater. *Solar Energy*, 82:602–612, 2008.

[37]   Agarwal R. K. and Garg H. P. Study of a photovoltaic and thermal system - thermisyphonic solar water heater combined with solar cells. *Energy Conversion and Management*, 35:605–620, 1994.

[38]   Kalogirou S. *Solar Energy Engineering: Processes and Systems*. Academic Press, Elsevier, Netherlands, 2009.

[39]   O'Hanlon F. J. *A Users' Guide to Vacuum Technology*. Wiley Interscience, New Jersey, 3rd edition, 2003.

[40]   Tyagi V.V., Kaushik S. C., and Tyagi S. K. Advancement in solar photo voltaic/thermal (PV/T) hybrid collector technology. *Renewable and Sustainable Energy Reviews*, 16:1383–1398, 2012.

[41]   Markus P. and Herald D. Testing of controllers for thermal solar systems. *Solar Energy*, 82:676–685, 2008.

[42]   Ibrahim A., Othman M. Y., Ruslan M. H., Mat S., and Sopian K. Recent advances in flat plate photovoltaic/thermal (pv/t) solar collectors. *Renewable and Sustainable Energy Reviews*, 15(1):352–365, 2011.

[43]   Tonui J.K. and Y. Tripanagnostopoulos. Improved pv/t solar collectors with heat extraction by forced or natural air circulation. *Renewable Energy*, 32:623 – 637, 2007.

131

[44] Tonui J.K. and Tripanagnostopoulos Y. Performance improvement of pv/t solar collectors with natural air flow operation. *Solar Energy*, 82(1):1 – 12, 2008.

[45] Assoa Y.B., Menezo C., Fraisse G., Yezou R., and Brau J. Study of a new concept of photovoltaic/thermal hybrid collector. *Solar Energy*, 81(9):1132–1143, 2007.

[46] Brogren M., Karisson B., Werner A., and Roos A. Design and evaluation of a low-concentrating, stationary, parabolic reflectors for wall integration of water cooled photovoltaic-thermal hybrid modules. *In Proceedings of the international Conference PV in Europe*, pages 551–555, Rome, Italy, October 2002.

[47] Garg H. P. and Adhikari R. S. Conventional hybrid photovoltaic/thermal air heating collectors: Steady state simulation. *Renewable Energy*, 11:363 – 385, 1997.

[48] Garg H. P., Agrawal P. K., and Hargava A. K. The effect of plane booster reflector on the performance of a solar air heater with solar cells suitable for solar dryer. *Energy Conversion and Management*, 32:543–554, 1991.

[49] Sopian K., Lui H. T., Kakac S., and Veziroglu T.N. Performance of a double pass Photovoltaic/thermal solar collector suitable for solar drying systems. *Energy Conservation and Management*, 41:353 - 365, 2000.

[50] REN21 Secretariat. *Renewables 2012 global status report*. Online, REN, 2012. Available from www.ren21.net accessed on 28/02/2014.

[51] Krauter S. and Ruther R. Considerations for the calculation of greenhouse gas reduction by photovoltaic solar energy. *Renewable Energy*, 29:345–355, 2004.

[52] Fthenakis V. M. and Kim H. C. Greenhouse-gas emissions from solar electric and nuclear power: A life-cycle study. *Energy Policy*, 35:2549–2557, 2007.

[53] Hottel H. C. and Whiller A. Evaluation of flat-plate solar collector performance. *In The conference on the use of solar energy,* volume 2, Tucson, Arizona, 1978. University of Arizona Press.

[54] Miroslav B., Bosanac S., Katic I., Svrensen H., Bruno N., and Jamal B. *Photovoltaic/thermal solar collectors and their potential in Denmark*. Final Report, EFP project 1713/00-0014, Copenhagen, 2003.

[55] Chow T. T. A review on photovoltaic/thermal hybrid solar technology. *Applied Energy*, 87:365–379, 2010.

[56] Incropera P. F., Dewitt P. D., Bergman L. T., and Lavine S. A. *Fundamentals of Heat and Mass Transfer*. John Wiley and Sons, U.S.A., 6th edition, 2007.

[57] Thorsell T. *Advances in thermal insulation, vacuum insulation pannels and thermal efficiency to reduce energy usage in buildings*. PhD thesis, KTH Roya Institute of Technology, 2012.

[58] Solar Energy Laboratory. *TRNSYS manual: Getting started*, volume 1. University of Wisconsin-Madison, U.S.A, 3rd edition, 2012. Accessed at http://sel.me.wisc.edu/trnsys on 29/10/2014.

[59] TRNSYS manual: *Using Simulation Studio*. University of Wisconsin-Madison, U.S.A, 2012.

[60] Solar Energy Laboratory. *EES manual: Getting started*, volume 1.University of Wisconsin-Madison, U.S.A, 3[rd]Edition, 2013. Accessed at http://sel.me.wisc.edu/trnsys on 29/10/2014.

[61] Zondag H. A. Flat plate pv-thermal collectors and systems: A review. *Renewable and Sustainable Energy Reviews*, 12:891–959, 2005.

Appendix A

Parameters used in the simulation and experiment

A.0.1   **Constant parameters**

Table A.1: List of constant parameters

Parameter	Value
Day of the year	234
Date	22nd August 2014
Time	7:30 am to 7:15 pm
Location	Durban($-29^{o}27^{'}S$, $30^{o}95^{'}E$, 8m)
Specific heat capacity of water	4190 J/kg
Absorptance of plate	0.94
Emittance of plate	0.9
Emittance of glass	0.88
Ground reflectance	0.4
Nusselt number	3.7
Surface Azimuth	0°
Thermal conductivity of Glass wool	0.040 W/mK
Thermal conductivity of copper	0.4 W/mK
Thermal conductivity of surrounding air	0.025 W/mK
Stephan Boltzmann's constant	5.67 x 10^{-8}
Collector inclination angle	35^{0}
Absorber plate area	1.4273 m^{2}
Absorber plate thickness	0.007 m
PV module area	1.125 m^{2}
External tube diameter	0.012 m
Internal tube diameter	0.106 m
Tube spacing	0.120 m

A.0.2 Measured parameters

Table A.2: List of constant parameters

Parameter	Value
Temperatures (^oC)	Inlet water
	Outlet water
	Ambient air
	Tank water
	Plate and PV
Voltage (V)	VIPV/T and PV/T
Current (A)	VIPV and PVT
Wind speeds (m/s)	Average
Solar radiation (W/m^2)	Global Horizontal Irradiance
	Diffuse Horizontal Irradiance
	Direct Normal Irradiance

A.0.3 Calculated variable parameters

A.0.3.1 Heat loss coefficient through the back of the collector

The heat loss coefficient through the back of the Module was considered to be the same for both PV/T and VIPV/T and calculated using the Equation A.1

$$U_b = \frac{k_{back}}{l_i} = \frac{0.040}{0.050} = 0.8 W/m^2 K \tag{A.1}$$

Heat loss coefficient through the edges of the collector

The heat loss coefficient through the edges of the collector was calculated using Equation A.2 as follows

$$U_e = \frac{(UA)_{edge}}{A_p} = \frac{(0.040/0.050) \times 2 \times 0.105 \times (1.640 + 0.87)}{1.4273} = 0.2954 W/m^2 K \tag{A.2}$$

Heat loss coefficient through the edges of the collector

135

$$U_t = \left[\dfrac{N}{\dfrac{c}{T_{pm}} \left(\dfrac{T_{pm} - T_a}{N+f} \right)^e} \right]^{-1} + \dfrac{\sigma(T_{pm} + T_a)(T_{pm}{}^2 + T_a{}^2)}{(\varepsilon_p + 0.00591 N h_w)^{-1} + \dfrac{2N+f-1+0.133\varepsilon_p}{\varepsilon_g} - N}$$

<div align="right">(A.3)</div>

The terms f, e and c are constants imposed for simplicity and are expressed as:

$f = (1+0.089h_w-0.1166h_w\varepsilon_p)(1+0.07866N) = (1+0.089\times16.636-0.1166\times16.636\times$

$0.94)(1 + 0.07866 \times 1) = 0.7089$

$c = 520(1-0.000051\beta^2) = 520(1-0.000051\times35^2) = 487.513$

$e = 0.430(1-100/T_{pm}) = 0.430(1-100/288.91) = 0.2982$

h_w = wind heat transfer coefficient $(W/m^{2o}C) = 2.8+3.0v = (2.8 + 3.0\times4.612) =$

$16.636W/m^{2o}C$

v = wind speed (m/s) = $4.612 m/s$

N = no of glass covers = 1

β = tilt angle of the collector (deg) = 35°

ε_g = glass cover emittance = 0.88

ε_p = absorber plate emittance = 0.9

T_a = ambient temperature (K). Since this was a measured variable parameter, the reading corresponding to 7:30 am = 15.91^oC (288.91K) was used for this calculation.

T_{pm} = Plate mean temperature (K). This was a measured variable parameter and the first entry corresponding to 7.30 am was recorded as 53.213^oC = 326.212K. Another way of determining T_{pm} would be by Equation A.4 as:

$$T_{pm} = T_{fi} + \dfrac{Q_u/A_c}{F_R U_L}(1 - F_R)$$

<div align="right">(A.4)</div>

The values of the parameters calculated indicated above were inserted into Equation A.3 and obtained U_t = 0.0688W/m^2K Therefore, the overall heat loss coefficient was calculated by adding all the three components as shown in Equation A.5.

$U_L = U_t + U_e + U_b = 0.8 + 0.2954 + 0.0688 = 1.1658 W/m^2K$ (A.5)

This is a typical calculation of the first term, the rest of the variable values corresponding to individual data points were automatically generated in an EES code.

Appendix B

Simulation and Experimental results

B.0.1 Simulation results

Time	Q_u		η_{th}		η_{el}		η_o	
	VIPV/T	PV/T	VIPV/T	PV/T	VIPV/T	PV/T	VIPV/T	PV/T
07:30	46.98	38.96	0.16	0.13	0.00	0.00	0.16	0.13
07:45	61.23	51.37	0.16	0.14	0.13	0.12	0.29	0.26
08:00	76.97	65.28	0.17	0.14	0.12	0.11	0.29	0.25
08:15	90.41	78.22	0.17	0.14	0.13	0.13	0.30	0.27
08:30	105.28	92.07	0.17	0.15	0.12	0.13	0.29	0.28
08:45	112.43	97.65	0.16	0.14	0.10	0.10	0.26	0.24
09:00	127.45	110.83	0.17	0.14	0.12	0.11	0.28	0.25
09:15	138.33	120.06	0.16	0.14	0.11	0.11	0.28	0.25
09:30	151.91	131.66	0.17	0.14	0.12	0.11	0.29	0.26
09:45	160.62	141.49	0.17	0.15	0.11	0.12	0.28	0.26
10:00	167.18	147.10	0.17	0.15	0.11	0.11	0.27	0.26
10:15	175.53	154.41	0.17	0.15	0.11	0.11	0.27	0.25
10:30	185.65	172.87	0.17	0.16	0.10	0.11	0.28	0.27
10:45	198.35	172.71	0.17	0.15	0.09	0.09	0.27	0.24
11:00	209.67	185.55	0.18	0.16	0.09	0.08	0.26	0.24
11:15	212.41	187.17	0.17	0.15	0.09	0.08	0.26	0.23
11:30	210.32	184.54	0.17	0.15	0.08	0.08	0.26	0.23
11:45	210.97	186.03	0.17	0.15	0.09	0.08	0.26	0.24
12:00	209.87	184.12	0.17	0.15	0.07	0.08	0.24	0.23
12:15	204.07	178.13	0.17	0.15	0.08	0.08	0.25	0.23
12:30	201.49	176.38	0.17	0.15	0.09	0.09	0.25	0.23
12:45	201.32	176.61	0.17	0.15	0.09	0.09	0.26	0.24
13:00	194.19	168.41	0.16	0.14	0.09	0.09	0.25	0.23
13:15	182.34	156.40	0.16	0.14	0.09	0.09	0.25	0.22
13:30	178.45	153.06	0.16	0.14	0.10	0.09	0.26	0.23
13:45	173.30	144.02	0.16	0.13	0.09	0.09	0.25	0.23
14:00	168.17	140.70	0.16	0.14	0.09	0.09	0.26	0.23
14:15	156.20	131.71	0.16	0.14	0.08	0.09	0.24	0.22
14:30	145.01	121.62	0.16	0.13	0.09	0.08	0.24	0.21
14:45	131.10	110.10	0.15	0.13	0.09	0.09	0.24	0.22
15:00	122.74	103.09	0.15	0.13	0.09	0.10	0.25	0.23
15:15	104.64	88.89	0.15	0.12	0.08	0.09	0.23	0.21
15:30	90.93	77.69	0.14	0.12	0.09	0.09	0.23	0.21
15:45	84.97	67.63	0.15	0.12	0.10	0.10	0.24	0.22
16:00	70.41	59.93	0.15	0.13	0.11	0.11	0.25	0.24
16:15	50.46	42.53	0.13	0.11	0.11	0.11	0.25	0.22
16:30	37.09	33.32	0.14	0.12	0.13	0.13	0.26	0.26
16:45	20.02	16.19	0.10	0.08	0.13	0.14	0.23	0.22
17:00	10.88	8.50	0.11	0.09	0.20	0.20	0.32	0.29
17:15	6.11	5.20	0.11	0.09	0.00	0.01	0.11	0.10

Time	Solar Radiation	T_i	T_a	T_Tank	Voltage (V)		Current (I)		POWER (W)	
					VIPV/T	PV/T	VIPV/T	PV/T	VIPV/T	PV/T
07:30	205.04	20.03	15.91	20.23	0.00	0.00	0.00	0.00	0.00	0.00
07:45	264.68	20.14	16.24	20.35	23.71	23.27	3.15	3.10	74.79	72.04
08:00	325.17	21.69	16.52	20.15	25.61	24.85	3.41	3.31	87.26	82.14
08:15	379.73	20.83	16.93	20.49	29.06	28.39	3.86	3.78	112.29	107.19
08:30	439.15	20.83	17.19	20.57	29.86	31.21	3.97	4.15	118.56	129.59
08:45	492.75	20.83	17.42	20.92	29.31	29.02	3.90	3.86	114.29	112.03
09:00	537.44	20.83	17.88	20.71	32.35	31.20	4.30	4.15	139.19	129.50
09:15	594.46	20.83	17.73	20.75	33.89	33.75	4.51	4.49	152.76	151.52
09:30	643.11	20.83	17.88	20.32	36.17	35.03	4.81	4.66	173.98	163.22
09:45	671.67	20.83	18.80	21.37	35.05	36.40	4.66	4.84	163.39	176.20
10:00	708.72	20.83	18.48	21.60	35.58	36.56	4.73	4.86	168.40	177.78
10:15	734.59	20.83	18.82	21.67	36.26	36.16	4.82	4.81	174.87	173.92
10:30	750.24	20.90	19.54	22.65	35.99	36.53	4.79	4.86	172.27	177.44
10:45	796.55	20.81	19.74	23.10	35.49	34.69	4.72	4.61	167.50	160.07
11:00	835.41	20.83	19.33	23.35	34.75	33.91	4.62	4.51	160.57	152.96
11:15	854.35	20.81	19.23	23.74	35.12	33.14	4.67	4.41	164.08	146.05
11:30	852.80	21.66	19.56	25.88	34.57	34.20	4.60	4.55	158.94	155.54
11:45	854.96	21.33	19.62	28.60	35.98	34.85	4.79	4.63	172.20	161.52
12:00	862.53	21.42	19.48	31.15	32.89	34.11	4.37	4.54	143.85	154.73
12:15	852.80	21.72	19.87	32.85	34.46	34.49	4.58	4.59	157.91	158.25
12:30	849.72	22.35	19.64	34.37	35.43	35.75	4.71	4.75	166.99	169.98
12:45	840.08	23.10	19.59	35.81	35.24	35.71	4.69	4.75	165.20	169.59
13:00	826.16	23.27	19.92	36.98	34.96	35.57	4.65	4.73	162.55	168.28
13:15	808.30	23.09	20.03	38.09	35.70	34.31	4.75	4.56	169.49	156.56
13:30	776.58	23.29	20.12	38.97	35.51	34.38	4.72	4.57	167.75	157.20
13:45	748.75	23.61	19.80	39.73	34.21	34.36	4.55	4.57	155.62	156.98
14:00	722.01	24.17	19.73	40.44	33.83	34.00	4.50	4.52	152.18	153.79
14:15	681.10	24.77	19.81	41.02	30.88	31.56	4.11	4.20	126.82	132.47
14:30	642.99	23.96	19.92	41.21	30.63	29.42	4.07	3.91	124.79	115.15
14:45	611.29	24.29	19.85	41.29	30.13	30.62	4.01	4.07	120.76	124.67
15:00	560.71	22.08	19.58	40.63	29.73	30.23	3.95	4.02	117.56	121.54
15:15	505.20	21.27	20.26	40.01	26.48	27.97	3.52	3.72	93.25	104.07
15:30	450.00	21.53	20.26	39.20	25.96	26.23	3.45	3.49	89.62	91.52
15:45	403.76	21.04	19.43	38.70	25.67	26.15	3.41	3.48	87.62	90.96
16:00	334.72	21.91	19.35	38.51	24.42	25.15	3.25	3.34	79.30	84.11
16:15	265.24	20.61	19.45	38.20	22.46	21.81	2.99	2.90	67.11	63.29
16:30	190.86	20.40	19.34	37.90	20.28	20.75	2.70	2.76	54.72	57.25
16:45	140.91	20.23	19.38	37.58	17.85	18.38	2.37	2.45	42.37	44.95
17:00	66.31	20.61	18.94	37.28	15.09	14.99	2.01	1.99	30.28	29.90
17:15	40.03	20.13	18.89	36.94	0.00	2.55	0.00	0.34	0.00	0.86

B.0.2 Experimental results

Time	Solar Radiation	T_{tank} (°C)	Ta	Inlet Temperature T_i (°C)		Outlet Temperature T_O (°C)		Voltage (V)		Current (A)	
				VIPV/T	PV/T	VIPV/T	PV/T	VIPV/T	PV/T	VIPV/T	PV/T
07:30	205.04	20.68	15.91	20.03	20.03	20.36	20.92	22.80	22.47	3.03	2.99
07:45	264.68	20.90	16.24	20.14	20.14	21.57	21.41	23.29	22.85	3.10	3.04
08:00	325.17	20.99	16.52	21.69	21.69	22.56	21.32	24.75	23.96	3.29	3.19
08:15	379.73	21.55	16.93	20.83	20.83	24.10	23.87	27.68	26.98	3.68	3.59
08:30	439.15	22.45	17.19	20.83	20.83	25.05	25.41	28.85	30.25	3.84	4.02
08:45	492.75	22.88	17.42	20.83	20.83	25.88	25.69	30.49	30.22	4.06	4.02
09:00	537.44	23.68	17.88	20.83	20.83	26.80	26.55	32.66	31.52	4.34	4.19
09:15	594.46	23.87	17.73	20.83	20.83	27.60	27.05	33.53	33.39	4.46	4.44
09:30	643.11	23.92	17.88	20.83	20.83	28.78	27.97	35.45	34.29	4.71	4.56
09:45	671.67	24.24	18.80	20.83	20.83	36.96	28.97	34.37	35.74	4.57	4.75
10:00	708.72	25.08	18.48	20.83	20.83	38.13	30.51	34.59	35.59	4.60	4.73
10:15	734.59	25.12	18.82	20.83	20.83	40.97	32.85	34.79	34.69	4.63	4.61
10:30	750.24	26.08	19.54	20.90	20.90	46.62	34.87	33.87	34.44	4.50	4.58
10:45	796.55	28.95	19.74	20.81	20.81	49.97	38.60	34.73	33.92	4.62	4.51
11:00	835.41	32.10	19.33	20.83	20.83	55.38	44.93	34.19	33.34	4.55	4.43
11:15	854.35	35.11	19.23	20.81	20.81	56.93	50.42	34.93	32.93	4.65	4.38
11:30	852.80	42.09	19.56	21.66	21.66	56.62	53.00	33.72	33.34	4.48	4.43
11:45	854.96	46.56	19.62	21.33	21.33	57.91	54.50	34.63	33.45	4.61	4.45
12:00	862.53	48.66	19.48	21.42	21.42	58.92	55.97	32.16	33.41	4.28	4.44
12:15	852.80	52.46	19.87	21.72	21.72	58.22	56.02	33.23	33.27	4.42	4.42
12:30	849.72	54.69	19.64	22.35	22.35	57.97	54.82	32.89	33.23	4.37	4.42
12:45	840.08	56.90	19.59	23.10	23.10	57.72	54.67	32.77	33.27	4.36	4.42
13:00	826.16	56.29	19.92	23.27	23.27	56.90	53.37	32.63	33.29	4.34	4.43
13:15	808.30	56.90	20.03	23.09	23.09	56.00	54.78	34.76	33.33	4.62	4.43
13:30	776.58	56.08	20.12	23.29	23.29	54.63	52.75	34.72	33.56	4.62	4.46
13:45	748.75	56.18	19.80	23.61	23.61	52.41	52.52	31.44	31.61	4.18	4.20
14:00	722.01	56.96	19.73	24.17	24.17	48.80	49.03	33.22	33.40	4.42	4.44
14:15	681.10	56.00	19.81	24.77	24.77	43.70	46.92	31.39	32.06	4.17	4.26
14:30	642.99	55.99	19.92	23.96	23.96	40.84	44.47	32.65	31.52	4.34	4.19
14:45	611.29	55.40	19.85	24.29	24.29	38.04	40.09	31.58	32.05	4.20	4.26
15:00	560.71	55.77	19.58	22.08	22.08	35.29	35.49	29.89	30.39	3.98	4.04
15:15	505.20	55.43	20.26	21.27	21.27	33.05	33.84	29.28	30.64	3.89	4.08
15:30	450.00	55.13	20.26	21.53	21.53	31.76	29.50	28.95	29.20	3.85	3.88
15:45	403.76	54.40	19.43	21.04	21.04	31.24	27.15	27.84	28.29	3.70	3.76
16:00	334.72	52.36	19.35	21.91	21.91	30.89	25.62	26.88	27.55	3.58	3.66
16:15	265.24	51.63	19.45	20.61	20.61	30.68	24.73	24.56	23.97	3.27	3.19
16:30	190.86	50.63	19.34	20.40	20.40	30.08	24.14	20.46	20.92	2.72	2.78
16:45	140.91	49.06	19.38	20.23	20.23	29.46	23.69	18.14	18.67	2.41	2.48
17:00	66.31	49.07	18.94	20.61	20.61	29.25	23.11	13.79	13.69	1.83	1.82
17:15	40.03	49.04	18.89	20.13	20.13	29.01	22.56	11.94	12.21	1.59	1.62

Time	Solar Radiation G(W/m²)	Useful Heat (Qu)		Eta_th		POWER _el (W)		Eta_el		Eta_overall		U_L	
		VIPV/T	PV/T	VIPV/T	PV/T	VIPV/T	PV/T	VIPV/T	PV/T	VIPV/T	PV/T	VIPV/T	PV/T
07:30	205.04	35.33	38.56	0.16	0.13	69.13	67.13	0.15	0.15	0.31	0.28	1.02	0.23
07:45	264.68	53.19	50.38	0.16	0.13	72.17	69.42	0.12	0.12	0.28	0.25	-0.50	0.23
08:00	325.17	61.05	61.29	0.16	0.13	81.49	76.37	0.11	0.10	0.27	0.24	0.28	0.23
08:15	379.73	72.87	72.23	0.16	0.13	101.92	96.82	0.12	0.11	0.28	0.25	0.07	0.24
08:30	439.15	83.42	84.09	0.16	0.13	110.66	121.69	0.11	0.12	0.27	0.26	0.44	0.25
08:45	492.75	93.33	94.67	0.16	0.13	123.68	121.42	0.11	0.11	0.27	0.24	0.65	0.26
09:00	537.44	119.46	103.85	0.16	0.14	141.84	132.14	0.12	0.11	0.27	0.24	-5.01	0.28
09:15	594.46	133.48	115.08	0.16	0.14	149.53	148.28	0.11	0.11	0.27	0.25	-5.65	0.28
09:30	643.11	141.44	124.68	0.16	0.14	167.10	156.34	0.12	0.11	0.27	0.24	-5.40	0.28
09:45	671.67	148.83	132.51	0.16	0.14	157.11	169.92	0.10	0.11	0.26	0.25	-7.75	0.28
10:00	708.72	157.42	140.13	0.16	0.14	159.11	168.49	0.10	0.11	0.26	0.24	-7.07	0.28
10:15	734.59	166.37	146.44	0.16	0.14	160.97	160.03	0.10	0.10	0.26	0.24	-9.60	0.30
10:30	750.24	174.28	151.90	0.15	0.14	152.58	157.74	0.09	0.09	0.24	0.24	-16.20	0.30
10:45	796.55	184.43	162.75	0.17	0.14	160.43	153.00	0.09	0.09	0.26	0.23	-19.80	0.39
11:00	835.41	191.90	175.59	0.17	0.15	155.43	147.82	0.08	0.08	0.25	0.23	-10.10	0.76
11:15	854.35	201.46	180.21	0.17	0.15	162.23	144.19	0.08	0.08	0.25	0.22	-12.68	0.78
11:30	852.80	207.71	179.58	0.17	0.15	151.19	147.80	0.08	0.08	0.25	0.22	-12.70	0.71
11:45	854.96	209.11	181.06	0.17	0.15	159.49	148.82	0.08	0.08	0.25	0.23	-15.49	0.91
12:00	862.53	212.99	183.16	0.17	0.15	137.53	148.42	0.07	0.08	0.24	0.23	-14.46	0.93
12:15	852.80	209.94	180.16	0.17	0.15	146.83	147.17	0.08	0.08	0.25	0.22	-15.11	0.96
12:30	849.72	206.94	179.41	0.17	0.15	143.88	146.87	0.08	0.08	0.24	0.22	-9.26	0.89
12:45	840.08	200.86	176.65	0.17	0.15	142.82	147.20	0.08	0.08	0.24	0.23	-5.95	0.95
13:00	826.16	197.32	172.45	0.17	0.15	141.63	147.36	0.08	0.08	0.24	0.23	-6.46	0.96
13:15	808.30	192.01	168.44	0.17	0.15	160.65	147.73	0.09	0.08	0.26	0.23	-6.71	1.01
13:30	776.58	184.96	161.10	0.17	0.15	160.37	149.82	0.09	0.09	0.26	0.23	-6.66	0.86
13:45	748.75	174.05	150.05	0.17	0.14	131.50	132.86	0.08	0.08	0.25	0.22	-5.22	1.09
14:00	722.01	171.01	144.73	0.17	0.14	146.78	148.39	0.09	0.09	0.26	0.23	-5.28	0.65
14:15	681.10	162.32	135.74	0.16	0.14	131.03	136.68	0.09	0.09	0.25	0.23	-5.03	0.33
14:30	642.99	141.16	127.64	0.16	0.14	141.79	132.14	0.10	0.09	0.26	0.23	-3.02	0.33
14:45	611.29	148.46	120.13	0.16	0.14	132.68	136.58	0.10	0.10	0.26	0.24	-6.09	0.28
15:00	560.71	132.83	110.11	0.16	0.14	118.85	122.84	0.09	0.10	0.26	0.23	-8.78	0.30
15:15	505.20	117.13	98.91	0.16	0.14	114.04	124.86	0.10	0.11	0.26	0.25	-17.85	0.26
15:30	450.00	99.60	87.71	0.16	0.14	111.48	113.38	0.11	0.11	0.27	0.25	-9.10	0.23
15:45	403.76	103.72	78.64	0.17	0.14	103.06	106.41	0.11	0.12	0.28	0.25	-15.40	0.20
16:00	334.72	62.83	64.95	0.16	0.14	96.12	100.93	0.13	0.13	0.29	0.27	1.06	0.23
16:15	265.24	51.65	53.12	0.14	0.12	80.25	76.43	0.13	0.13	0.28	0.25	1.43	0.16
16:30	190.86	38.69	38.78	0.14	0.12	55.66	58.19	0.13	0.14	0.27	0.26	0.30	0.22
16:45	140.91	22.98	29.23	0.13	0.12	43.78	46.36	0.14	0.15	0.27	0.26	7.62	0.29
17:00	66.31	9.40	13.35	0.14	0.11	25.30	24.93	0.17	0.17	0.31	0.28	2.96	0.60
17:15	40.03	4.27	7.91	0.12	0.11	18.96	19.82	0.21	0.22	0.33	0.33	3.54	0.58

Appendix C

The Experimental Equipment Technical Specifications

Table C.1: The experimental equipment technical specifications

Component	Property	Value
Solar battery	Model	BSB Regulated valve sealed
	Nominal voltage	$12V$
	Nominal capacity	100Ah (20^oC)
	Charge status	Constant voltage charging
	Cycle use	$14.4 - 14.8V$
	Standby use	$13.6 - 13.8V$
	Initial current	Less than 25A
Solar circulation pump	Model	CS-0512HM-12M (Grandfos)
	Rated voltage (V_m)	12V dc
	Rated total capacity	4 liters/minute
	Rated head	Not $< 1.3m$
	Maximum flow rate	10kg.f/cm^2
	Power consumption	$8W$
	Operating current	$0.65A$
	Temperature range	$-20^oC - 90^oC$
	Max relative humidity	95 %
Charge controller	Model	TriStar-45
	Rated voltage	$12,24,48V\ dc$
	Maximum rated current	$45A$ continuous
DataTaker DT80	System voltage	10-30Vdc
	Analogue channels	10 (expandable to 100)
	Digital channels	8 (bi-directional)
Component	Property	Value
	Inputs	Inter-channel isolation:100V Analogue section isolation:100V Input impedance: 100K, >100M Common mode range: ±3.5V
	Accuracy	±0.15 % (5^oC to 40^oC) ±0.35 %(-45^oC to 70^oC)
	Interfaces	RS232, USB 1.1
	Data capacity	128MB
	Software	- dEX
	Measured parameters	- Temperatures - Module current - Battery voltage - State of Charge (SOC)
	Physical properties	Dim. 180 x 137 x 65mm Weight: 1.5 kg

		Temp. range: -45^oC to 70^oC
Sunshine Pyranometer	Overall accuracy	±5 % daily integrals ±5 %$\pm10Wm^{-2}$ % hourly average ±8 %$\pm10Wm^{-2}$ individual readings
	Resolution	$0.6Wm^{-2} = 0.6mV$
	Range	0 to $> 2000Wm^{-2}$
	Analogue output sensitivity	$1mV = 1Wm^{-2}$
	Analogue output range	$0 - 2500mV$
	Sunshine status threshold	$120Wm^{-2}$ in the direct beam
	Accuracy: Sunshine status	±10 % sun hours with respect to the threshold
	Accuracy: Cosine Correction	±2 % of incoming radiation over $0 - 90^o$ Zenith angle
	Accuracy: Azimuth angle	±5 % over 360 rotation
	Temperature coefficient	±0.02 % per ^oC typical ($-20 to + 70^oC$)
	Temperature range	$-40 to + 70^oC$
	Response time	< 200ms
	Spectral Response sensitivity	$400 - 2700nm$
	Spectral sensitivity variation	10 % typical
	Latitude capability	-90° to $+90^o$
	Power requirement	$2mA$ (excluding heater power),$5V$ $15V$ DC
	Heater power	$12V$ $15V$ DC, up to $1.5A$